FUNCTIONALLY GRADED STRAIN HARDENING CEMENTITIOUS COMPOSITES FOR IMPROVING CONCRETE DURABILITY

by

Pavel Trávníček

A Dissertation

Submitted to

The Department of Civil Engineering

Yokohama National University

In Partial Fulfillment of the Requirements for the Degree of

Doctor of Philosophy

Department of Civil Engineering

YOKOHAMA NATIONAL UNIVERSITY

Yokohama, Japan

September, 2017

Abstract

The strain hardening cementitious composite (SHCC) is an interesting type of fibre reinforced material, predominantly used as a patch repair material mainly due to its beneficial self-controlled tight crack width. Main difference between the ordinary fibre reinforced concrete (FRC) and SHCC is tensile performance characteristic for its capability of sustaining or increasing load capacity after the first cracking up to relatively large strain values up to, but not limited to 3%.

All structures, and concrete is not an exemption, are undergoing deteriorative processes of a different rate when exposed to environmental loading, that can be of natural or artificial cause, such as air, moisture, temperature, salt diffusion, freezing and thawing, etc. It is the tight cracking and large strain capacity creating a material of high fracture energy, that makes SHCC materials especially suitable to be used as a repair layer to substitute old deteriorated concrete covers that cannot protect reinforcing steel bar.

It is then natural to get an idea of creating a functionally graded material, that would be optimized to highlight those beneficial characteristics of SHCC. This evolution can be called FG-SHCC (functionally graded SHCC), and it is a kind of material formed by layers of SHCC of different material characteristics to create better functional protection against penetration of harmful substances from the surface throughout its multi-layer structure. The goal of this dissertation is to investigate the possibilities of FG-SHCC, discuss and analyse some of it's potential drawbacks, and propose an optimal function describing the distribution of layers in the FG-SHCC.

Diffusion is a result of random molecular motions causing transport of diffused matter from one area to another in the absence of convection currents or pressure difference. Theory of diffusion is based on the hypothesis that the speed of transfer of diffusing material through unit area of a section is proportional to the concentration gradient.

Cracks in the cementitious material are inevitable even under the service load conditions, and increased material diffusivity needs to be understood. From experimental research it is understood that diffusion coefficient through the crack increases with the increasing crack width and becomes almost constant when the crack width is approximately 80-100microns, which is highly harmful for protection of steel rebars against penetrating substances. For the diffusion analysis, the so-called apparent diffusivity coefficient is usually used. Apparent diffusivity of a material depends on concentration of the solution and other conditions. In case of CO_2 diffusion, higher concentration causes densification of the surface layer causing reduction of diffusivity.

Numerical error of diffusion analysis is examined on two different analytical solutions. First, semi-infinite domain of constant diffusivity with constant boundary concentration and secondly a two-layer semi-infinite domain. It has been found that for accurate estimate of concentration distribution, a certain "backfield" domain is necessary to model a finite domain (FG-SHCC) attached to a large domain (concrete) beyond the steel reinforcement.

Layering of SHCC, i.e., creation of FGM (functionally graded material), is examined and an effect of layer order and composition on crack width distribution caused by mechanical load is observed. FGM is widely observed in natural structures, such as for example the internal structure of bamboo, with graded distribution of longitudinal fibrous structure, or in organs, such as a bone structure. It is presumed that, layered SHCC compared to a single layer can further improve durability, due to finer cracks distributed over a large area. FG-SHCC material can further provide a tool to control the diffusion of chlorides. Diffusion through the different FGM is analysed and firstly presented on three layer material. Step-wise functions are used to approximate linear function distribution, concave function and convex function. Those functions are using different diffusivity ratios (quality index) such as 0.5:1.0:1.5, where 1.0 is assumed to be an average quality. From the analysis results, it can be concluded that the steepest function gradient offers the best performance and that the concave function show almost the same durability as the linear gradient, when same external layer is used. FG-SHCC is then studied by using the test data of different SHCC mixtures, and corrosion initiation time at the location of crack is studied. Main conclusion here is

that the formed crack highly increases the initial apparent diffusivity of sound material, resulting into penetration depth to be more than 20-times larger in the crack location. Durability time is then defined as the time until corrosion is initiated, but even after reaching the durability time, the corrosion rate of SHCC might be different from the one of single layer mortar due to so-called micro-cell corrosion.

Experimental work to verify bond behaviour of layered material subjected to tensile loading and the surface cracking of the repaired FG-SHCC material applied on the mortar beam is examined. Tensile bond test on the layered structure applied on a concrete surface in three 5mm layers showed no signs of mechanical de-bonding and the failure zone was within the first layer, i.e., the surface layer. This performance was obtained even without using a special primer and with 24 hours time gap between each layer application. The flexure test of the pre-cracked beam repaired with FG-SHCC showed that crack width is well bellow the allowable limit, and that at service load there are no residual cracks, i.e, only elastic deformation. An anisotropic modelling of FG-SHCC is newly presented, showing more realistic cracking behaviour compared to homogeneous model.

Optimization utilizing the random trial and error method for chloride ion diffusion from the surface through the multi-layer structure of FG-SHCC is performed. Limitation factors are the ultimate SHCC material local strain and fibre content causing cracks not wider than 100μm due to the risk of crack localization. 6 layers are here assumed and the ideal distribution with given constrains at linear variable strain and constant strain is suggested. Main design limits are use of minimum possible fibre content at the interface with old concrete that would still prevent localization at the given strain and use of maximum amount of fibres at the surface layer to reduce crack width. When linear variable strain is applied on the structure, the best quality material is suitable to be used on the surface, the relatively weakest material layer should be used inside the FGM, and the average quality at the interface. This distribution creates a polynomial functional gradient.

Proposed FG-SHCC repair material can provide higher durability compared to homogeneous distribution. The beneficial behaviour is presented by numerical models. From the experiment it is concluded that risk of de-bonding at the initial life span

is not present. Performance of the bond quality with respect to time is suggested as a subject of a future study. FGM is a suitable material structure especially for 3D printed concrete. Such application can open further possibilities of optimization, i.e., the optimization can be performed not only with respect to layers (direction x), but also along the surface (direction y,z).

Acknowledgements

The presented research in this dissertation would not be possible without the help of many people. My deepest gratitude and sincere thanks goes to my research advisor, Prof. Tatsuya Tsubaki, for his professional, genuine guidance and valuable advice to accomplish the dissertation on time.

I am thankful to Associate Prof. Akira Hosoda, concrete laboratory at Yokohama National University, for his ideas and valuable discussions during any presentation to improve this research significantly.

I am grateful to Research Associate Satoshi Komatsu, concrete laboratory at Yokohama National University, for his valuable ideas and comments throughout the years of my research and especially during the experimental works.

I wish to express sincere appreciation to the members of examination committee Prof. Koichi Maekawa, Prof. Yoshiyuki Nakamura, Associate Prof. Akira Hosoda, and Associate Prof. Mamoru Kikumoto, for their contribution in reviewing this research work and their guidance during the last stage of this research. The author appreciates the comments on this dissertation and their good will to improve this research to reach the final stage.

Grateful appreciation goes to the Ministry of Education, Culture, Sports, Science, and Technology of Japan for the allocation of financial support.

Finally, I would like to thank to my family, without their support and encouragement I would not be able to pursue this journey. I am grateful towards all the members of the laboratory for providing the pleasant atmosphere to work in. My special thanks is due to my great friends, who were all the time here for me.

Contents

List of Figures

List of Tables

Chapter 1

Introduction

The main summary of the research significance, basic concepts and definitions used in the dissertation are presented in this first chapter. Main problem is described and used solution techniques to provide us with answers are also mentioned. This first chapter is completed with a note on the dissertation organization itself.

1.1 Research significance

Corrosion of embed reinforcement is probably one of the foremost discussed and researched issue in the concrete structures, as it is the key for long structural durability. Corrosion of reinforcement can be observed by leaching of corrosion product to the surface, later followed by cracking and spalling of the surface layer and progress of corrosion. The deterioration rate is highly dependent not only on the quality of a concrete structure itself, but the environment exposure is of the same importance. Japan, and many other countries having structures of high importance near the most severe environment, such as highways, tunnels and bridges near a coastline, are facing the durability problems the most. But also landlocked countries, especially the ones with temperatures regularly under the freezing point are facing a similar problem. Some marine environment can show deterioration of the surface, e.g., cracking and de-lamination, already during 5 to 10 years following construction. [20] Very severe deterioration can occur in structures, where many harmful conditions are combined [29], [91], [27]. In Japan, up to 20% of tunnel structures, and around 15% of river structures, culverts and superstructures build before year 1964 show at least minor

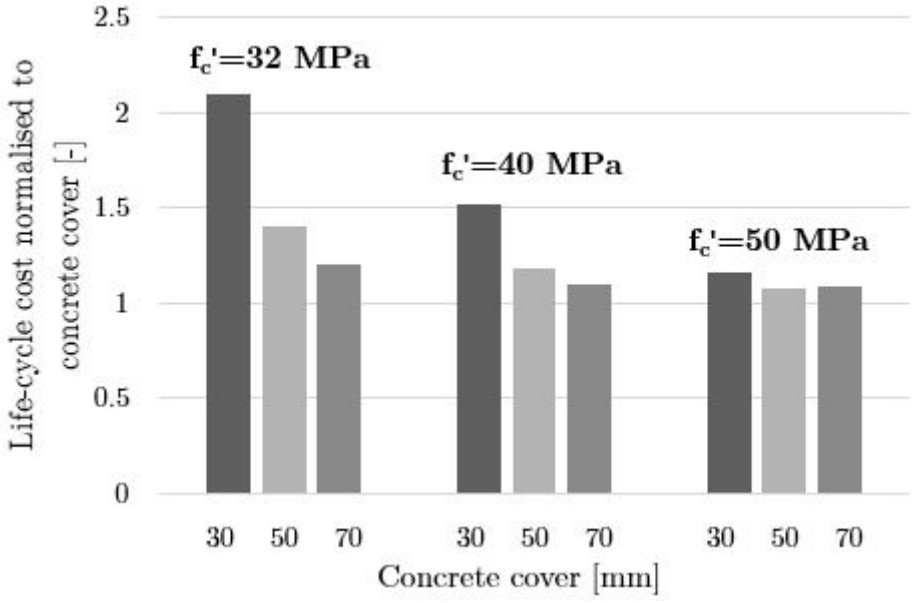

Fig. 1.1.1 Mean life-cycle costs in splash zone [94]

deterioration, i.e., structure is still safe to use, but would not be in future [105]. Some 5.9% of structures are ranked as remarkably deteriorated, where remedy is need to consider [105].

Highest reason for this deterioration is reported low-quality concrete and shortage of concrete cover [105]. The mostly used repair method is use of a pre-packed concrete for refacing of structures, jacketing, filling of cavities in and under structures. Second most common repair method is applying a paint, followed by patching repair materials [105]. From the visual inspection, 85% of the repaired structures within 100m from coastline show again after 5-10 years some signs of re-deterioration, rendering the repair method ineffective. This is calling for development of preventative maintenance scheme, or more effective repair methods to reduce cost of a structure over it's whole life-cycle.

Example of determined life-cycle cost of a structure at splash zone for a service life of 100 years is in the Fig.1.1.1, from which can be seen, that higher quality material, or thicker cover layer and the combination of both can provide a reduction in cost of retrofitting over the life-cycle. The life-cycle costs includes cost of construction, quality assurance, maintenance and cost of inspections. With an inadequate design, life-cycle cost can be more than doubled.

Fig. 1.1.2 Example of deteriorated structure

1.2 Objectives

The main objective of this study is to find optimal multi-layer structure material, that would provide higher durability for the main deterioration factors, such as chloride ions ingress, carbonation and salt scaling, and to study factors affecting this process. By examining these factors, functionally graded strain hardening composite structure can be obtained.

To achieve the objectives of this study following steps were performed:

1. Studying the mechanical behaviour of functionally graded strain hardening cementitious composites under various strain levels, crack width formation and number of cracks.

2. Studying how salts and carbon dioxide can penetrate inside the sound and cracked functionally graded strain hardening cementitious structures, and the rate of those processes.

3. Studying the physical behaviour of strain hardening cementitious composites, and how fibre content, water to binder ratio and matrix composition affects it's material properties, such as apparent diffusivity of chloride ions, carbonation and

salt scaling.

4. Design different models of functionally graded material and optimize for a different deterioration by implied strain, see if the different type require a different kind of functionally graded material structure.

5. Studying how FG-SHCC can be optimized for salt scaling phenomenon.

1.3 Literature review

General overview of used expressions and parameters that are defined and need to be understand the problem are briefly introduced. Additional details of presented expressions that this thesis is dealing with are to be specified in later chapters.

1.3.1 Diffusion

Diffusion is a result of random molecular motions causing transport of diffused matter from one area to another in the absence of convection currents or pressure difference. This can be illustrated by a column of clear water placed on top of material of a colour, such as iodine solution. After sharp separation of the coloured part, the whole solution becomes after sufficient time uniformly coloured. Theory of diffusion is based on the hypothesis that the speed of transfer of diffusing material through unit area of a section is proportional to the concentration gradient, expressed as

$$F = -D\frac{\partial C}{\partial x} \tag{1.3.1}$$

where F is the speed of transfer, C is the substance concentration along the distance normal to the section x and D is a diffusion coefficient [21]. Differential equation of diffusion can be than for a one-dimensional gradient of concentration written as

$$\frac{\partial C}{\partial t} = D\frac{\partial^2 C}{\partial x^2} \tag{1.3.2}$$

1.3.2 Diffusion in SHCC

It is well established, that cracked material in general shows lower resistance to diffusion of a substance from environment [86, 56]. From experimental research it is understood,

Table 1.1 Mean apparent diffusion coefficients [16]

Concrete type	Content $[kg/m^3]$	Apparent chloride diffusivity $[\times 10^{-12} m^2/s]$			
		6 months	12 months	18 months	30 months
Portland cement	325	2.67	4.48	8.21	1.82
	400	1.44	2.52	2.04	2.21
Slag cement (75% slag)	325	1.30	1.10	1.01	0.88
	400	1.26	0.77	0.87	0.71
Silica fume	325	0.87	0.72	0.89	0.79
	400	1.06	0.72	0.78	1.00
Natural silica	325	1.28	1.40	1.33	1.62
	400	0.40	0.40	0.31	0.33

that diffusion coefficient through the crack increases with the increasing crack width and becomes almost constant, when the crack width is approximately 80-100microns or more [26, 43, 46]. Some researchers testing different kind of material, such as steel fibre reinforced concrete are reporting, that cracks smaller than 100μm seem to do not affect the permeability [82]. This assumption is probably done based on the seemingly insignificant diffusion difference in between crack width of 50μm and 100μm. It was shown, that aggregates play an important role on chloride diffusion, when embedded in the crack [111] and chloride transport is very rapid along the crack boundary [41]. A different technique to characterise the cracking behaviour using acoustic emission was also developed, that can distinguish matrix cracking and fibre slippage/rupture [75].

For the diffusion analysis, it is the so called apparent diffusivity coefficient used. Difference between the actual and apparent diffusivity is that the latter is the mean value of the actual diffusion over the period of exposure, i.e., from the initial exposure till the final determination of the chloride profile in the structure. Apparent diffusivity coefficients for various types of cementitious materials and exposure duration is in the Table.1.1, also showing how apparent diffusivity can change with respect to time, generally showing declining tendency [16, 24, 109]. Migration of chloride ion under the electric field is presented as a reliable method for determining diffusion coefficient [116].

Apparent diffusivity of a material is depended to concentration of the solution. In

Fig. 1.3.1 Gradient distribution of longitudinal fibrous structure of bamboo [32]

case of CO_2 diffusion, higher concentration causes densification of the surface layer causing reduction of diffusivity [23, 33]. Depth of carbonation in concrete can be determined exactly using thermogravimetric analysis (TGA), x-ray diffraction analysis (XRDA) and FTIR instruments, or conventionally by using phenolphthalein indicator. Depth of colourless region representing the carbonated zone estimated using phenolphthalein indicator is approximately half of what TGA, XRDA or Fourier transform infra-red (FTIR) determines. The pH value around 9.0 indicates the degree of carbonation around 50% and when pH value is around 7.5, it is assumed 100% degree of carbonation [12].

Permeability of cracked compared to sound SHCC, which is similar to that of sound concrete, can be increased by one or two orders, when the strain of 0.2 to 1.0% is applied [115].

1.3.3 Functionally graded material (FGM)

A summary on previous work on diffusion through multi-layer media is given in Appendix A. Layering of SHCC, i.e., creation of FGM, is examined and effect of layers order and composition on cracks distribution caused by mechanical load is observed. FGM is widely observed in natural structures, such as for example the internal structure of bamboo with a gradient distribution of longitudinal fibrous structure, Fig.1.3.1 . It is presumed that, layered SHCC compared to a single layer can further improve durability, due to finer cracks distributed over larger area. Functionally gradient SHCC material can further provide a tool to control the diffusion of chlorides.

1.4 Outline

Diffusion analysis is used to study the functionally graded strain hardening cementitious (FG-SHCC) material and it's possibilities to improve concrete structures durability by

crack control, when applied as a repair material layer. Different kind of SHCC were used to model gradients of various order to resist against chloride penetration, carbonation, salt scaling, and to study the effect on crack formation. Experiments were conducted to test different FG-SHCC to study the tensile bond characteristics in between layers and performance when used as a repair layer on the surface of cracked concrete.

Following this introductory the chapter 1, in the chapter 2, a short description on environmental conditions surrounding structures is discussed. This includes chloride attack, chloride transport and the mechanism of chloride induced corrosion of rebars. Following is the carbonation of concrete and the mechanism of carbonation induced corrosion, salt scaling and the mechanism of salt scaling.

In chapter 3, strain-hardening cementitious composite used as a crack control functionally graded material is studied. The created SHCC material model is compared to available mechanical properties from the literature, and it is used as a base for creating new models with different fracture energy, which are used for the FGM. Materials are applied on a pre-cracked beam as a repair surface layer. Load capacity and the crack pattern of a single layer model determined was compared to the literature test data, and based on the analysis of different kind interfaces, the rigid connection was selected. multi-layer SHCC models, i.e., FG-SHCC is the tested on the same concrete model, where a step-wise linear function of fracture energy distribution is used. Model showed, that using the layer with the lowest fibre content on the surface produce more cracking together with better prevention of crack opening in the pre-cracked beam model. Opposite gradient was beneficial for a higher load capacity and lower amount of surface cracks. Behaviour of this layering was further studied in the chapter 6 by an experiment. Conclusion from the chapter 3 is that layering where the material with the highest fracture energy is on the interface with the pre-cracked beam, the crack width opening is almost as in the homogeneous model.

In chapter 4, diffusion through the different FGM is analysed, presented on three layer material. Step-wise functions are used to approximate linear function distribution, concave function and convex function. Those functions are using different diffusivity ratios from 0.5:1.0:1.5 to 0.3:1.0:1.7 and different layer order. From the analysis results, it can be concluded, that the steepest function gradient offers the best performance and that the concave function show almost the same durability as the linear function,

both utilizing the steepest gradient. FG-SHCC is then studied by using the test data of different SHCC mixtures, and corrosion initiation time at the location of crack is studied. Main conclusion here is that the formed crack highly increase the apparent diffusivity, where penetration can be more than 20-times larger. Reason for different corrosion resistance of mortar and SHCC is then attributed to the width of a crack, causing so called micro-cell corrosion, which rate is smaller compared to macro-cell corrosion of a reinforced concrete or mortar.

In chapter 5, optimization for chloride ion diffusion from the surface through the multi-layer structure of FG-SHCC is performed with consideration of the limitations to the ultimate material local strain at different fibre content SHCC. 6 layers are here assumed and the ideal distribution with given constrains at linear variable strain and constant strain is suggested. Main design limits are here are use of minimum possible fibre content at the interface with old concrete, that would still prevent localization at the given strain and the second limit is using maximum amount of fibres at the surface layer. The linear variable strain distribution showed that for 6 layer FGM, the best quality material is suitable to be used on the surface, and the relatively weakest material layer should be used inside the FGM.

In chapter 6, diffusion of carbonation through the crack in the SHCC is examined whilst using equivalent diffusivity for carbonation. It can be noted, that effect of gradient is reduced with crack opening, and the effect of FGM can be observed as the size of the area between the worst and best material concentration distribution. For the proposed linear relationship between the crack width and material diffusivity, it can be concluded, that layering beneficial for chloride diffusivity resistance is beneficial also against carbonation.

In chapter 7, conclusions obtained in the present study and derived recommendations for future work are presented

Chapter 2

Environmental conditions surrounding structures

In a long term, concrete structures are subjected to the effect of moisture, heat and chemical attack. Main focus here is given to one of the major reasons of deterioration, i.e, chloride attack [3]. Moisture content, on the other hand, from the tensile strength point of view is neglected, as the it is reported to have a very small effect on the split-tensile strength, as in the case of compressive strength [13].

2.1 Chloride attack

Concentration of total salts concentration in seawater varies with temperature, where in colder regions it's lower and higher in warmer seas, especially in shallow coastal areas due to high evaporation rate [1]. Methods to estimate diffusion of chloride ions is presented in Appendix B.

2.1.1 Chloride transport

Penetration of chloride ions into cementitious material is a complex process of ionic diffusion, capillary sorption, dispersion, permeation, etc. The most rapid diffusion is observed in highly saturated structure, where chloride ions enter the material due to gradient in concentration between the exposed surface and inner structure. Total amount of diffused chloride can be divided into free chloride, i.e., dissolved in the solution, and binded chloride, i.e., chloride that chemically or physically bound to cement hydrates, such as C_3A, C_4AF and their hydration products resulting into formation of Fridel's salt. Binding of chloride ions is reducing the apparent diffusivity, as there is less moving ions, thus reducing the amount of free chlorides at the reinforcing steel. It

is only the free chloride causing the reinforcement corrosion [51].

2.2 Mechanism of chloride induced corrosion

Corrosion of steel rebars in concrete is an electro-chemical phenomenon. In sound material, this process is very long, but generally all the structures contain certain amount of cracks, that provides quicker access to chlorides, air and moisture [76]. Because of the tight cracking width, SHCC showed better protection against not only diffusion of chlorides, but also can reduce the corrosion rate due to formation micro-cathodes and micro-anodes, resulting into up to a half to a quarter of corroded material, compared to a cracked mortar [37].

2.3 Carbonation

The penetration of CO_2 is mainly a diffusion phenomenon that depends on concrete quality and exposure conditions, such as the CO_2 concentration and moisture content. Methods to estimate diffusion of chloride ions is presented in Appendix C.

2.3.1 Mechanism of carbonation induced corrosion

Schematic carbonation mechanism is presented in Fig.2.3.1. Highly alkaline nature of concrete with pH values above 12.5 is creating a film of oxide on a reinforcement to prevent corrosion initiation. When carbon dioxide from the environment penetrates into concrete, the alkaline environment is being neutralized, and when the pH value become less than 11, corrosion of the steel rebar can be initiated [73, 72, 58].

2.4 Salt scaling

Salt scaling is one of the major durability issues of concrete causing material surface degradation by gradual spalling off of a thin layers of the material, compared to ordinary freeze-thaw cycles of the material, that causes degradation of material in bulk [89, 83, 84, 74]. It is reported, that mechanically loaded engineered cementitious composites have almost 10times higher resistance to scaling, i.e., 10times lower mass of scaled-off

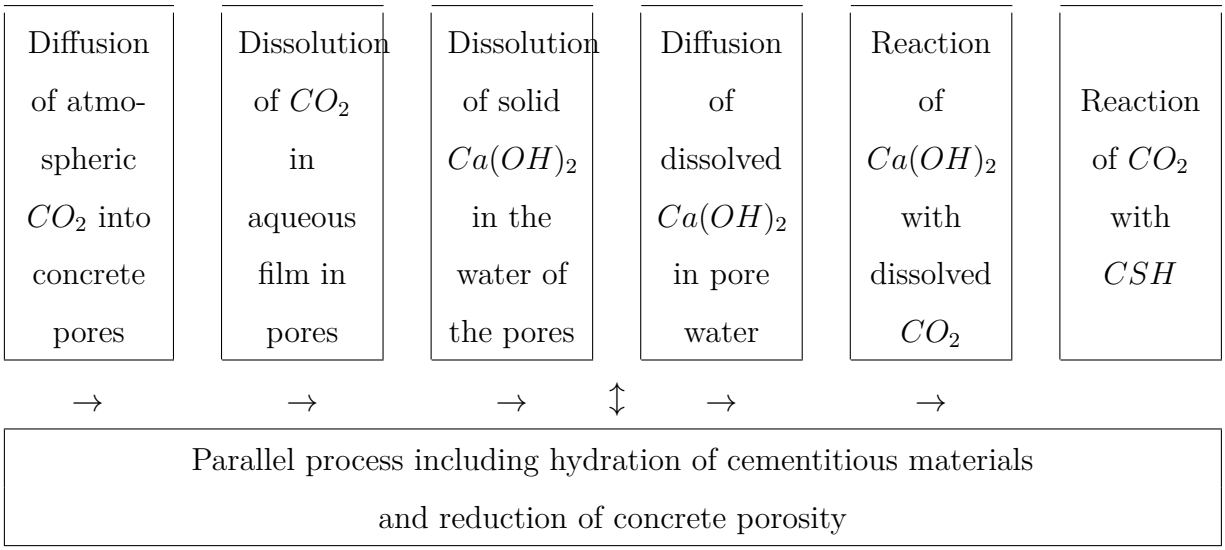

Fig. 2.3.1 Physico-chemical process of concrete carbonation

material [85]. The damage is increased when the minimum temperature of the thermal cycle is lower than -10 degrees. Next, it was showed, that increase in damage is larger for temperature reduced from $-16°C$ to $-18°C$ then for reduction from $-11°C$ to $-13°C$ [95]. Freezing of SHCC with higher W/B ratio and hydrophilic fibres reduces it's ductility [112]. Salt scaling resistance is increased when using air entrained agents, lower water to binder ratio, or Portland cement without pozzolanic or latent hydraulic additions [34, 69, 98, 60], although some researchers are pointing out, that by adding minerals, such as fly ash or ground-granulated blast-furnace slag can reduce chloride ingress due to slightly denser pore structure [14]. This discrepancy might be attributed to the effect of curing, because cement materials with latent hydraulic components require longer time for hydration.

2.4.1 Mechanism of salt scaling

Mechanism of salt scaling was addressed by many researchers (Powers 1965, Hansen 1963, Snyder 1965, Harnic 1980, Binbin 1988, Star and Ludwig 1997, and Valenza and Scherer 2004). Salt scaling in proposed theories is explained by various mechanisms, such as combined effect of hydraulic and osmotic pressures, dilation pressure due to salt crystal growth, concentration gradient through the depth of concrete, thermal shock from application of de-icing agents, decrease of resistance of material against the frost salt attack due to chemical reaction, and a mechanism referred to as "glue spall"

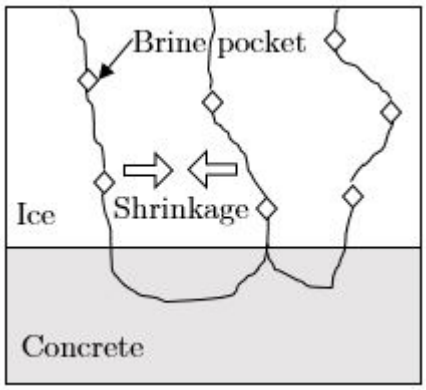

Fig. 2.4.1 Scheme of frost salt scaling mechanism

explaining the mechanism by stress from ice acting upon a concrete surface. Glue-spall mechanism amongst others is the one mostly accepted, but even though being able to explain the pessium salt concentration, the theory cannot account for beneficial effect of air entrainment.[18, 19, 95, 96, 97, 50]

According to a theory based on "glue-spall" mechanism, de-icing salts are entrapped in the freezing salt solution layer on top of the surface. This creates weak pockets inside the ice ice layer and depending on the salt concentration, cracking of the brine causes salt scaling due to the layer shrinking. Depending on solution concentration, three possible outcomes are to expect. First, if the concentration is less than 0.1%, ice layer doesn't crack and so no scaling occurs. Second, when the solution reaches pessium concentration, i.e., 1-3% independent of the type of solute, tensile stress exceeds the tensile strength of ice and initiate the surface scaling. Third option is when the solution concentration is 10-20%, the ice layer become too soft to exert enough stress to the surface layer and scaling does not occurs. Also, no scaling occurs, when the pool of a solution is not present on the surface [18, 19, 95, 96, 97, 50]. Effect of salt scaling is modelled by reduction of the analysis thickness domain with more details in Appendix D.

2.5 Durability of concrete structures

2.5.1 General

Durability is by standard ISO-13823 defined as the "capability of a structure or any component to satisfy, with planned maintenance, the design performance requirements over a specified period of time under the influence of the environmental actions, or as a result of a self-ageing process". Concrete is due to it's low cost and high durability the most widely used structural material. Many of those structures are build in areas with highly aggressive environment, such as seashore or freezing areas where salt is applied, where unsatisfactory durability is observed [72, 71]. Deterioration of concrete structures usually comes from chemical changes to the cover layer caused by attack of acids, salts, carbon dioxide, alkali-aggregate reactions, freezing and thawing cycles, etc. [57]. Effect of the combined attack is reviewed in Appendix E.

2.5.2 Material related durability

Durability is usually treated by selection of suitable material. Key material parameter for not only durability is water to cement ratio; the lower the ratio, the higher durability is expected. Example on how w/c and relative humidity affect carbonation penetration is shown in Fig.2.5.1. Concrete chemical resistance is then determined by the type of cement and other mix constituents, concrete mix proportions and compaction and curing. All these factors are affecting porosity of concrete [57, 101, 66, 71, 78].

2.5.3 Structure related durability

Cracking of concrete structures is inevitable, leading to reduced durability by increased diffusion of aggressive agents, but it is important to understand the different source of cracking. Cracking in concrete can occur from very early age, when concrete is still plastic due to settlement or crazing. Overview of type of cracking, their primary cause and location is given in Table 2.1 .

Table 2.1 Types of cracks

Type of cracking	Subdivision	Common location	Primary cause
Plastic settlement	Over reinforcement	Deep sections	Excess bleeding
	Arching	Top of columns	
	Change of depth	Trough and waffle slabs	
Plastic shrinkage	Diagonal	Pavements and slabs	Rapid early drying
	Random	Reinforced concrete slabs	
	Over reinforcement	Reinforced concrete slabs	Rapid early drying or steel near surface
Early thermal contraction	External restraint	Thick walls	Excess heat generation
	Internal restraint	Thick slabs	Excess temperature gradients
Long-term drying shrinkage		Thin slabs and walls	Inefficient joints
Crazing	Against form-work	Walls	Impermeable formwork
	Floated concrete	Slabs	Over-trowelling

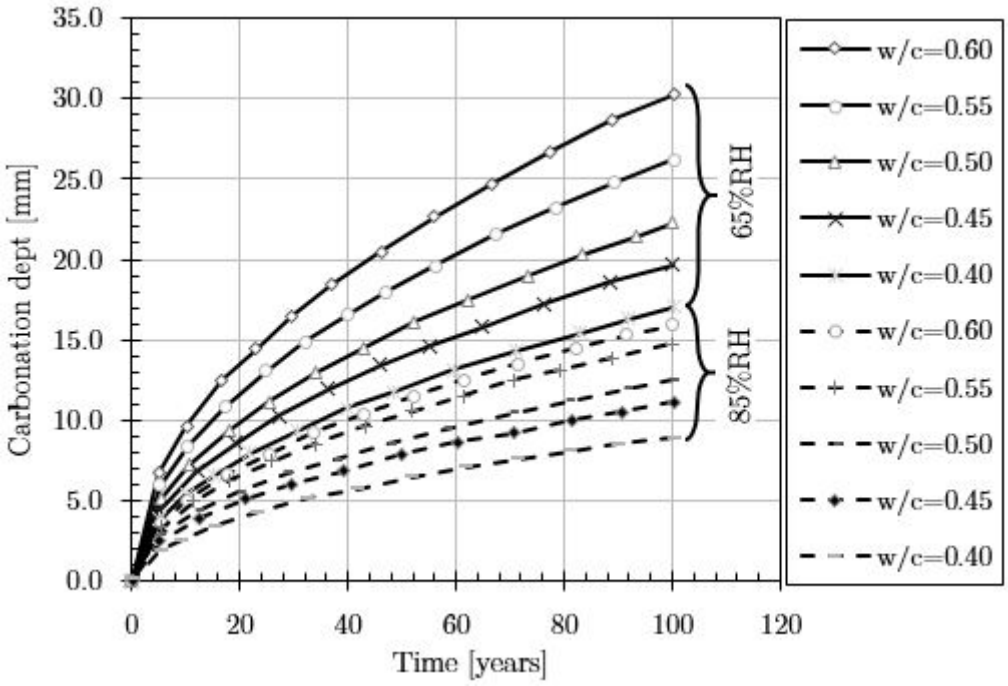

Fig. 2.5.1 Carbonation depth for different w/c and relative humidity

Chapter 3

FG-SHCC multi-layer structure with constant gradient for crack width control and chloride diffusion resistance

Strain hardening cementitious composite (SHCC) material used as external layers on plain concrete specimen as the only reinforcement is considered in this study. By layering, one can create functionally gradient material (FGM) to control crack spacing, localization and opening. As a variable function in this study fracture energy and effect on distribution of layers are examined. Compared to ordinary RC cracks, formation of micro-cracks increases resistance to moisture, gas and salt penetration, the key for cement-based materials durability. This numerical study uses finite element method (FEM) software, with material model tailored to available SHCC mixture test results. SHCC material model was designed through numerical uniaxial tensile testing, followed by a bending test of a two-layer material composed of one layer of plain concrete and one layer of SHCC. FGM is then created by layering the SHCC of various fracture energy and the obtained crack formation is studied.

Strain hardening cementitious composites (SHCC) is a type of fibre-reinforced cement-based material. Tensile strength is generally achieving range of $3 - 8$MPa with pseudo strain-hardening tensile behaviour and ultra-ductility (up to and beyond 3% of tensile strain) caused by fibres bridging cracks. SHCC can form multiple, closely spaced cracks of narrow crack widths, generally below 100μm, as shown in stress strain diagram in Fig. 3.0.1.

Damage of cement based materials is accredited to moisture, salts and gas penetration and their combination. Crack width control is a proven method in RC design standards and codes, with suggested critical values for different environmental condi-

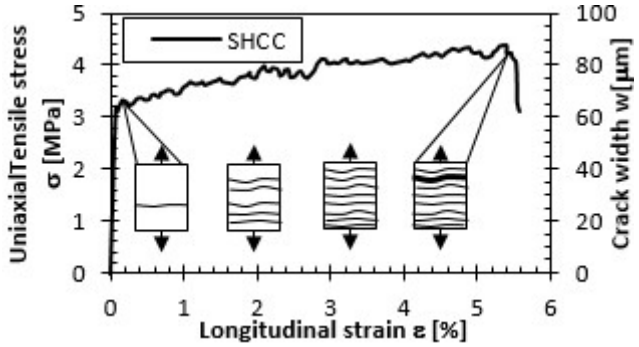

Fig. 3.0.1 Stress-strain response of SHCC [101]

tions, as in Table 3.1. SHCC offers a strong potential for higher durability structures due to its pseudo strain-hardening nature and increasing load capacity.

Micro-cracks afford these materials the potential for self-healing, indicating their ability to recover it's properties, such as mechanical (strength, stiffness and ductility) and transport (chloride ingress, carbonation)[101].

Reduced penetration depth of SHCC versus reinforced mortar/concrete was observed in a comparative flexure test of the same deflection. The apparent diffusion coefficient of SHCC is reported as linearly proportional to the number of cracks, whereas the coefficient of reinforced mortar is related to the square of the crack width [101]. SHCC can be further used in combination with ordinary steel rebars, for better load capacity. The crack width of SHCC is thought to be an intrinsic material property, independent on a steel reinforcement, contrasting to ordinary reinforced concrete structures, where crack width is highly depended on the steel reinforcement ratio.

Foremost effect on the required mesomechanical behaviour, like formation of multiple fine cracks, has the fibre-matrix interfacial bond characteristics at micro-scale level. By investigation of the chloride exposure effect on various micro-mechanical parameters of SHCC, tests revealed that cycles of exposure to chlorides and drying significantly reduce the chemical bond strength, while frictional bond showed a slight increase. This phenomenon is due to decreased local elastic modulus on the interface transition zone (ITZ) of fibre and matrix. Stable value is gradually reached at about 30μm from the fibre. This effect is attributed to increased matrix porosity of the ITZ near the fibre surface. Initiation of finely spaced cracks from matrix imperfections is controlled by matrix fracture toughness, which has been reported as almost unaffected by chloride treatment, when tested of 3-point bending notched beams.[101].

Table 3.1 Allowable crack width in RC structures for durability [101]

Exposure condition	Allowable crack width [mm]
ACI 224R, 90	
Dry air or protective membrane	0.41
Humidity, moist air, soil	0.30
De-icing chemicals	0.18
Seawater and seawater spray, wetting and drying	0.25
Water retaining	0.10
ACI 318-89	
Interior	0.41
Exterior	0.33
ACI 350R-89	
Normal	0.27
Severe	0.22
CEB/FIP Model Code 1990	
Humid, deicing agents, seawater	0.30

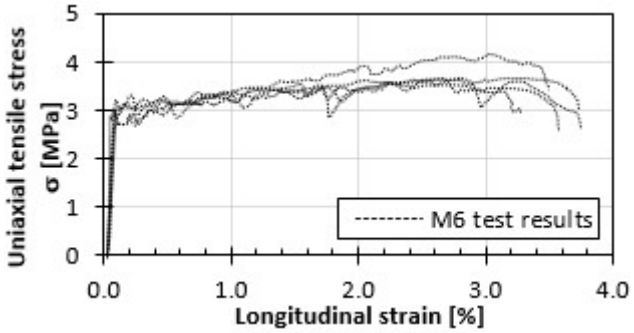

Fig. 3.1.1 Stress-strain curves of mix M6 with average tensile strain capacity of 3.3% [61]

3.1 SHCC material model

For the numerical analysis, mixture M6 [61] was selected as a SHCC material, Fig. 3.1.1. Specimen with dimensions of $15x5x60$mm has ultimate tensile stress of 4MPa at 3.3% of strain and 3MPa first cracking strength. M6 contains by volume 2% of PVA fibres and blast furnace slag to portland cement ratio of 2.32. This mixture shows very tight crack width of 57μm[113]), measured at load level after the tensile test.

A detail description of crack width calculation is presented in Appendix B.As a FEM model of M6, non-linear fracture–plastic constitutive rotational crack model was selected [10, 9], which allows to define history evolution laws for selected material parameters, such as Young's modulus, tensile and compressive strength. Fully rotational crack model is used, because direction of the principal stress coincides with the direction of the principal strain. The material model *CC3DNonLinCementitious2User* [10] provides user defined laws for selected material laws, such as: diagram for tensile and softening behaviour, shear retention factor and the effect of lateral compression on tensile strength. Apart from other parameters, the most important one to define was function for tension behaviour after cracking, that is behaviour of SHCC and crack opening localization strain, see Fig. 3.1.2, where σ_t' is tensile stress and f_t' is tensile strength.

In Fig. 3.1.3, cracked FE model used for tensile test of SHCC is presented. Model is simply supported on left edge, with applied displacement on right edge through steel plate, Fig.3.1.4. SHCC specimen for the analysis has identical dimensions as the test data (15x5x60mm). Load is applied in small steps incrementally, with step size of 1.2×10^{-5}m. Magnified detail in Fig. 3.1.3 shows 5 deformed elements in x

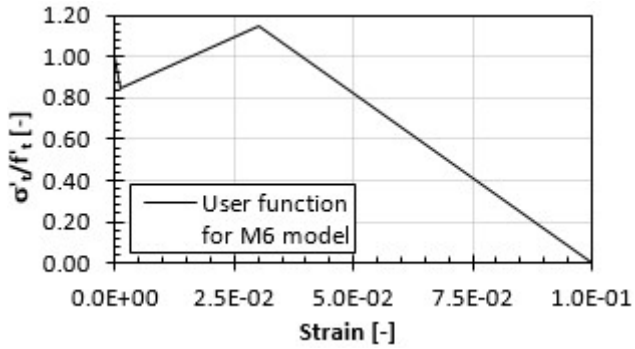

Fig. 3.1.2 Tension function for material mix M6 [10]

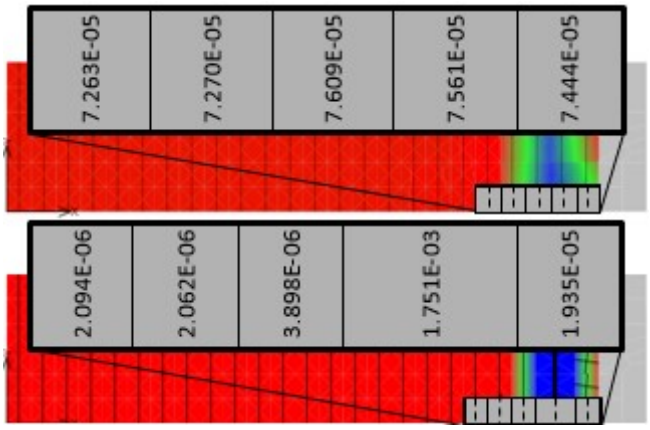

Fig. 3.1.3 Calculated crack width: (top) before localization, (bottom) after localization (Unit: m)

direction affected by crack localization with respective crack width. Crack in tension is represented by discrete failure plane in the finite element analysis. The crack width is calculated as $w = \epsilon_{cr} L_t^{'}$, where ϵ_{cr} is the crack opening strain and $L_t^{'}$ is the failure band for tension. Calculation of crack width is described more in detail in Appendix F.

The meshing size was selected with respect to computational efficiency and possible representing of number of cracks on the element body. In open cracks, stress is trans-

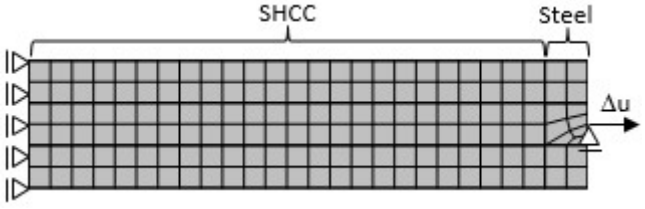

Fig. 3.1.4 FEM mesh for tensile test with boundary conditions.

mitted only by fibres. Stress is gradually redistributed to the matrix, with zero value at the crack edge, increasing with the distance from the crack. In certain distance from crack, the condition for matrix cracking may not be fulfilled, therefore cracks must maintain certain minimum spacing x, to ensure that the condition for matrix cracking is satisfied. To ensure that the crack spacing does not become less than x, presented analysis utilises regular meshes with finite element size equal to approximately $2x$, noting that the 4-noded quadrilateral element employed may accommodate a maximum of two semi-parallel cracks [48]. Average crack spacing is $2 - 7$mm at about 3% strain [100]. In this model, mesh size is 2.5×2.5mm. To avoid possible mesh dependency in results, this meshing size is used for all analysis in this study.

When the prescribed displacement was applied on the model, cracks were immediately formed over the whole area of the model and linearly opened until the failure. This is in contradiction with the behaviour of SHCC, having gradual formation of cracks with certain limiting minimum and maximum values of crack width in given strain rates, Fig. 3.1.5. At ultimate strain SHCC model of M6 material, further declared as material "N", shows crack localization with crack opening in the order of millimetres. Cracks outside the localization area are reduced by the value of elastic strain which is caused by stress release in area of the localization, Fig. 3.1.3. Right before localization, the model shows equal crack width over all domain, ranging from 72.6μm up to 75.8μm, which is within the range of SHCC expected behaviour. Due to the linear formation of those cracks during the loading, one cannot consider the crack width as a representation of real behaviour without further improving the model with more data on crack formation. In this analysis, the area of cracked elements and relative ratio of crack width will be used as a comparison tool alongside with crack opening on surface and in the SHCC.

Other SHCC models, presented in Table 3.2 have been scaled from N, here f_t represents tensile and f_c compressive strength of the material. Model H, having approximately 150% of the N fracture energy, and model L, having 50%. Apart from different load capacity, models also have altered ultimate strain. This has been done to allow different crack localization in tensile test of FGM model, where three different material layers are utilised.

All created models are presented in tensile stress-strain curves in Fig. 3.1.6. Model

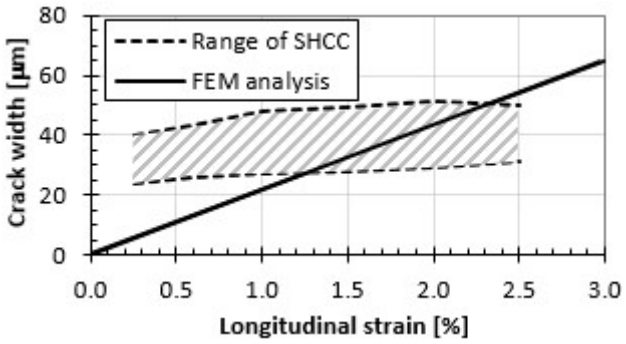

Fig. 3.1.5 Range of crack width in SHCC compared to FEM analysis [68]

Table 3.2 SHCC material parameters in FEM vs test data

Material	E [GPa]	f_t [MPa]	f_c[MPa]
Test data			
Matrix N	20	3.5	-10f_t
Fibres	40	1640	-f_t
FEM input data[*)]			
Model N from tensile test	20	3.5	-10f_t
Model H derived from N	25	4.5	-10f_t
Model L derived from N	20	2.5	-10f_t
[*)]Effect of fibre defined by user tension function			

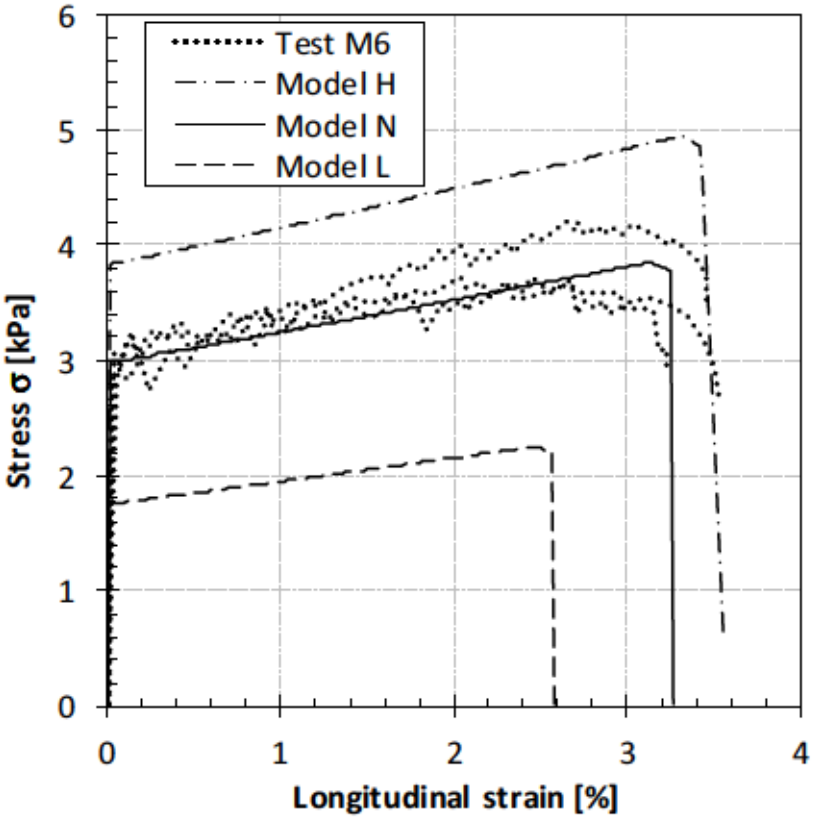

Fig. 3.1.6 Tensile stress–strain plots of SHCC

N is represented by a solid line and is compared to the N test data, which is represented by a dotted line. All represented models are used in the following analysis.

Drying shrinkage of SHCC, which is depended on cement type, is not modelled. Restrained drying shrinkage can cause up to $30-50\mu m$ crack width at 50% of relative humidity. This can be treated by use of low alkali cement, which can reduce free shrinkage by 5% and 30% lower crack width [106].

3.2 Beam test with one SHCC layer

In this section, beam test model is discussed. One of the first things to determine was the material properties of the plain concrete layer. Specified input values such as Young's modulus, tensile strength and compressive strength for the model are identical to the matrix material of SHCC. Fracture energy of this model then has to be adjusted for representation of the test data. As observed, fracture energy of base concrete affects behaviour mainly after the peak load, with maximum load relatively identical.

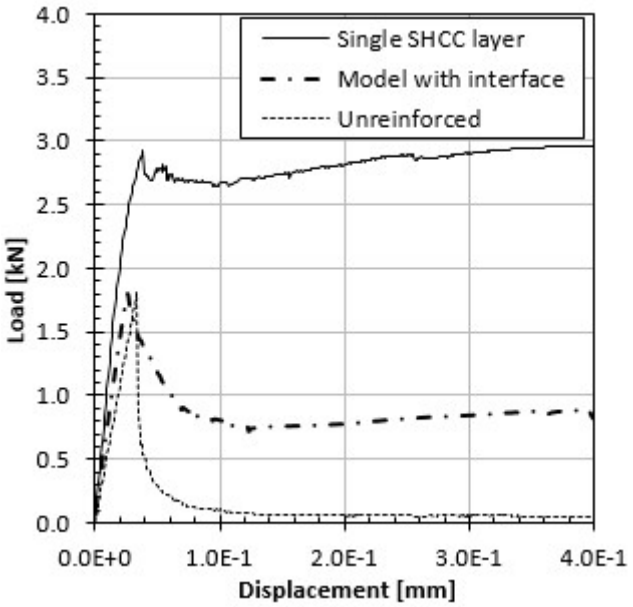

Fig. 3.2.1 Bending load-displacement plots of SHCC

Next, behaviour of the interface between the concrete and SHCC layer, as well as interface between each layers of SHCC has to be determined. For this purpose, a model with interface was created. Interface parameters have been determined based on manual recommendation [10]. The following parameters have been specified: initial stiffness per unit width of the interface in tangential and normal direction as $(Ec/t) * 1000$; tensile strength as up to 50% of concrete tensile strength; and cohesion set to 2 times the interface tensile value. Here, E_c represents Young's modulus of the weaker interface materials and t represents thickness of the interface. Thickness is set to minimum value of 0.1mm to represent direct contact of each layers. Model with such interface properties has been analysed, and force-displacement is recorded in Fig.3.2.1. Interface model values represent the stiffest interface in current case possible, as further improvement on interface tensile strength would reach or exceed the tensile strength of weaker joined material, which has from modelling point of view no justification and therefore perfect bond model is preferred. Crack pattern from interface test are presented in Fig. 3.2.2, a slip along the interface can be observed in the analysis. Experimental data does not show such a shear slip along the interface, so the perfect bond model is more favourable to use. This perfect bond is supported by the experimental testing of the beam with the SHCC layer in Appendix G.

In real life application, the interface of concrete and SHCC is treated with excellent

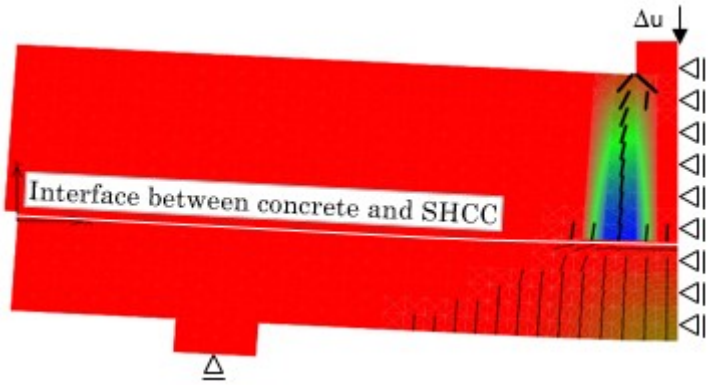

Fig. 3.2.2 Crack pattern of tested beam with defined interface between SHCC and concrete. ($\Delta u = 3.0 \times 10^{-4} m$)

primer and other surface preparation techniques. Scaling of different SHCC layers can be avoided by continuous preparation. It is of every manufacturer's interest to create perfect bonding conditions. In further analysis from above mentioned reasons used is only the perfect bond in between each layers of SHCC, as well as for interface between concrete and SHCC. Perfect bond crack model compared with test data [61] in white cracks is presented on Fig. 3.2.3, where a) shows all cracks in model and b) shows only cracks larger than 20μm, as they are not expected to be visible in real test. White frame represents frame of photo in referred paper [61].

The effect of using SHCC as reinforcing layer is observed when compared with unreinforced plain concrete model (Fig.3.2.4) of identical thickness such as the model containing SHCC. Compared to concrete reinforced by SHCC layer, model fails due to opening one crack in the middle of the span.

3.3 Multi-layer SHCC models

Single layer model of SHCC on three-point bending test (Fig. 3.2.3) showed good agreement with compared test data in peak load obtained from crack opening (COM) test [61], see Table 3.3. At this point, SHCC material model N can be used with two other different models extrapolated from N in various order for studying the effect of variable fracture energy on crack formation, expected crack branching behaviour is shown on Fig.3.3.1. SHCC formed in layers with various fracture energy is used to create FG-SHCC (Functionally Gradient Strain Hardening Cementitious Composite).

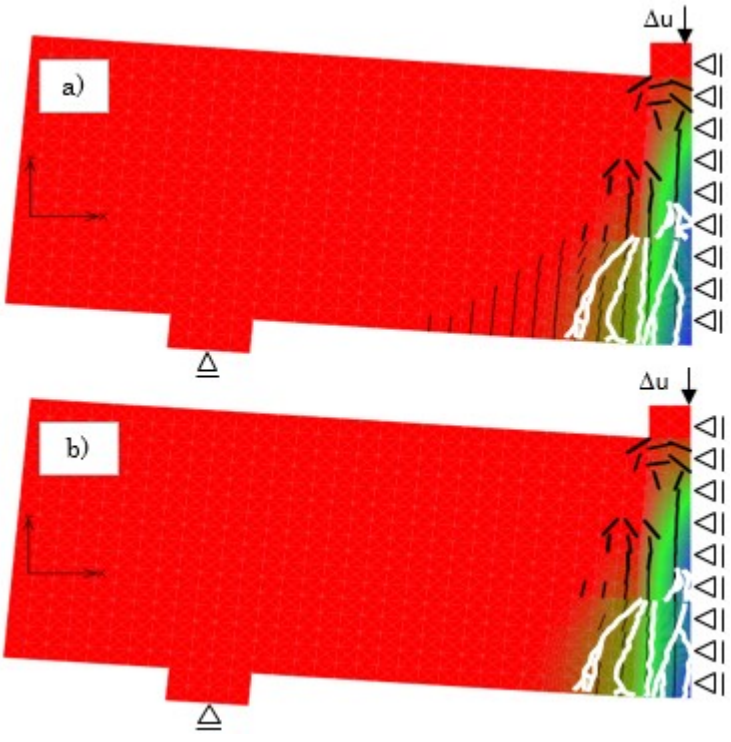

Default

Fig. 3.2.3 Crack pattern of tested beam with test data [61] in white frame a)No crack width limit; b)20μm crack width lower limit. Cracks in SHCC in black line are wider than 20μm.($\Delta u = 3.0 \times 10^{-4} m$)

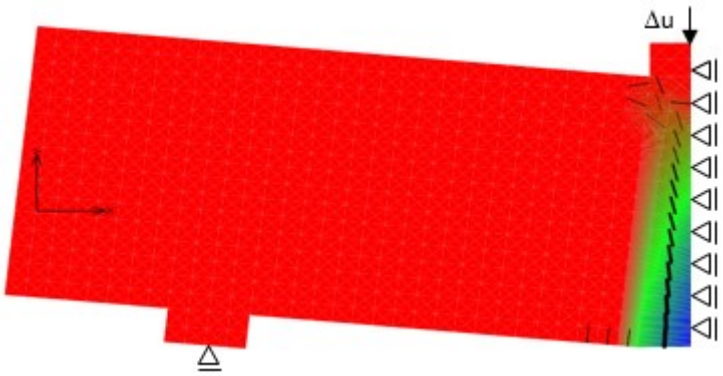

Fig. 3.2.4 Crack pattern on tested beam without reinforcing SHCC layer. ($\Delta u = 3.0 \times 10^{-4} m$)

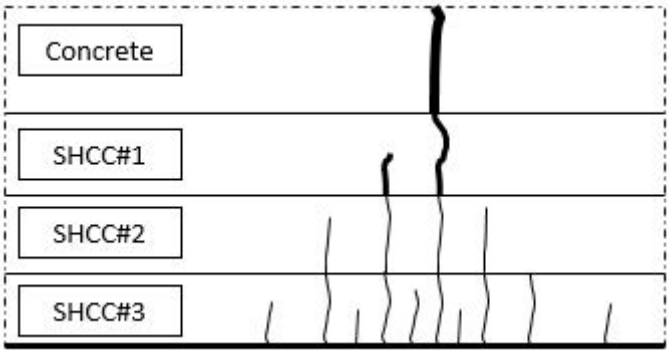

Fig. 3.3.1 Crack redistribution in layered material

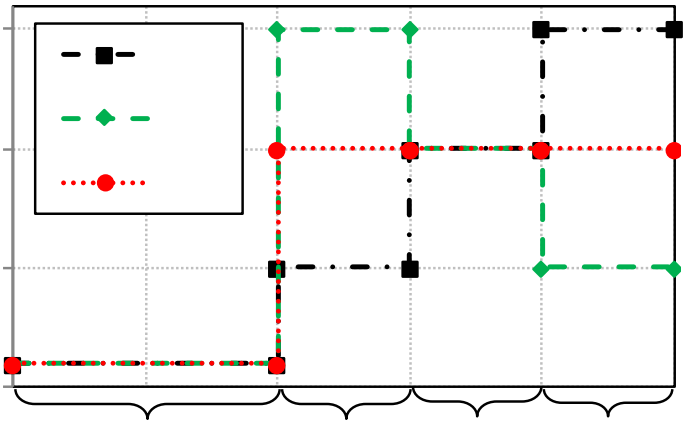

Fig. 3.3.2 Stepwise linear fracture energy distribution schemes

Change of function is represented by stepwise linear function, as a representation of stepwise quadratic function of expected real distribution, selected for simple approach, Fig.3.3.2. In concrete layer, homogeneous fracture energy distribution is assumed.

FG-SHCC is applied in 3 layers of total thickness of 15mm. This value is selected as the smallest value (lower bound), especially from the fabrication point of view. FG-SHCC of large thickness (upper bound) is tested in later Chapters 4 and 6.

For the multi-layer simulation, concrete material parameters are identical to one layer SHCC. N material model is also used unchanged, completed with new SHCC models of different fracture energies, as well as maximum load capacity, first cracking strength and total strain. Pseudo strain hardening remains identical in between various models.

All test results are compared to original homogeneous, i.e. one layer SHCC to study

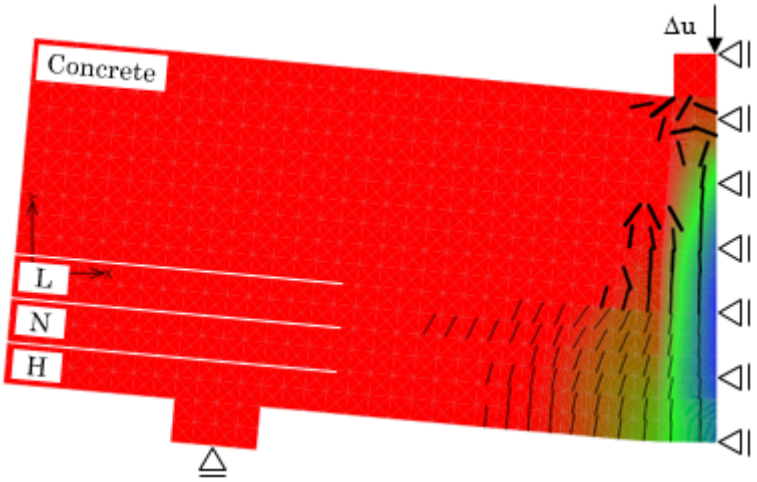

Fig. 3.3.3 Bending test crack distribution for layers LNH. ($\Delta u = 3.0x10^{-4}m$)

the effect of FGM on crack formation.

For layer LNH, Fig.3.3.3, peak loads and maximum displacements are showing similar behaviour to that of single layer compared to multi-layer. FGM shows increase of only 1.6% in load capacity and 2.2% in maximum displacement. One can compare obtained results in the manner of crack affected area, assuming that larger area of cracks can be understood as smaller crack width and smaller affected area predicts larger width of cracks. This effect is due to different energy dissipation. Softer layer L1 placed directly in contact with concrete, having only 50% of fracture energy of layer N, works as a cushion for localized stress from a crack opened in plain concrete.

In case of opposite order of the layers to HNL, Fig. 3.3.4, FGM shows 7.1% of reduction on maximum load capacity, but the overall cracked area is larger, see Table 3.3. This is due to location of the layer with highest fracture energy closer to the centre of the specimen. Order of this layer is studied to see the effect of layers order.

3.3.1 Application of multi-layer SHCC

From the SHCC application point of view, SHCC layer should be acting in tension, without effect of bending or shear, same as in the case of previous tests. In presented models, ratio of SHCC layer to concrete layer is 37.5% of SHCC and 62.5% of concrete layer thickness. In ordinary applications of SHCC, the repair layer can, at the most, form around 10% of the structure thickness, or less. In case of application on a slab, one can assume that SHCC will act in tension only, with negligible contribution of

Table 3.3 Bending test results at equal displacement

	Test [61]	Models		
	M6	NNN	HNL	LNH
Centre deflection [m]	Not measured	0.0004	0.00034	0.00034
Load at first cracking [kN]	2.80 - 3.25	2.90	2.49	2.66
Surface crack opening [μm]	Not measured	206.67	211.70	206.31
Largest crack [μm]	Not measured	60.56	63.15	61.34
Cracked SHCC area [mm^2]	Not measured	3250.0	4062.5	3625.0
FGM Gradient type [-]	—	—	Negative	Positive
Function gradient [N/m]	—	—	1	1
Peak load [kN]	2.80 - 3.25	2.96	2.78	2.99

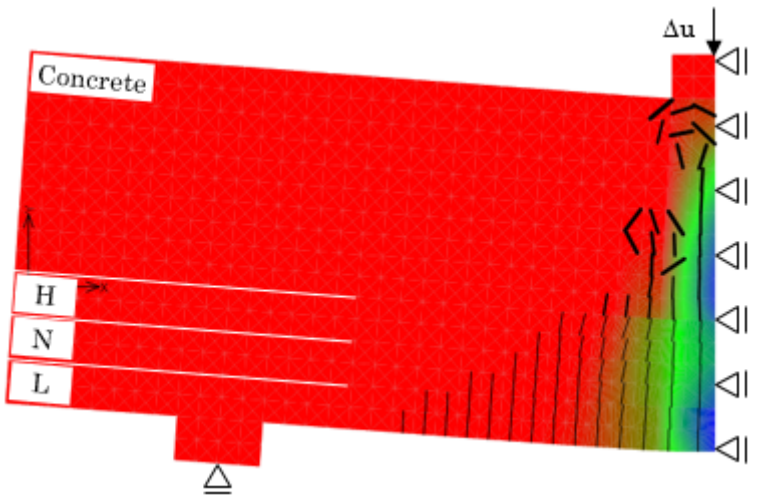

Fig. 3.3.4 Bending test crack distribution for layers HNL.

shear or bending.

3.3.2 Tensile test of multi-layer SHCC

For this reason, identical specimen was loaded in pure tension. To initiate the cracking at given location, concrete layer contains simulated crack modelled by reducing the out of plane thickness. Displacement is introduced directly in the model on the line, to exclude effects of restriction caused by the plate that is to simulate centre part of longer specimen, where pure tension is imagined. To capture the resulting load, summation of reactions over the load area has to be performed. Crack patterns for different layer orders are presented on Fig. 3.3.5. Compared to homogeneous layer, FGM shows larger cracked area, mainly in the weaker layer. This shows possibility of smearing the cracks over larger area, with smaller crack width. Crack widths are further compared in next section.

Goal of this simulation is to observe crack propagation from initiated place in concrete layer into SHCC layers and observe effect of different fracture energy of each layer. As a base comparing model, homogeneous SHCC layer consisting of N material is modelled. Results from tension tests are presented in Fig.3.3.6 and Fig.3.3.7 as a function of crack width normalised by applied force in respective location. FGM shows almost the same horizontal crack width distribution along the bottom surface as the uniform material, see Fig.3.3.8.

3.4 Crack formation results of SHCC FGM

In the bending test, reduced load capacity after the peak load in case of layer order HNL is prominent, Fig.3.4.1. Compared crack formation of layering LNH, Fig.3.3.3 and single layer N, Fig.3.2.3 one can see larger cracked area mainly in layer close to the interface-L1. Crack affected area is 11% larger for the layering, identical displacement, but at 9% lower load.

Bending test does not show benefits for layering of SHCC, as can be seen on crack width in Fig.3.4.2. Vertical axes represent crack width denominated by acting load in the SHCC, from interface to surface. Layer LNH, i.e. L1 close to the interface, shows from 0.1mm displacement faster softening, Fig.3.4.3. That is attributed to the fact,

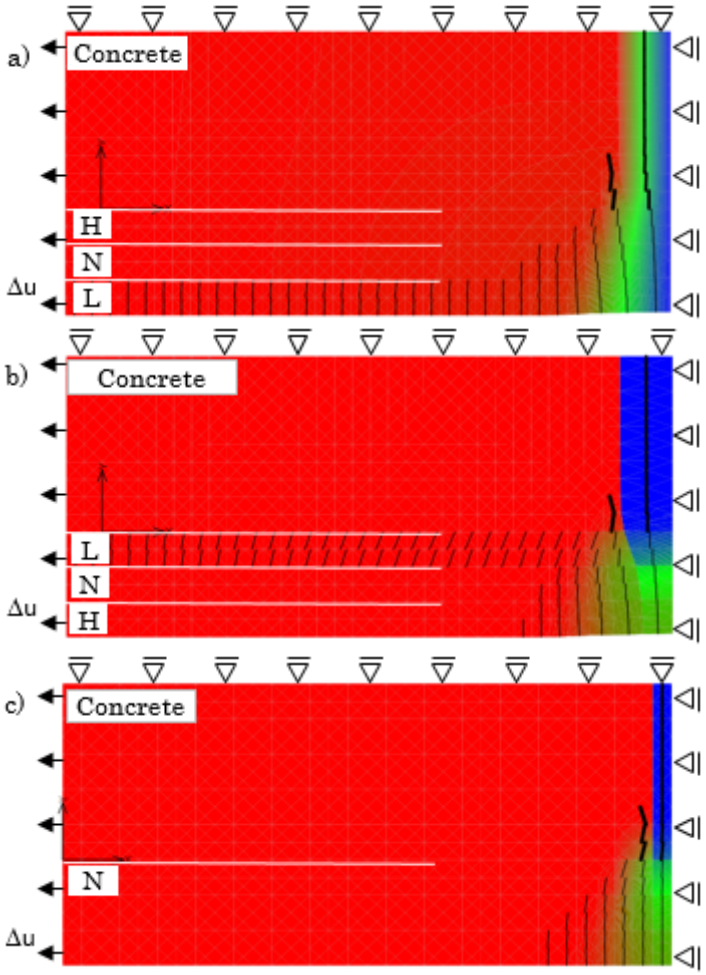

Fig. 3.3.5 Tension test crack distribution in a) HNL, b) LNH, c) N. ($\Delta u = 3.5 \times 10^{-4} m$)

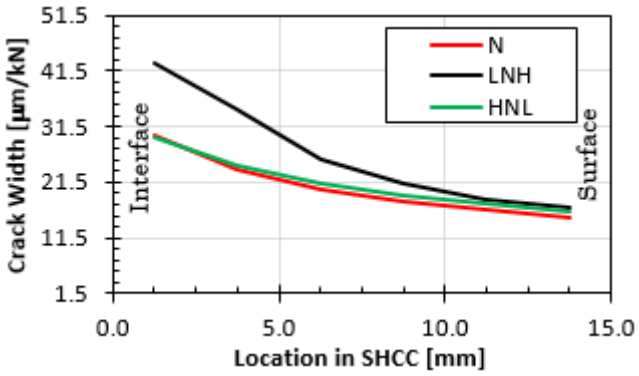

Fig. 3.3.6 Crack width in SHCC from tension test

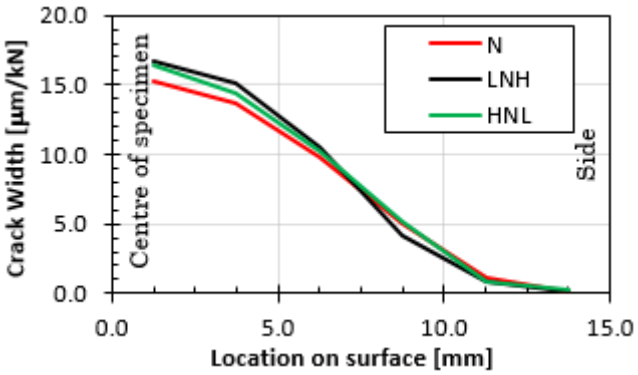

Fig. 3.3.7 Crack width on surface from tension test

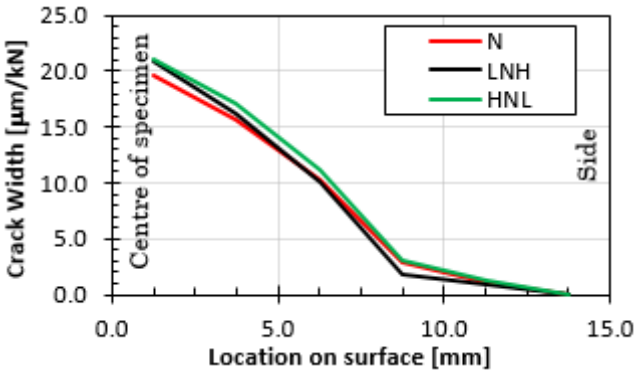

Fig. 3.3.8 Crack width on surface from bending test

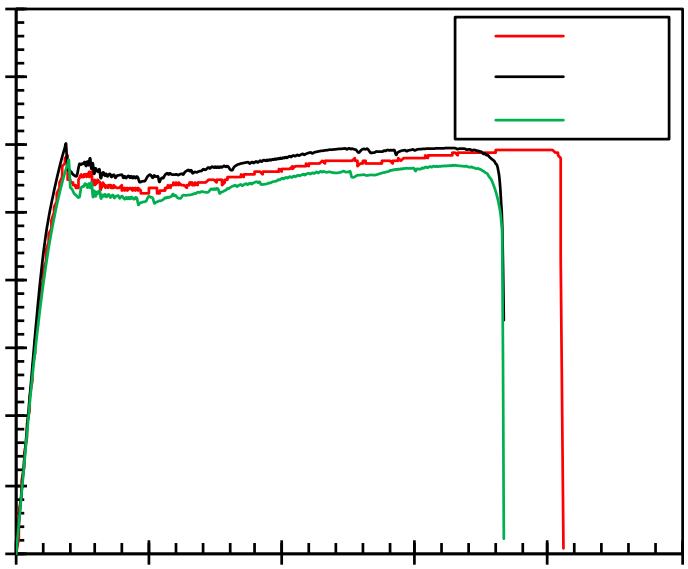

Fig. 3.4.1 Load-displacement curves for different layering in bending model

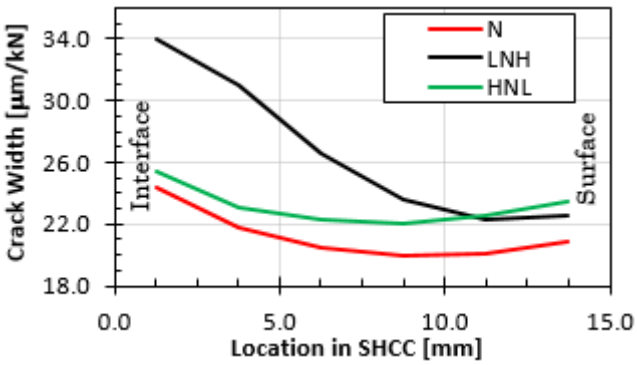

Fig. 3.4.2 Crack opening in SHCC from bending test

that weak layer L1 was not able to sustain the same load on the interface as layer E1. That caused cracking the whole L1 layer and early strain localization, with large crack width in all SHCC, see Fig.3.3.6. FGM materials shows almost the same horizontal crack width distribution along the bottom surface as the uniform material, see Figs. 3.3.7, 3.3.8. FGM with negative function gradient shows smaller vertical crack width distribution along the centre line of specimen, see Figs.3.3.6, 3.4.2. The above facts in bending and uniaxial tension implies the possibility of material use optimization to get improvement of durability of concrete structures.

3.5 Analytical study on functionally gradient strain-hardening cementitious composite for high durability

A method to improve the durability is investigated analytically for the case where SHCC is used as a functionally gradient repair material. The SHCC part is divided into multiple layers and the material properties of each layer are set functionally gradient. Then, it has been shown that the time needed for corrosion initiation can become longer depending on the selection of material properties of each layer. Also, the influence of crack width of the SHCC part is clarified.

Strain hardening cementitious composite (SHCC) material used as a repair material on reinforced concrete structures for protection against environment exposure is considered in this study. By layering different SHCC mixtures, one can create functionally gradient material (FGM) to control crack spacing, localization and opening. FGM is

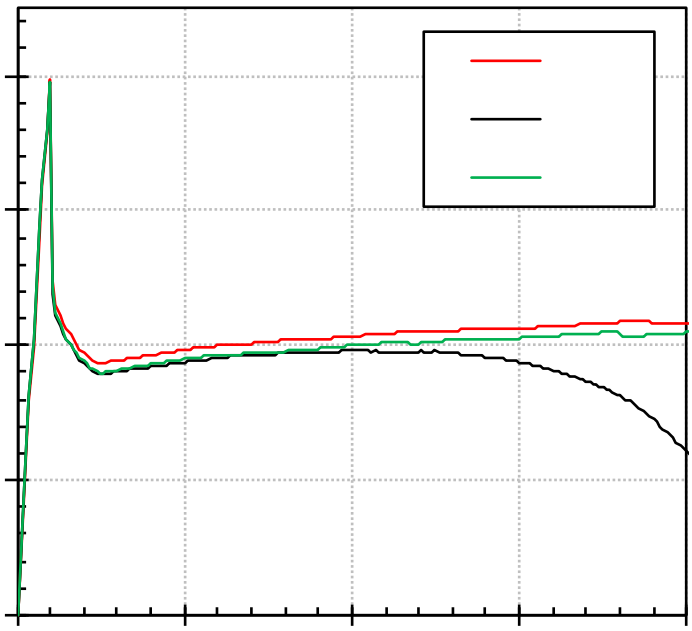

Fig. 3.4.3 Tension test load-displacement curves for different layering

described as a material property variation in structure changed gradually over volume. Compared to cracks in ordinary RC, formation of micro-cracks increases resistance to moisture, gas and salt penetration, the key to cement-based material durability. Another benefit of fine crack width in SHCC is its ability for intrinsic self-healing, recovering transport and mechanical properties.

Transport of chloride ions through the cementitious material using the pore liquid as a medium is usually described with Fick's 1st law equation, i.e., the flux of diffusing substance (e.g., chloride ions) is proportional to the gradient of the distribution of the diffusing substance. The proportional coefficient is called diffusion coefficient.

Penetrability and transport properties, i.e., diffusion of chloride ions in the pore liquid and convection of chloride ions in the pore liquid by liquid transport are retarded by the chloride binding to the cement gel. Another significant influence on the binding capacity of the chloride solution has the chemical composition [6]. The use of $CaCl_2$ instead of $NaCl$ increases the amount of bound chlorides [25]. Furthermore, the diffusion coefficient depends on the hydration level and the pore humidity RH of the pore system. Presented analysis of FG-SHCC (Functionally Gradient SHCC) uses diffusion coefficients of the unfavourable conditions, where material is subjected to cycling wet-

ting and drying conditions, i.e., full pore saturation or dry material causing negligible diffusion of chloride is not considered. Cycling of wetting and drying is unfavourable, because this cause deeper penetration of salts into the material. Some researchers pointed out, that during test of chloride diffusion into SHCC salts are collected on the other face of specimen [108]. This is a case of thin samples and it is not expected in this analysis, because the concrete slab is thicker and evaporation from unexposed surface is negligible.

Goal of this analysis is to inspect possible durability improvement by layering SHCC of different material properties. Layered material is usually found in nature as the most efficient material distribution. Firstly, this idea should be confirmed by analysis of sound SHCC with constant layer thickness, as the most basic concept and find the ideal material distribution whilst using available SHCC mixtures. When this concept is proven to be working and ideal distribution is found, effect of cracks from mechanical loading must be understood and estimated durability is presented.

3.6 Diffusion of chlorides in FG-SHCC without cracks

In the following diffusion analysis, diffusivity of the place with the largest crack is examined. The mesh size and time step size is selected so the result of the analysis is close to the known semi-infinite solution [21]. For diffusion analysis, the space-time finite element method is applied with a Crank-Nicolson integration method [2]. Time step is set to 0.01 year and the element size is 1mm, i.e., 5 elements in a single layer of SHCC. In this analysis, concentration of chloride at the reinforcement is monitored and durability is defined as a time, until which corrosive environment is not initiated, i.e., concentration of chloride at 1.2kg/m^3. Concentration on the surface is assumed constant at 3%. Rebar, which is not modelled, is in an un-repaired concrete with a cover thickness 25mm, i.e., located 40mm deep from the surface of repair material. Therefore, critical concentration of chlorides is controlled on the edge of a model. Location of the analysed detail is schematically represented in Fig.3.6.1. The detail is located on the bottom part of a slab repaired with an FG-SHCC material. Old concrete slab contains a crack, in the detail modelled on the right side, area of cracked elements is 62.5mm^2, i.e., 10 elements in crack analysis. Axisymmetric model has size

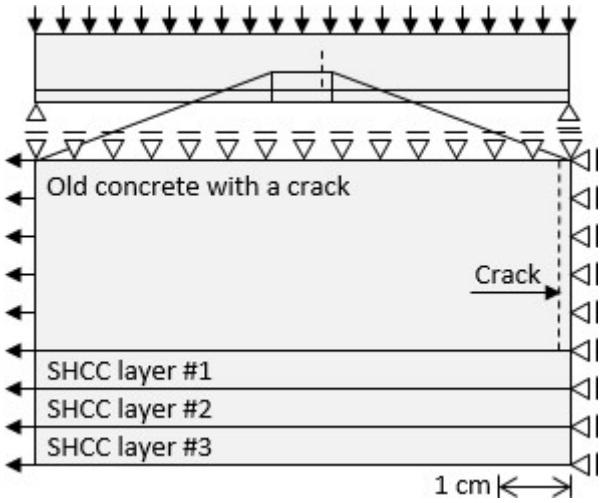

Fig. 3.6.1 Location of the detail in the structure

$80x40$mm, where SHCC layer is 15mm thick in total, i.e. the same dimensions of the model as for the crack analysis in previous chapters.

Diffusion of chloride ions is obtained by modifying the apparent diffusivity parameter and monitoring the concentration in the location of the rebar using a known boundary chloride concentration, time and a thickness from experiments [53, 77]. Numerical error of diffusion analysis is examined in Appendix H.

FGM is created by layering SHCC of different material properties. Different diffusion can be achieved mainly by varying the amount of fibres in a matrix, water to binder ratio or possible admixtures, e.g. water repellent [108]. FGM in this study is understood to be identical to a homogeneous layer when summary of relative material quality is identical, i.e., three identical layers of SHCC have 100% of fracture energy each, compared to FGM, where this ratio can vary (e.g. 50%, 100%, 150%).

Three layers of SHCC with identical constant thickness of 5mm are used for optimization for the best performance of sound FG-SHCC. Four different materials are used. Mechanical performance of adopted mixture N [113] is used as a base material for homogeneous SHCC distribution. An average value of chloride diffusivity based on the W/C ratio is assigned to the mixture N. From this base N material, three materials of different apparent diffusivity and mechanical performance are assumed by extrapolation of their respective properties. In Table 3.4, equivalent diffusivity of a material to form FGM is represented as a ratio, e.g., L1 at 2.3 has 230% of diffusivity of N and E1 has 30% diffusivity of N.

Table 3.4 Durability of sound SHCC repair material, sealed at the position of rebar (a case of effective primer)

Layers	Apparent diffusivity [cm^2/year]				Ratio (Quality Index) [-]				Durability [years]
	SHCC			Concrete	SHCC			Concrete	
LNH	0.575	0.1	0.075	2.5	2.3	0.4	0.3	10	24.37
HNL	0.075	0.1	0.575	2.5	0.3	0.4	2.3	10	21.39
NNN	0.25	0.25	0.25	2.5	1	1	1	10	11.58

note: layer order noted from the interface

Table 3.5 Durability of sound SHCC repair material, no seal at the position of rebar (direct contact or non-effective primer)

Layers	Apparent diffusivity [cm^2/year]				Ratio (Quality Index) [-]				Durability [years]
	SHCC			Concrete	SHCC			Concrete	
LNH	0.575	0.1	0.075	2.5	2.3	0.4	0.3	10	64.64
HNL	0.075	0.1	0.575	2.5	0.3	0.4	2.3	10	61.46
NNN	0.25	0.25	0.25	2.5	1	1	1	10	31.49

note: layer order noted from the interface

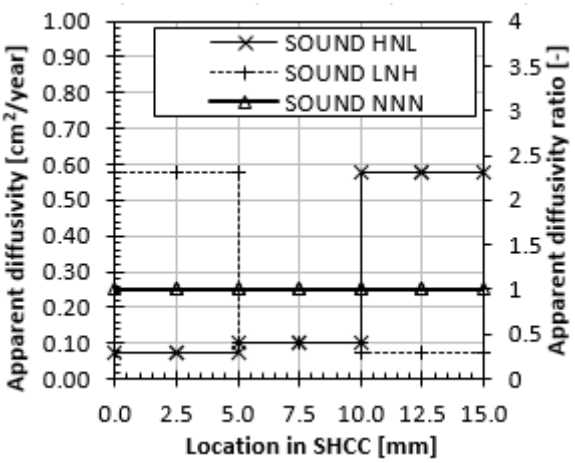

Fig. 3.6.2 Distribution of apparent diffusivity in sound FG-SHCC

For a case of effective primer used at the location of the rebar, results compared to a homogeneous layer of SHCC, FG-SHCC shows better performance of up to 210% of durability time of sound SHCC, see durability years in Table 3.4. Ratios of apparent diffusivity of such FGM are 2.3, 0.4 and 0.3, i.e., negative gradient, see the layering L1M1E1 in Fig.3.6.2. The resulting respective chloride ion concentration for each layering order is presented in Fig.3.6.3. Best used material layer for this analysis has equivalent diffusivity of 0.067cm^2/year, which is a diffusivity of the UHP-SHCC (Ultra-High Performance SHCC) material [65]. This analysis uses the apparent diffusivity of UHP-SHCC as the best material, but with progress in research of SHCC mixtures, formed function can be even more effective. The lowest performing material has apparent diffusivity of 0.575cm^2/year.

For a case of non-effective primer used at the location of the rebar, results compared to a homogeneous layer of SHCC, FG-SHCC shows better performance of up to 205% of durability time of sound SHCC, see durability years in Table 3.5. The resulting respective chloride ion concentration for each layering order is presented in Fig.3.6.4.

3.7 Diffusion of chlorides in FG-SHCC with cracks

This part of the analysis studies the effect on diffusion of cracked FG-SHCC, because material parameters are changing due to applied mechanical load. Effect of creep and other sources of cracks are not modelled, because the beneficial effect of FGM can be shown on an average width crack distribution from live load. One must understand,

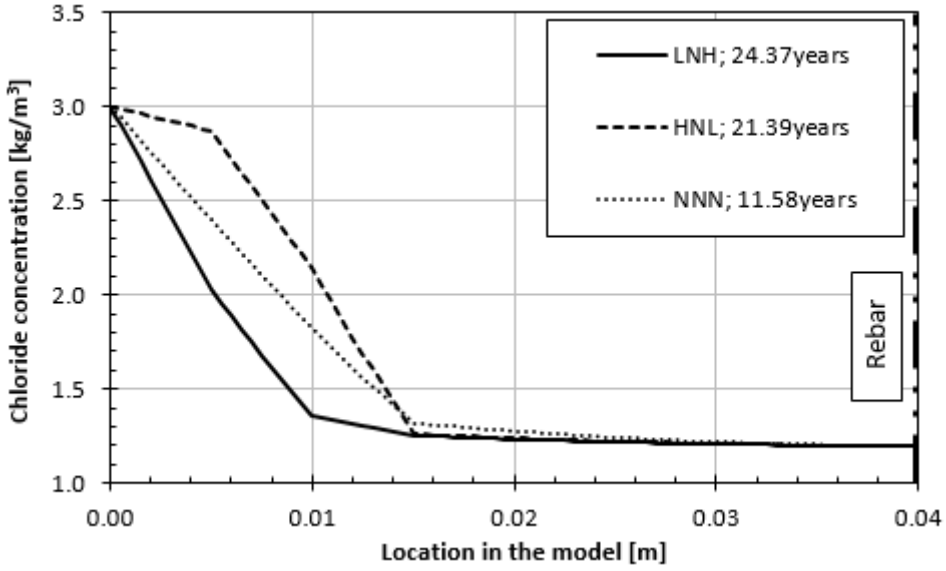

Fig. 3.6.3 Diffusion profile of different sound FG-SHCC, sealed at the position of rebar (a case of effective primer)

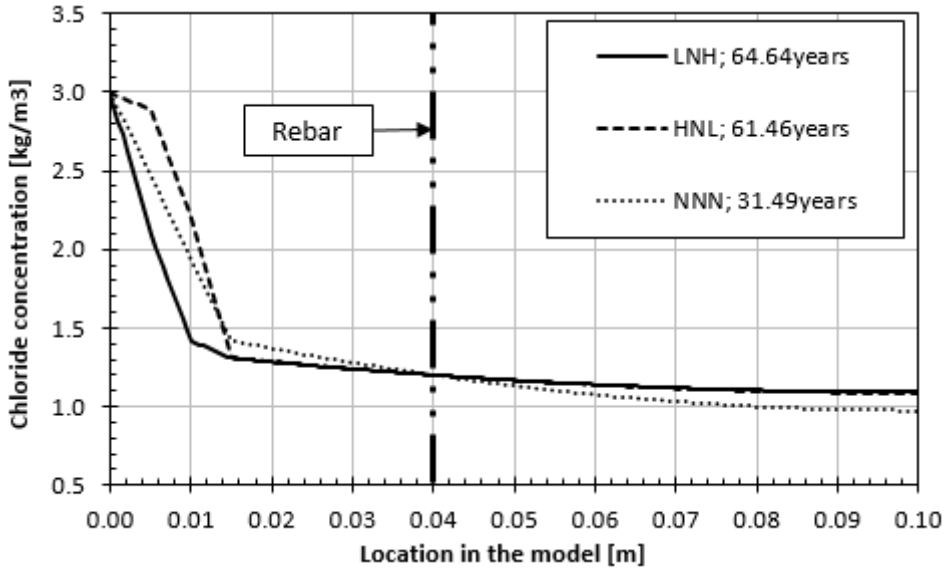

Fig. 3.6.4 Diffusion profile of different sound FG-SHCC, no seal at the position of rebar (direct contact or non-effective primer)

that not only the material properties are changed because of formed cracks, but also because of chemical changes due to chloride ion penetration.

SHCC under chloride exposure suffers from a decreased chemical bond strength between fibres and a matrix, with reduction of up to 40% [49]. On the other hand, mechanical bond strength is increased up to 125%, [65]. It is presumed, that this is caused by salt crystals growing on the interface and providing better contact. Such changes in the interfacial transition zone (ITZ) cause reduced fracture energy, therefore formation of smaller number of cracks, but with a larger average crack width resulting in reduced durability.

Prepared FEM model is firstly pre-loaded using the crack analysis to obtain the crack width at the stage after repair and application of first live load. Material's equivalent diffusivity is then updated due to newly formed cracks.

3.7.1 Average crack width

Using the FEM analysis, 2D non-linear model of an SHCC repair material on a concrete slab was created. Analysed model represents a small part of a repaired structure Fig.3.6.1, where a 25mm layer is representing an old concrete with a crack and 15mm layer is representing the SHCC repair material. Layers of SHCC of various mechanical and physical properties forms an FGM. Thickness of the 2D model is 40mm, except FEM elements that represents a crack, where thickness is set to 15mm. Stress in the thinner area is reaching the material strength earlier than in other elements, and the early formed crack can simulate the pre-cracked specimen. As it is recommended [79], boundary conditions are applied on the model through steel plates, Fig.4. Special interface material must be modelled in between the plate and the cementitious material to remove a tangential displacement restriction causing incorrect crack propagation. In the model with the rigid connection in between the steel plate and the cementitious material, the plate is confining the model against a lateral contraction, causing incorrect cracking. Cracked model with layering E1M1L1 is presented in Fig. 3.7.2, where red is a minimal stress and blue is the highest with graphical representation of formed cracks by vertical lines, where 1D diffusion analysis is carried at the place of the widest crack, i.e. under the single crack in concrete. Boundary condition allows shear slip between two loading plates, i.e., loading steel plate is not connected to the boundary

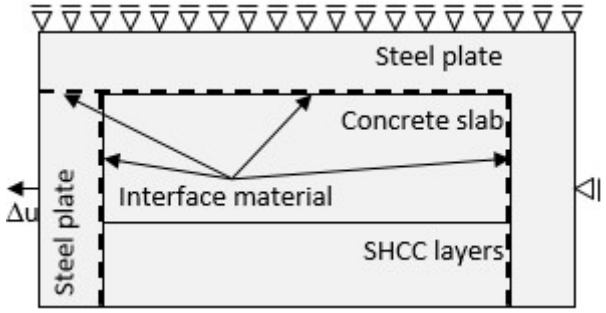

Fig. 3.7.1 Plain tensile test, ($\Delta u = 4.0 \times 10^{-5} m$)

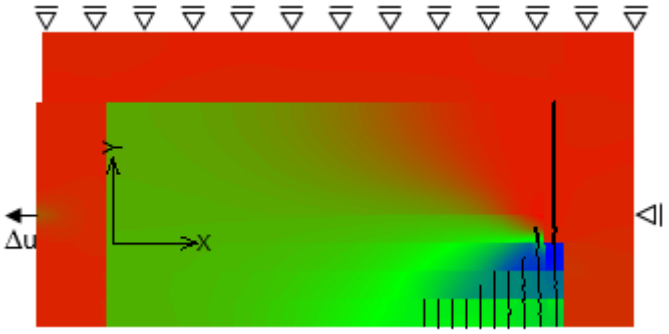

Fig. 3.7.2 Crack distribution from crack analysis and stress distribution, (red=min, blue=max)

steel plate due to applied interface, hence no shear forces are generated. Material input data are summarized in Table 3.6, where E is the Young's modulus of elasticity, f_t is the ultimate tensile stress and f_c is the ultimate compressive stress.

The interface material has high stiffness in a normal direction, so the model has an identical stiffness when loaded. This was tested on a modified model presented in Fig.3.7.3, where model with an interface and a model with a rigid connection were compared. Material properties of the interface set so the stiffness of both rigid and interface model have identical normal stiffness are summarized in Table 3.7. Tangential stiffness must satisfy two main conditions, former the reaction from displacement up to a value of transversal compression must be negligible and latter condition is a numerical stability of the analysis.

One meshing size was selected with respect to computational efficiency and possible representing of number of cracks on the element body. In open cracks, stress is transmitted only by fibres. Stress is gradually redistributed to the matrix, with zero value at the crack edge, increasing with the distance from the crack. The condition for a matrix cracking may not be fulfilled in a certain distance from a crack, therefore cracks

Table 3.6 SHCC material parameters in FEM vs test data

Test data	E [GPa]	f_t [MPa]	f_c [MPa]
M6 matrix	20	3.5	-10f_t
Fibre material	40	1640	-f_t
FEM input data			
Model N simulating M6	20	3.5	-10f_t
Model H upscaled from M6	25	4.5	-10f_t
Model N downscaled from M6	20	2.5	-10f_t

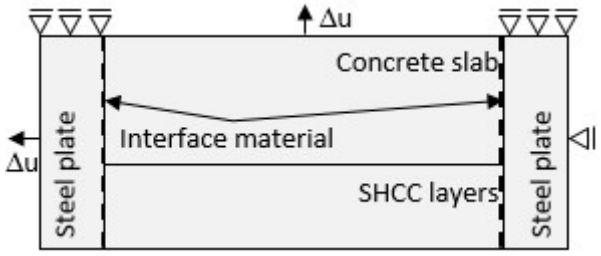

Fig. 3.7.3 Interface test model, ($\Delta u = 5.0x10 - 6m$)

Table 3.7 Interface material parameters

Parameter type	**Value**	**Units**
Normal stiffness, K_{NN}	1.00E+17	[MN/m^3]
Tangential stiffness, K_{TT}	1.00E-05	[MN/m^3]
Tensile strength, F_t	4.5	[MPa]
Cohesion, C	5	[MPa]
Friction coefficient	8.5	[-]
Thickness	0.001	[m]

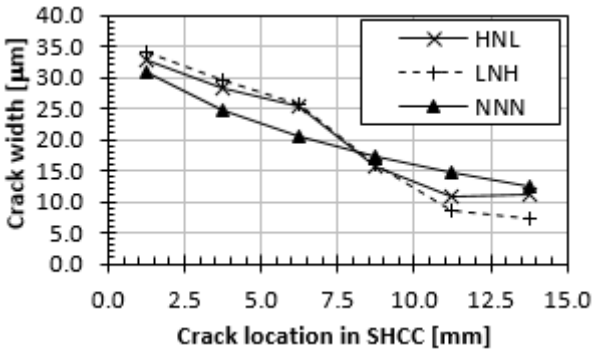

Fig. 3.7.4 Crack width profile in SHCC from live load, (Plain tensile test avr. strain: $\epsilon = 5 \times 10^{-4}$)

must maintain certain minimum spacing x. To ensure that the crack spacing does not become less than x, presented analysis utilizes regular meshes with finite element size equal to approximately $2x$, noting that the 4-noded quadrilateral element employed may accommodate a maximum of two semi-parallel cracks. In this model, mesh size is $2.5x2.5$mm.

Based on a repair method, repair material is generally subjected only to stress from a live load. Stress increase form a live load in a reinforcement is generally around 100MPa, i.e., with Young's modulus of a steel at 200GPa expected strain from a live load is 5×10^{-4}. Model is pre-loaded up to the specified strain, and then the strain is kept constant, while diffusion of chloride takes place. Cracks width formed in SHCC of different material layers caused by live load strain $\epsilon = 5 \times 10^{-4}$ are presented in Fig.3.7.4.

3.7.2 SHCC crack analysis precision

Case of a zero loading step has to be examined. It has been observed, that certain material models are showing spurious deformations and change of crack width during non-loading steps, which are necessary to be applied for a combination of mechanical loading with an environmental load causing change in the material properties.

NonLinCementitious2User material model is selected as the most suitable for SHCC. Compared to the SBETA material model, width of cracks is changing during non-loading steps, i.e., when the constant B.C. is applied. In this model, interface from Table 3.7 and a limit of 40 iterations is used. Iteration limit was reached in all steps. Cracked model with location of monitored cracks is presented on Fig.3.7.5. Crack

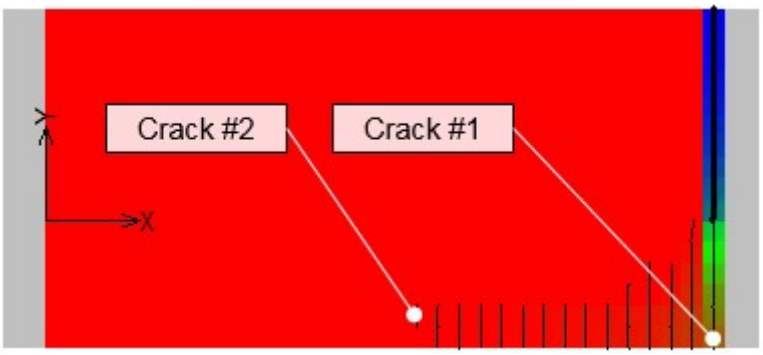

Fig. 3.7.5 Cracked model with monitored cracks

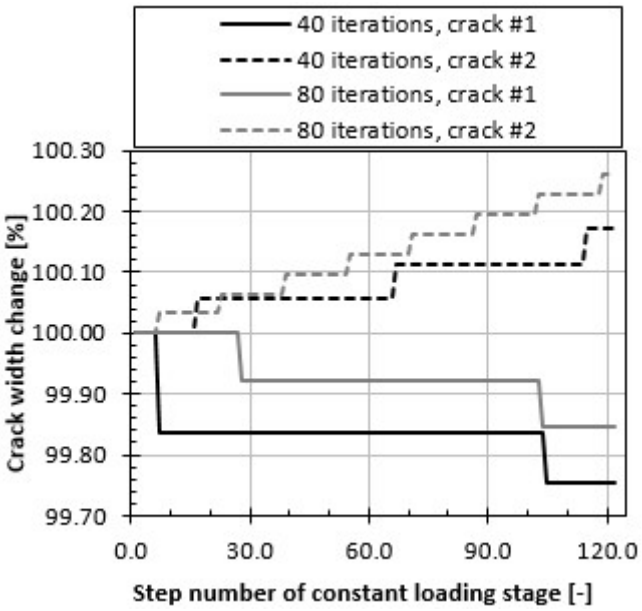

Fig. 3.7.6 Crack change during constant loading stage

change is presented on Fig.3.7.6, where width of crack #1 at first constant loading step is 1.211×10^{-6}m and width of crack #2 is $1.753x10^{-10}$m. For the case of 80 iterations, width of the crack #1 starts at 1.285×10^{-6}m and crack #2 at 3.075×10^{-9}m. Fig.3.7.5 compares relative change within one model, difference when comparing 40 and 80 iterations is 6.11% for the crack #1 and 5.7% for the crack #2.

When loading is applied directly on the cementitious material, maximum number of iteration is not reached, but change of crack width is larger, mainly during first 30 constant loading steps, see Fig.3.7.7.

Crack width change during constant loading steps can be controlled by modifying used tolerance values. Satisfying results were achieved by reducing tolerances as presented in Table.3.8. Effect of changed tolerance on results with the loading history

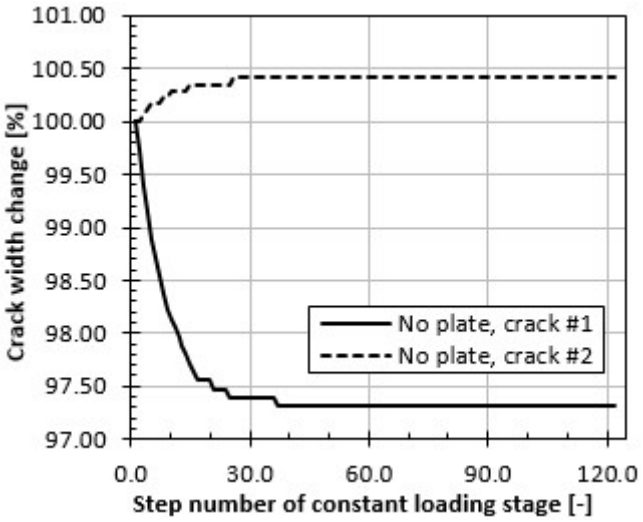

Fig. 3.7.7 Crack change during constant loading stage, load applied directly on cementitious material (tension test)

Table 3.8 Tolerance values in crack analysis

Tolerance	**Default tolerance**	**Introduced tolerance**
Displacement error	0.01	0.0005
Residual error	0.01	0.0005
Absolute residual error	0.01	0.0005
Energy error	0.0001	0.000005

is presented in Fig.3.7.8, Fig.3.7.9 and Fig.3.7.10 respectively.

3.7.3 Diffusivity of cracked SHCC

Cracked versus sound material has in general higher diffusivity. The difference in diffusivity between a cracked and a sound SHCC foremost depends on average width of cracks, number of cracks and maximum crack width. That is, two SHCC materials can have identical average crack width, but diffusivity of the one with higher number of cracks is larger.

One way of measuring chloride penetration depth is to use silver-nitrate sprayed solution for a non-direct testing [77]. Area with a changed colour after application of a silver-nitrate solution is understood as to be prone for steel corrosion, and a measured penetration depth can be used in the diffusion analysis. Silver-nitrate applied on a

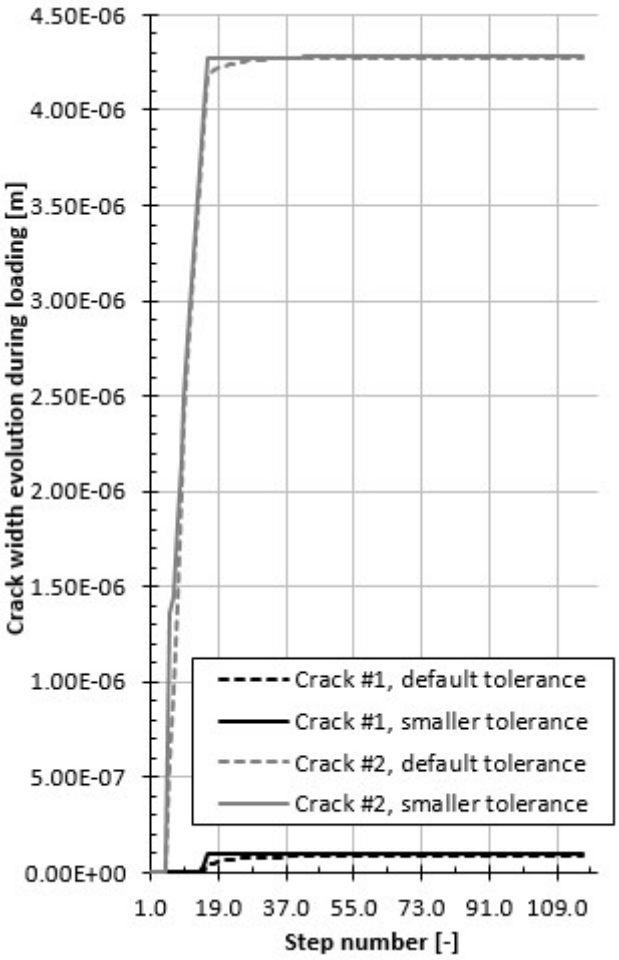

Fig. 3.7.8 Change of crack width

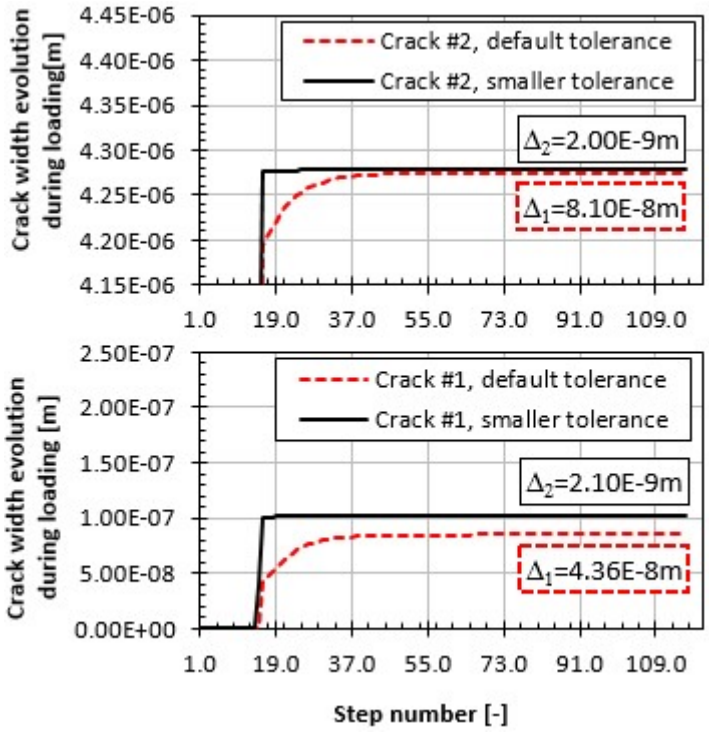

Fig. 3.7.9 Change of crack width, detail of Fig.3.7.8

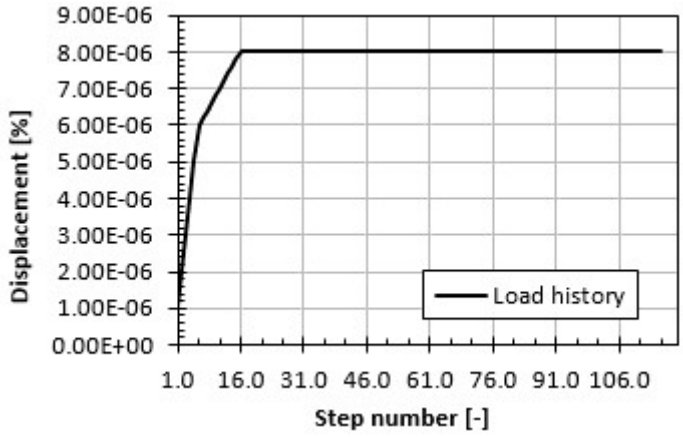

Fig. 3.7.10 Loading history for evaluation of crack width difference of a different tolerance

cementitious material reacts by changing a colour, when concentration of chlorides is in a range of 0.28% to 1.41% by binder mass [70].

Other way is measuring direct concentration profiles by method of X-ray fluorescence (XRF) [108]. For each result was calculated equivalent diffusivity parameter using known boundary concentration, depth of chloride penetration and time of a corrosion initiation.

Calculated equivalent diffusivity parameters for diffusion analysis are presented in Table 4 with ϵ as strain and w as crack width values of the respective test data. Using the test data, a parameter D0 describing the effect of cracks in SHCC can be obtained using following equation for diffusivity defined in Eq.4.3.1 [44] as

$$D_{eff} = D_k + D_0 log_{10}\left(\epsilon w^2\right) \tag{3.7.1}$$

where D_k [m^2/year] is diffusivity of uncracked SHCC, D_0 [m^2/year] is a parameter for cracks in SHCC, ϵ[%] is average strain of SHCC and w [μm] is an average crack width of SHCC.

Calculated parameter D_0 (Table 3.9) is used for prediction of crack width effect on SHCC, Fig.3.7.11. Data from [43] are used for scaling the equivalent diffusivity to create two SHCC materials L1 and E1, where L1 has at zero crack width 230% larger diffusivity and E1 30% of equivalent diffusivity, see Fig. 3.7.11. As can be seen in Fig.3.7.11, equivalent diffusivity became almost constant with average cracks larger than 100μm. Similar behaviour was found by Suvash C. P. [77] and Seung Y. J. [43] on a cracked concrete specimen, where for cracks $80-100\mu$m chloride diffusion is constant and independent of crack width. Difference is observed in crack range $0-30\mu$m, where chloride diffusion of concrete is almost unchanged, but SHCC has a logistic growth. In crack range from 30μm up to 100μm, the diffusion in concrete has linear increase, somewhat like SHCC. It must be noted, that even though shape of functions is similar, diffusivity of concrete is much larger.

3.7.4 Influence of crack width on durability

For the given strain at 5.0×10^{-4} causing crack width up to 35μm, diffusivity of cracked SHCC layer E1 increases up to 242%. For the case of effective primer, resulting distri-

Table 3.9 Effect of cracks in SHCC

Ref.	D_d [cm^2/year]	D_k [cm^2/year]	ϵ [%]	w [μm]	D_{d0} [-]
[25]	0.259	0.37	0.6	21	0.03
[65]	0.260	0.57	0.2	40	0.12

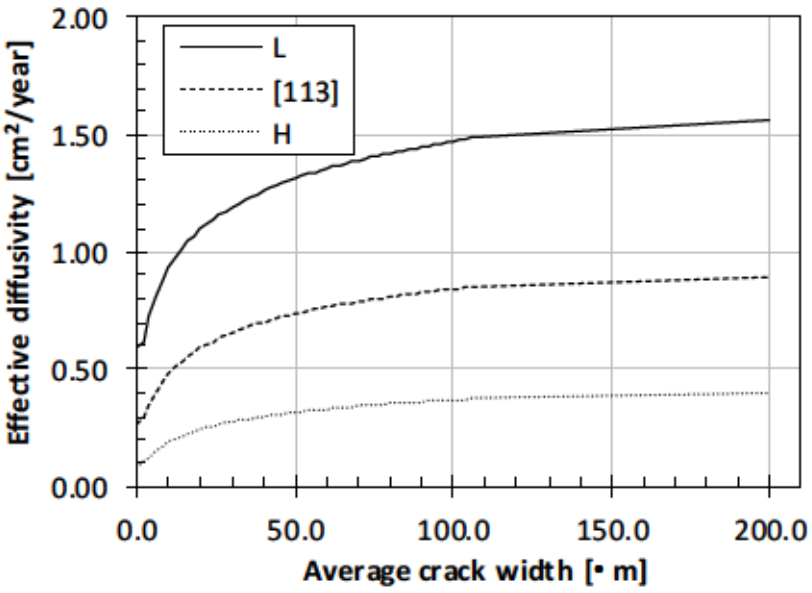

Fig. 3.7.11 Apparent diffusion as a function of crack width of SHCC

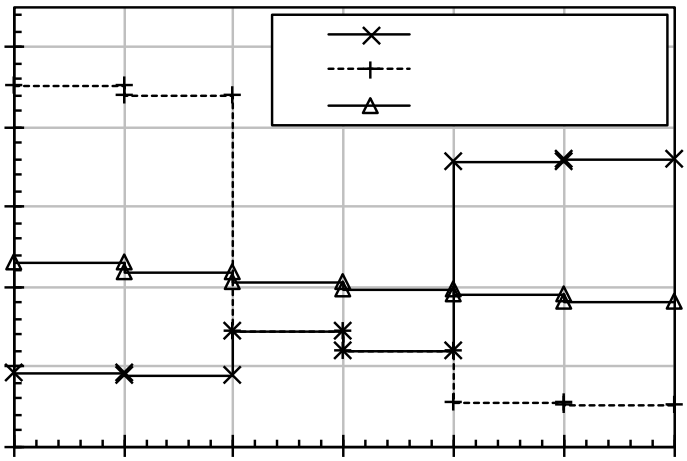

Fig. 3.7.12 Distribution of apparent diffusivity in cracked FG-SHCC

bution modified by the effect of cracks on apparent diffusivity is shown in Fig.3.7.12 with respective chloride ion concentration in Fig.3.7.13 showing the distribution of each layering at the time of corrosion initiation. Cracked FG-SHCC shows better durability compared to cracked homogeneous, with up to 193% of homogeneous durability time. FG-SHCC with the lowest diffusivity on the exterior surface shows better (147%) performance of FG-SHCC of identical layers but inverse order, Table 3.10. This is due to good quality surface layer, that is not affected by cracking as much as the layer at the interface with concrete substrate and combination of low apparent diffusivity.

Chloride ion concentration for a case of direct contact or non-effective primer is in Fig.3.7.14. Cracked FG-SHCC shows better durability compared to cracked homogeneous, with up to 189% of homogeneous durability time. FG-SHCC with the lowest diffusivity on the exterior surface shows better (138%) performance of FG-SHCC of identical layers but inverse order, Table 3.11. The above facts in diffusion and crack analysis implies the possibility of material use optimization to get improvement of durability of concrete structures.

The gradient orientation shows higher importance for the cracked FG-SHCC, due to assumed lower degradation of a surface layer in a form of a narrower crack width, compared to the width near the interface, i.e., from the diffusivity point of view it is beneficial to place the best performing layer in a place of lowest deterioration.

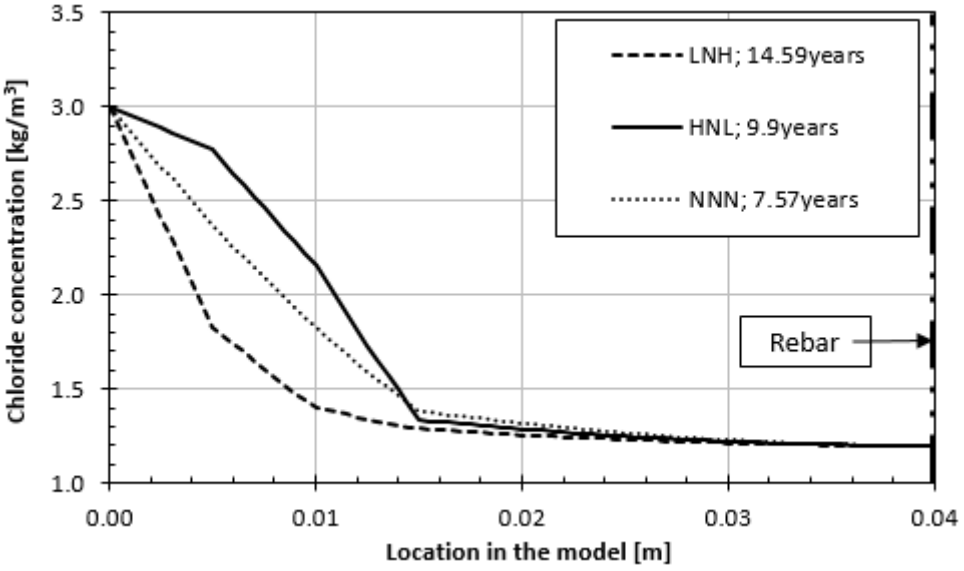

Fig. 3.7.13 Diffusion of different cracked FG-SHCC, sealed at the position of rebar (a case of effective primer)

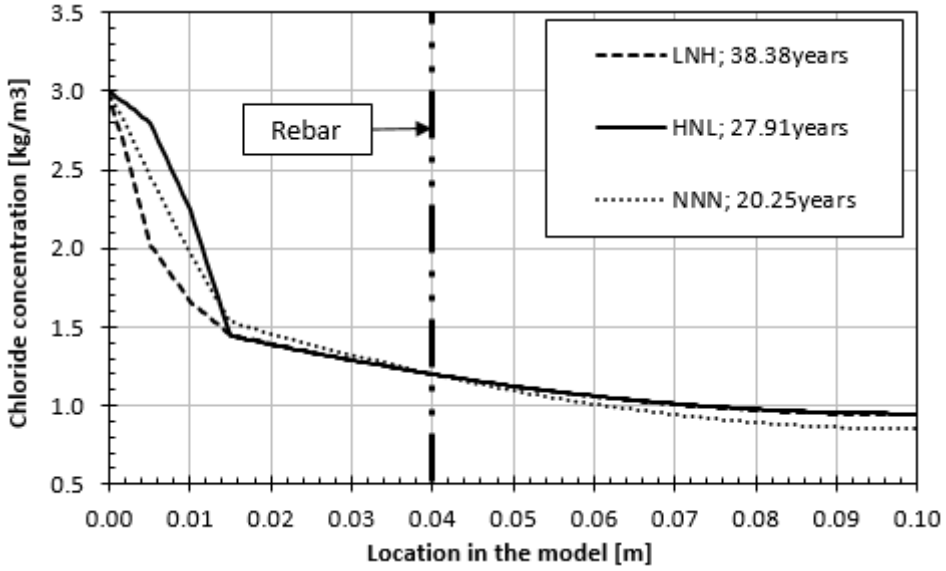

Fig. 3.7.14 Diffusion of different cracked FG-SHCC, no seal at the position of rebar (direct contact or non-effective primer)

Table 3.10 Durability of cracked FG-SHCC material, sealed at the position of rebar (a case of effective primer)

Layers	Apparent diffusivity [cm^2/year]							
	SHCC						Concrete	
LNH	0.903	0.881	0.289	0.238	0.110	0.101	2.5	
HNL	0.182	0.174	0.287	0.236	0.716	0.722	2.5	
NNN	0.458	0.434	0.41	0.395	0.378	0.362	2.5	
Layers	Ratio (Quality Index) [-]							Durability
	SHCC						Concrete	[years]
LNH	3.612	3.524	1.156	0.952	0.440	0.404	10	14.59
HNL	0.728	0.696	0.148	0.944	2.864	2.888	10	9.90
NNN	1.832	1.736	1.656	1.580	1.512	1.448	10	7.57

note: layer order noted from the interface

Table 3.11 Durability of cracked FG-SHCC material, no seal at the position of rebar (direct contact or non-effective primer)

Layers	Apparent diffusivity [cm^2/year]							
	SHCC						Concrete	
LNH	0.903	0.881	0.289	0.238	0.110	0.101	2.5	
HNL	0.182	0.174	0.287	0.236	0.716	0.722	2.5	
NNN	0.458	0.434	0.41	0.395	0.378	0.362	2.5	
Layers	Ratio (Quality Index) [-]							Durability
	SHCC						Concrete	[years]
LNH	3.612	3.524	1.156	0.952	0.440	0.404	10	38.38
HNL	0.728	0.696	0.148	0.944	2.864	2.888	10	27.91
NNN	1.832	1.736	1.656	1.580	1.512	1.448	10	20.25

note: layer order noted from the interface

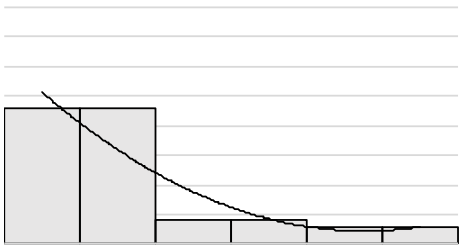	Uncracked No seal +105% durability time Seal +110% durability time Gradient: Table 3.4 and 3.5 Exponential gradient
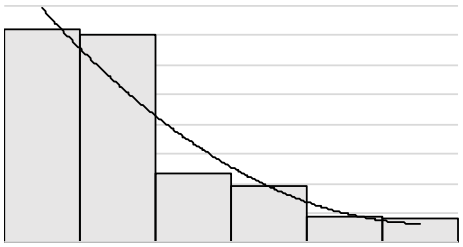	Cracked No seal +89% durability time Seal +93% durability time Gradient: Table 3.10 and 3.11 Exponential gradient

Fig. 3.8.1 Cracked and uncracked FG-SHCC diffusivity gradients

3.8 Remarks

A material with high fracture energy should be placed on the interface to efficiently transfer stresses from crack. Distribution of a gradient is presented in Fig.3.8.1. The sealed condition is showing a higher effectiveness of the FGM, but due to faster accumulation of chlorides at the rebar, the absolute durability time is lower than that of unsealed condition. The effect of FGM is also reduced due to formation of cracks, ultimately a sufficiently wide crack would cause no benefit of FGM. Thus, crack localization should be prevented. A material with higher fracture energy is showing larger loading capacity, that is crucial at the interface location. From the diffusivity point of view, such a distribution is also beneficial, as data from other researchers [[75, 42, 100, 47]] suggest that material with higher fracture energy tend to have a larger maximum crack width, on Fig.3.8.2.

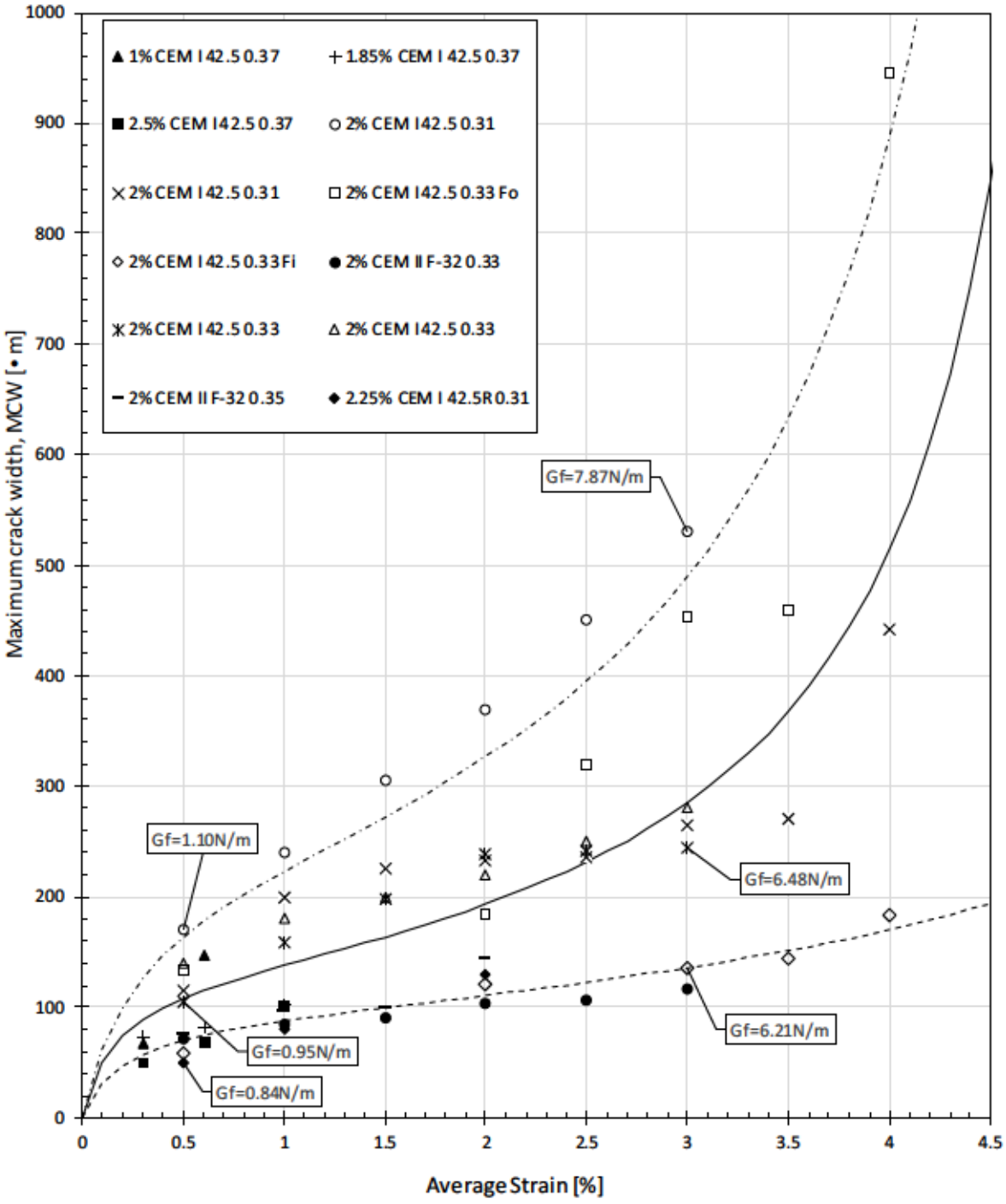

Fig. 3.8.2 Fracture energy vs maximum crack width

Chapter 4

FG-SHCC multi-layer structure with variable gradient for chloride diffusion resistance with and without crack

Strain hardening cementitious composite (SHCC) material used as a repair material on reinforced concrete structures for protection against environmental exposure is considered in this study. By layering different SHCC mixtures, one can create functionally gradient material (FGM) to control crack spacing, localization and opening. Compared to cracks in ordinary RC, formation of micro-cracks increases resistance to moisture, gas and salt penetration, the key to cement-based material durability. As variable functions in this study equivalent diffusivity of carbonation and chloride ions in assumed crack width are used to examine the effect of layer distribution. FGM is then created by layering the SHCC of various material properties and the obtained durability as a function of time for corrosion initiation is studied. From the numerical simulation, it is found that the corrosion initiation time of sound FG-SHCC is extended significantly compared to uniform SHCC and this beneficial behaviour is found in cracked FG-SHCC as well. FG-SHCC compared to homogeneous material shows both for chloride attack and carbonation moderate to high increase in durability, based on the crack width. Effect of layering decreases with increasing crack width. Due to the nature of crack width limit of SHCC, beneficial behaviour of layering to form FG-SHCC during service load is always present.

The durability potential of functionally graded SHCC (FG-SHCC) is studied when applied as a repair material on a mortar substrate. SHCC material compared to ordinary mortar or FRC material provides better durability due to tight crack width beneficial for low diffusivity of deteriorating substances, such as chloride ions or CO_2

causing carbonation, as studied by many researchers [37, 51, 53, 11, 76]. Another benefit of tight crack width is lower steel deterioration rate due to micro-cell corrosion. Steel reinforcement corrosion surrounded by SHCC is suppressed due to a large anode/cathode area ratio due to the fact, that the anodic reaction in the cracked region is restrained by SHCC's crack width control capability and crack dispersibility. To benefit from this behaviour, it is recommended to use a cover layer of at least 10mm to utilize the crack width control capability [44]. To theoretically spread the crack effect from a layer to another layer, each layer is selected to be 10mm thick for the diffusion analysis in this chapter.

During repair work, the deteriorated old surface layer is removed to expose reinforcing bars and heavily corroded bars are changed. Patch repair material is applied in the following steps, a layer of FRC can be used to cover reinforcing bars, followed by layers forming the FG-SHCC. In this study, it is assumed that the reinforcing bar is directly under the SHCC layers and diffusion analysis is carried out only in those layers.

4.1 Effect of a different function representing diffusivity distribution

FG-SHCC can is here created to form various functions. Concept of different functions is presented by different step-wise functions, which are to represent a linear or an exponential distribution of a different order. The mechanism behind the FGM is explained in Appendix I.

4.1.1 Linear function approximation, sealed at the position of rebar

Linearly distributed diffusivity is presented on Fig.4.1.1 to Fig.4.1.3, different gradients are presented. Layer thickness is increased from 15mm to 30mm, for the case of easier fabrication, and to study whether the effect of FGM will differ from the case of 15mm FG-SHCC thickness. For this case of 30mm FG-SHCC layer, the base durability time of the homogeneous layer is 24.74years. Gradients with the best performing layer on

the surface are showing the best improvement of durability time. For the gradient 0.5-1-1.5 it's improvement of +31% of durability time, compared to the homogeneous layer. With steeper gradient, i.e. 0.3-1-1.7 the improvement is +81% of durability time, compared to the homogeneous layer.

4.1.2 Concave function approximation, sealed at the position of rebar

Concave diffusivity distribution is presented on Fig.4.1.4 to Fig.4.1.6, different gradients are presented. The base durability time of the homogeneous layer is 24.74years. Gradients with the best performing layer on the surface are showing the best improvement of durability time. For the gradient 0.5-1.5-1.0 it's improvement of +30% of durability time, compared to the homogeneous layer. With steeper gradient, i.e. 0.3-1.7-1.0 the improvement is +79% of durability time, compared to the homogeneous layer.

4.1.3 Convex function approximation, sealed at the position of rebar

Convex diffusivity distribution is presented on Fig.4.1.7 to Fig.4.1.9, different gradients are presented. For this case of 30mm FG-SHCC layer, the base durability time of the homogeneous layer is 24.74years. Gradients with the best performing layer on the surface are showing the best improvement of durability time. For the gradient 1.0-0.5-1.5 it's improvement of +22% of durability time, compared to the homogeneous layer. With steeper gradient, i.e. 1.0-0.3-1.7 the improvement is +57% of durability time, compared to the homogeneous layer.

4.1.4 Linear function approximation, no seal at the position of rebar

Linearly distributed diffusivity is presented on Fig.4.1.10 to Fig.4.1.12, different gradients are presented. For this case of 30mm FG-SHCC layer, the base durability time of the homogeneous layer is 62.82years. Gradients with the best performing layer on the surface are showing the best improvement of durability time. For the gradient

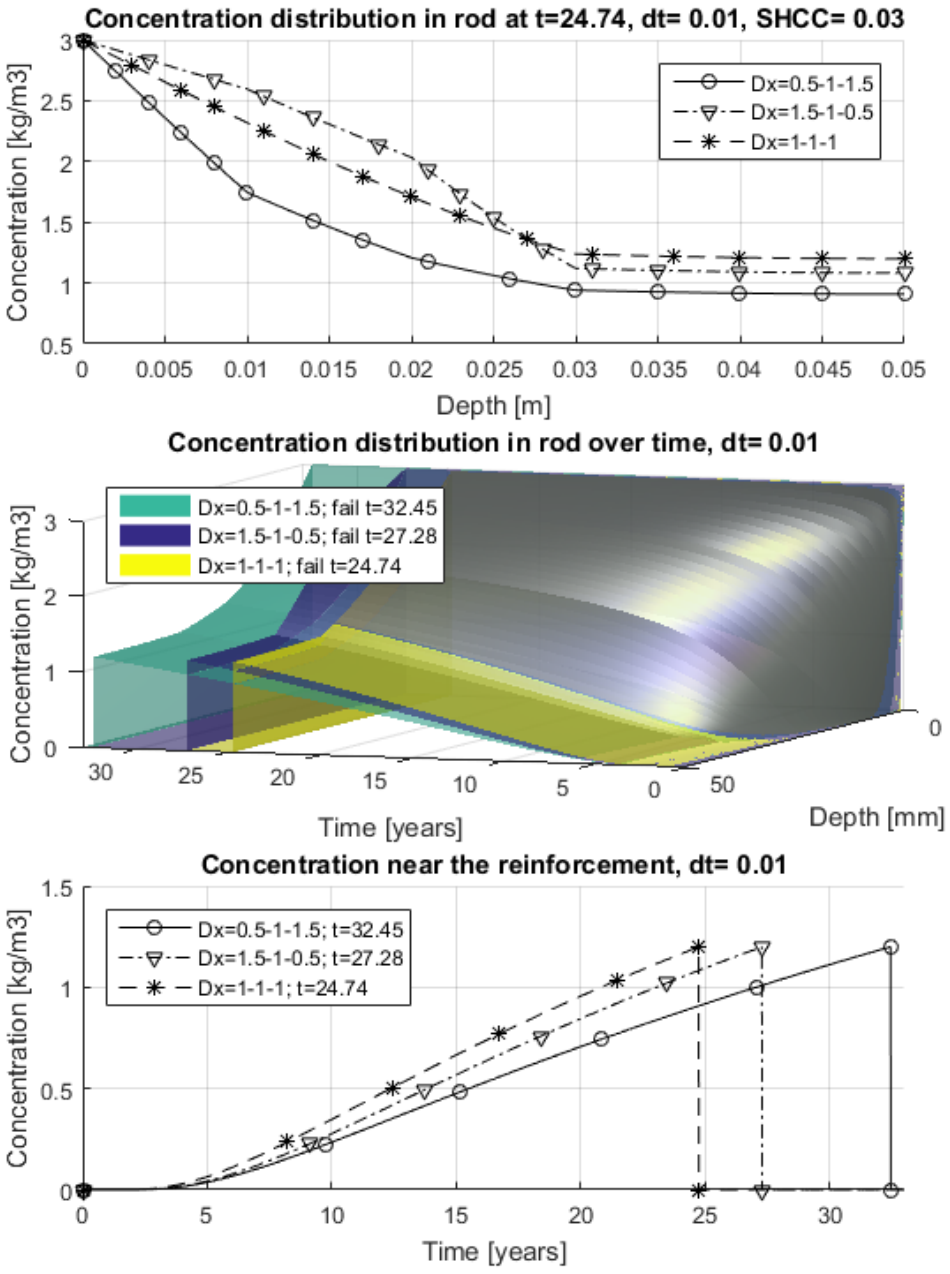

Fig. 4.1.1 Linear step wise function (Apparent diffusivity ratios 0.5:1.0:1.5)

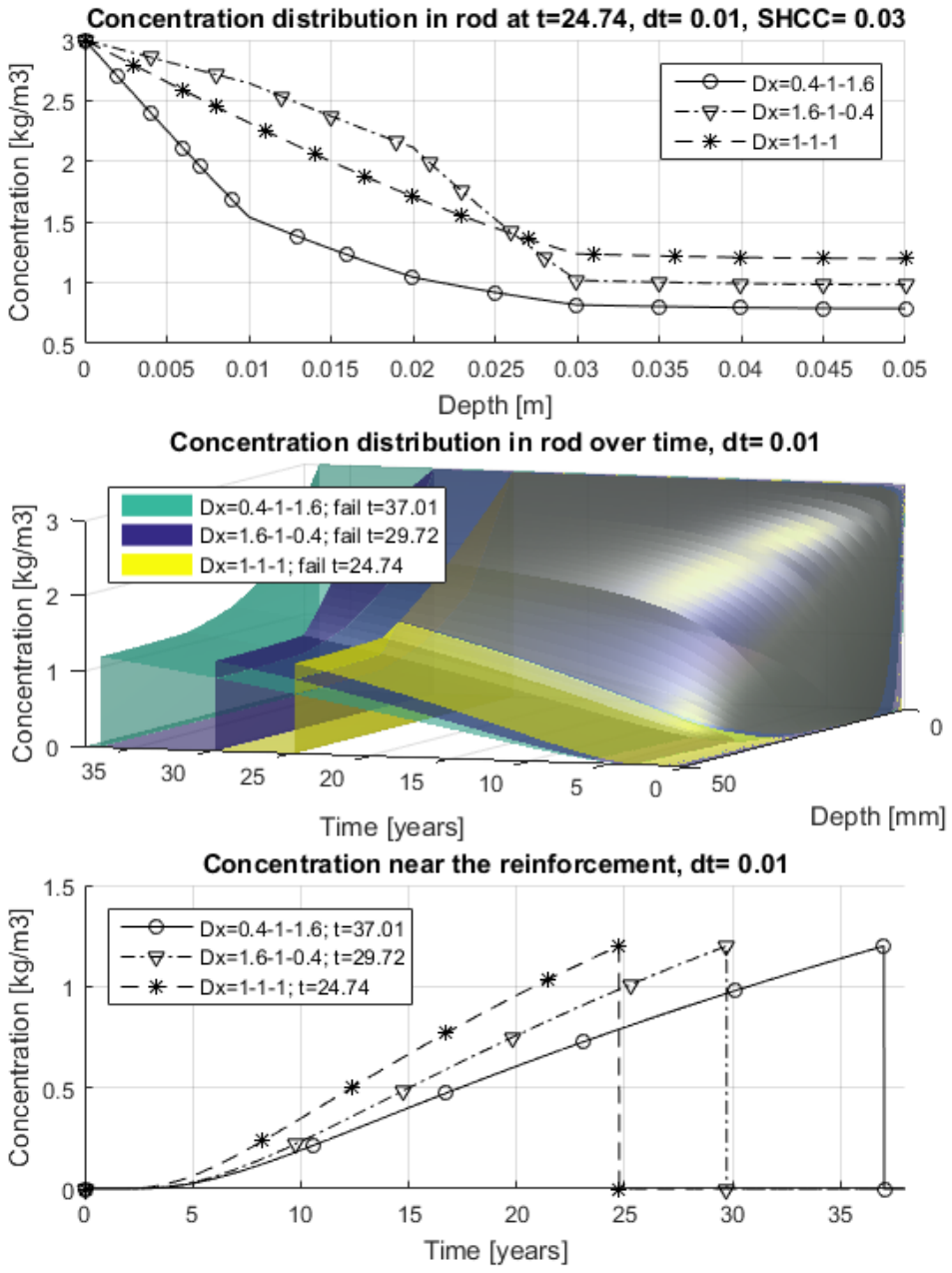

Fig. 4.1.2 Linear step wise function (Apparent diffusivity ratios 0.4:1.0:1.6)

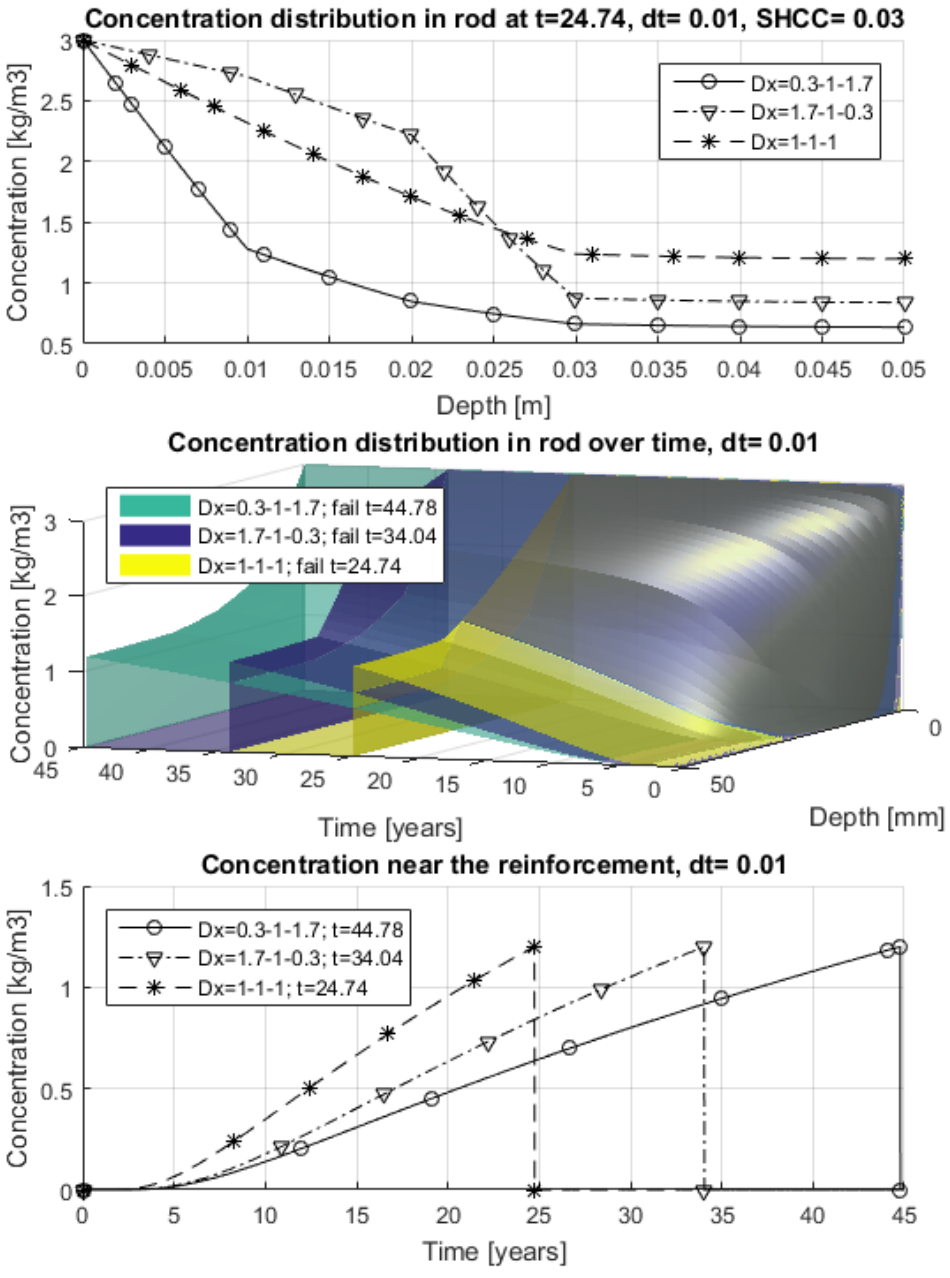

Fig. 4.1.3 Linear step wise function (Apparent diffusivity ratios 0.3:1.0:1.7)

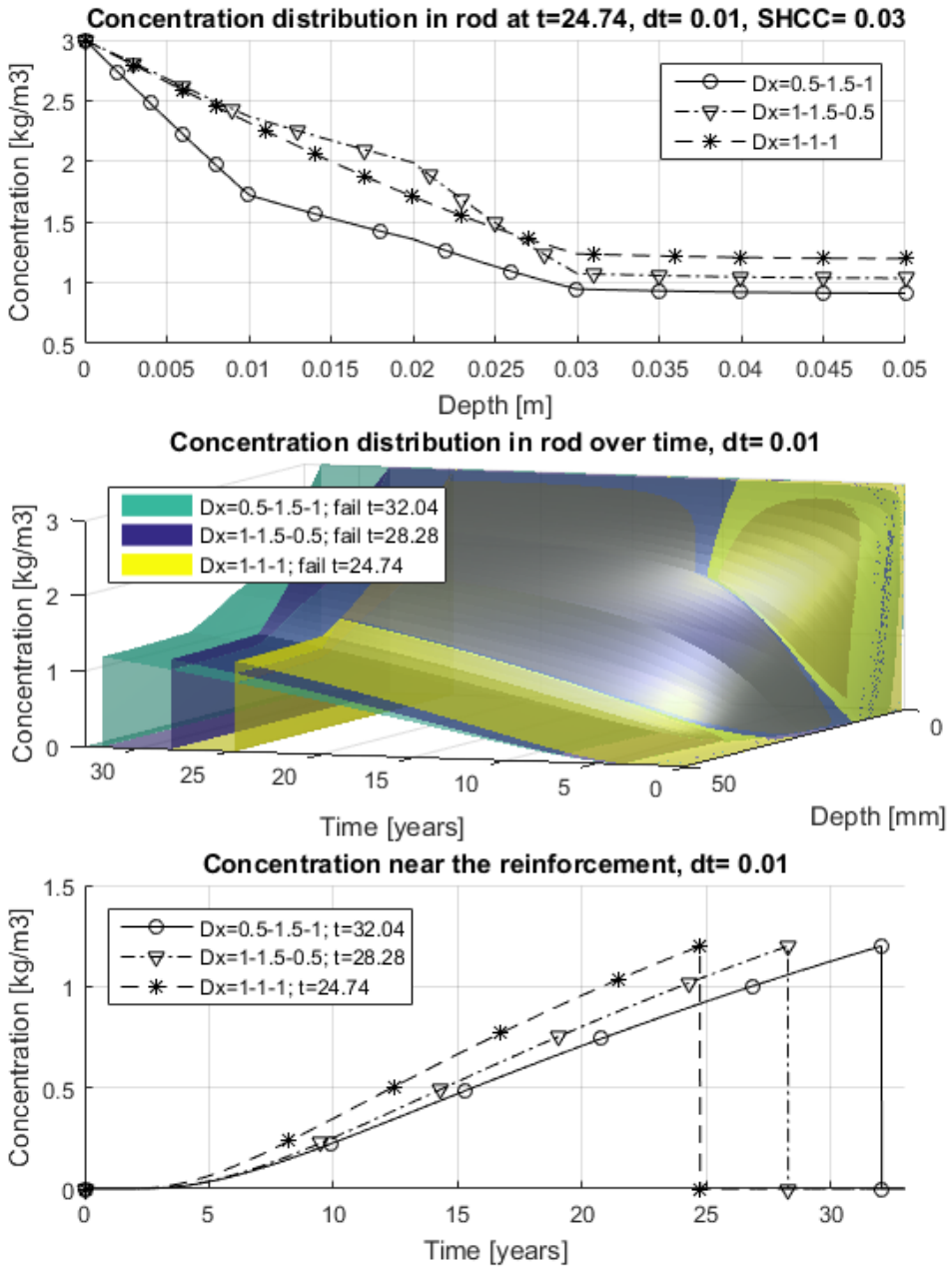

Fig. 4.1.4 Concave step wise function (Apparent diffusivity ratios 0.5:1.5:1.0)

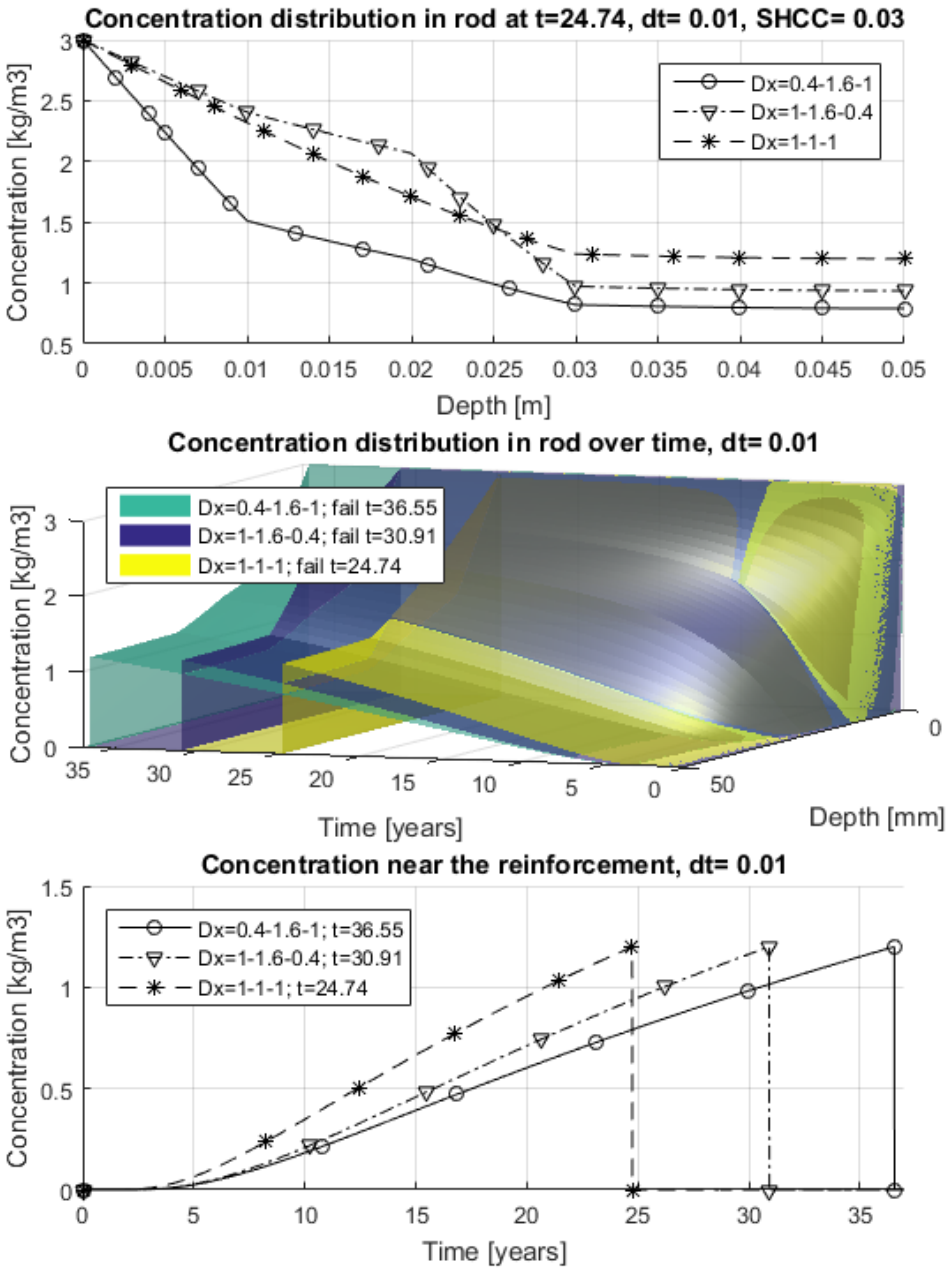

Fig. 4.1.5 Concave step wise function (Apparent diffusivity ratios 0.4:1.6:1.0)

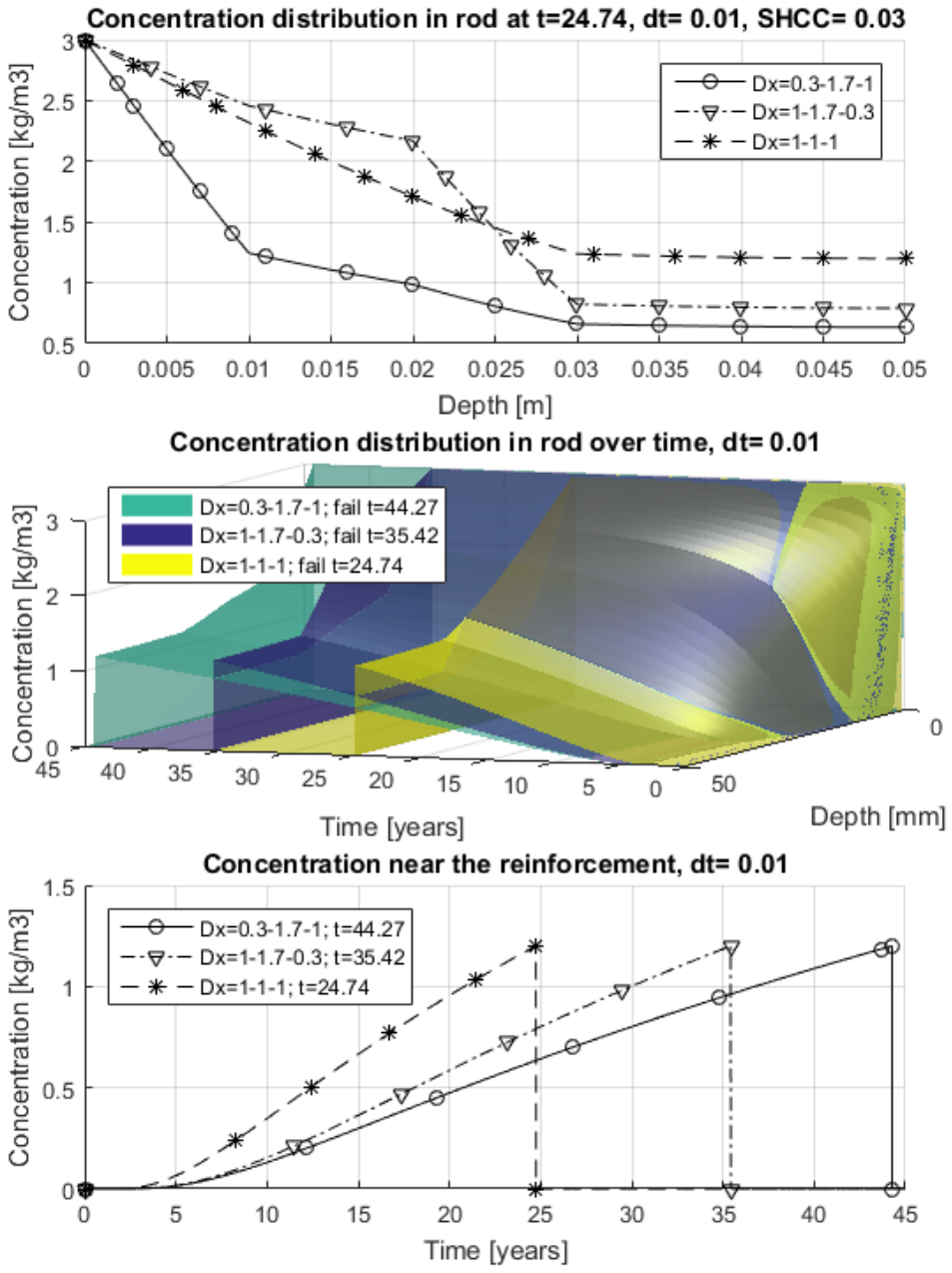

Fig. 4.1.6 Concave step wise function (Apparent diffusivity ratios 0.3:1.7:1.0)

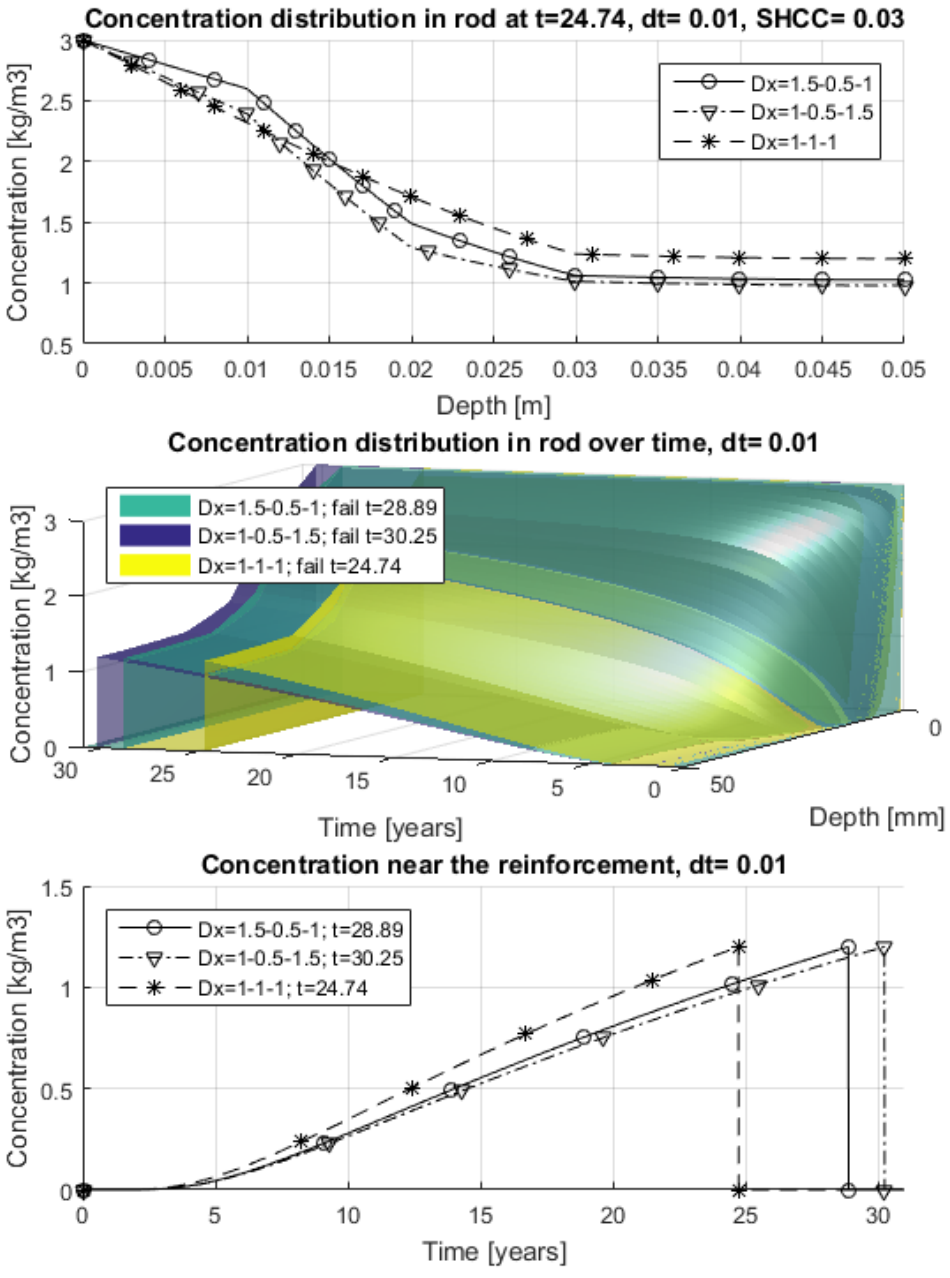

Fig. 4.1.7 Convex step wise function (Apparent diffusivity ratios 1.5:0.5:1.0)

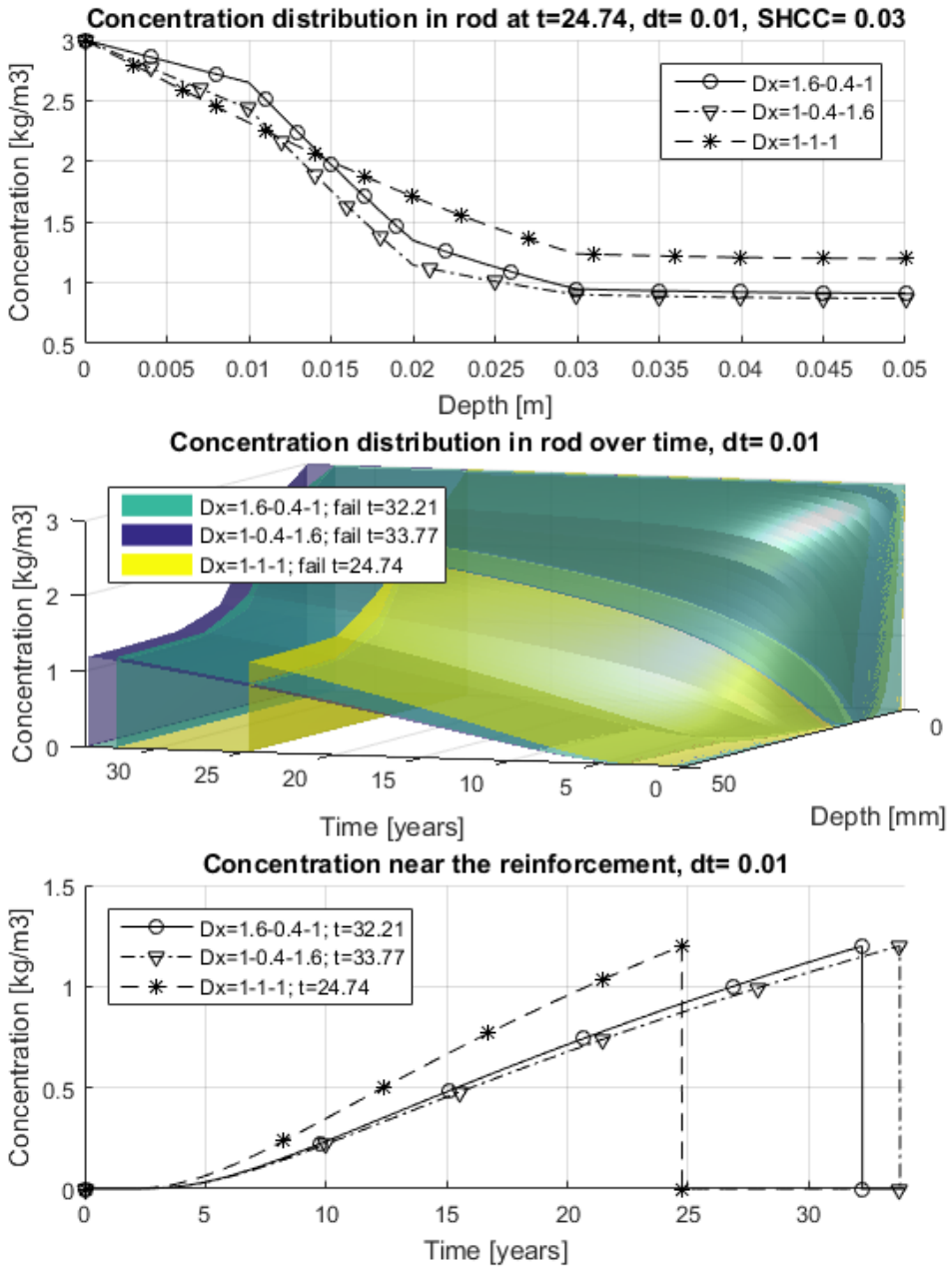

Fig. 4.1.8 Convex step wise function (Apparent diffusivity ratios 1.6:0.4:1.0)

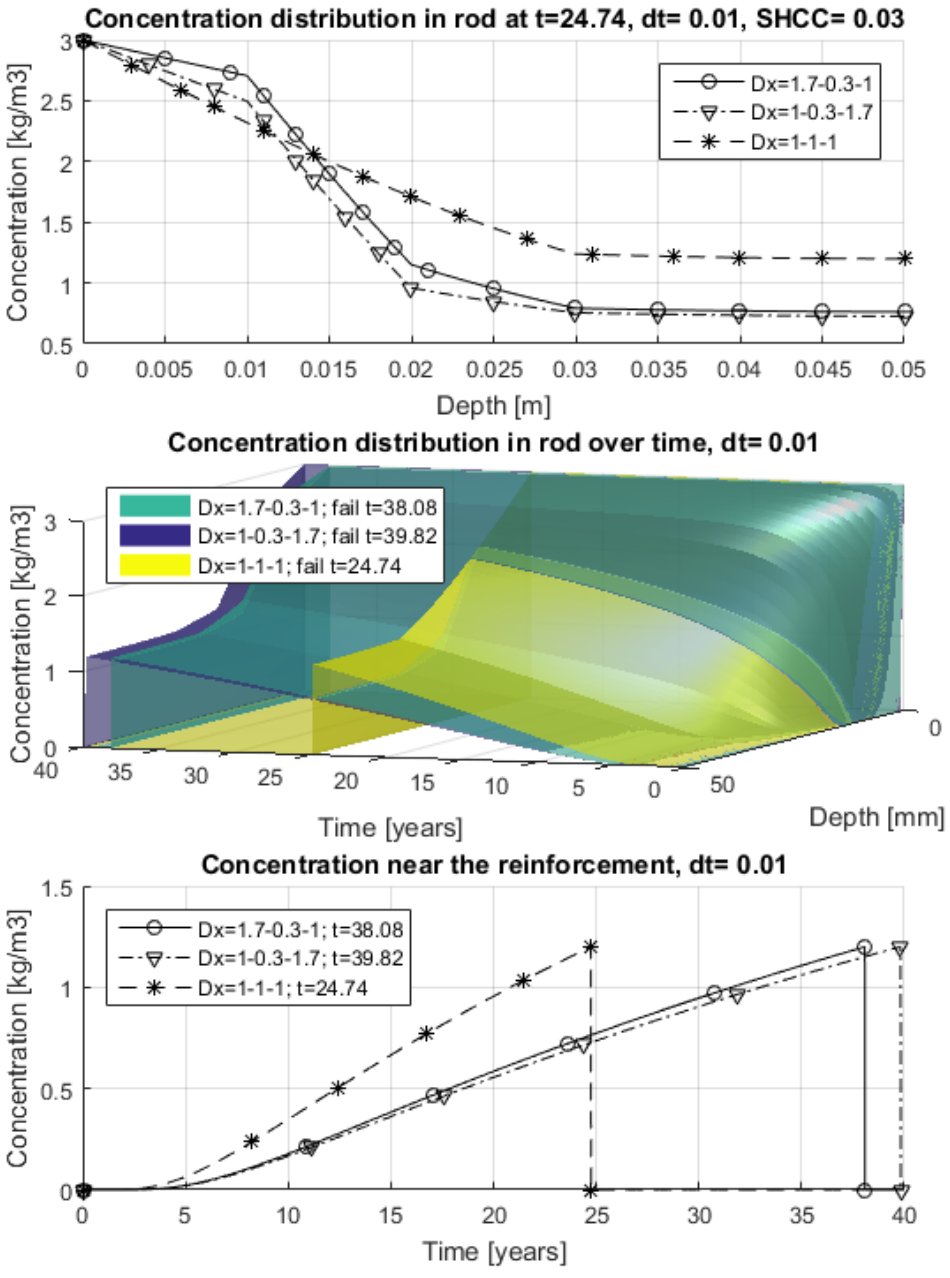

Fig. 4.1.9 Convex step wise function (Apparent diffusivity ratios 1.7:0.3:1.0)

0.5-1-1.5 it's improvement of +26% of durability time, compared to the homogeneous layer. With steeper gradient, i.e. 0.3-1-1.7 the improvement is +70% of durability time, compared to the homogeneous layer.

4.1.5 Concave function approximation, no seal at the position of rebar

Concave diffusivity distribution is presented on Fig.4.1.13 to Fig.4.1.15, different gradients are presented. The base durability time of the homogeneous layer is 62.82years. Gradients with the best performing layer on the surface are showing the best improvement of durability time. For the gradient 0.5-1.5-1.0 it's improvement of +31% of durability time, compared to the homogeneous layer. With steeper gradient, i.e. 0.3-1.7-1.0 the improvement is +69% of durability time, compared to the homogeneous layer.

4.1.6 Convex function approximation, no seal at the position of rebar

Convex diffusivity distribution is presented on Fig.4.1.16 to Fig.4.1.18, different gradients are presented. The base durability time of the homogeneous layer is 62.82years. Gradients with the best performing layer on the surface are showing the best improvement of durability time. For the gradient 1.0-0.5-1.5 it's improvement of +19% of durability time, compared to the homogeneous layer. With steeper gradient, i.e. 1.0-0.3-1.7 the improvement is +59% of durability time, compared to the homogeneous layer.

Model is improved for testing all possible combinations with defined minimum and maximum limit, step size, and constant average value, Fig.4.1.19. Values at the ternary plot are limited by the current achievable minimum diffusivity and a maximum diffusivity from test data. Three main cases are highlighted, showing the actual distribution of relative diffusivity in three layers. On the horizontal axis, a layer number 1 is assumed to be placed on the interface, and layer number 3 is the surface layer. On a vertical axis, it is a ratio of diffusivity normalized to the mean value of diffusivity, i.e. 0.25cm^2/year. Minimum ratio of 0.3 is equal to 0.075cm^2/year, and the maximum

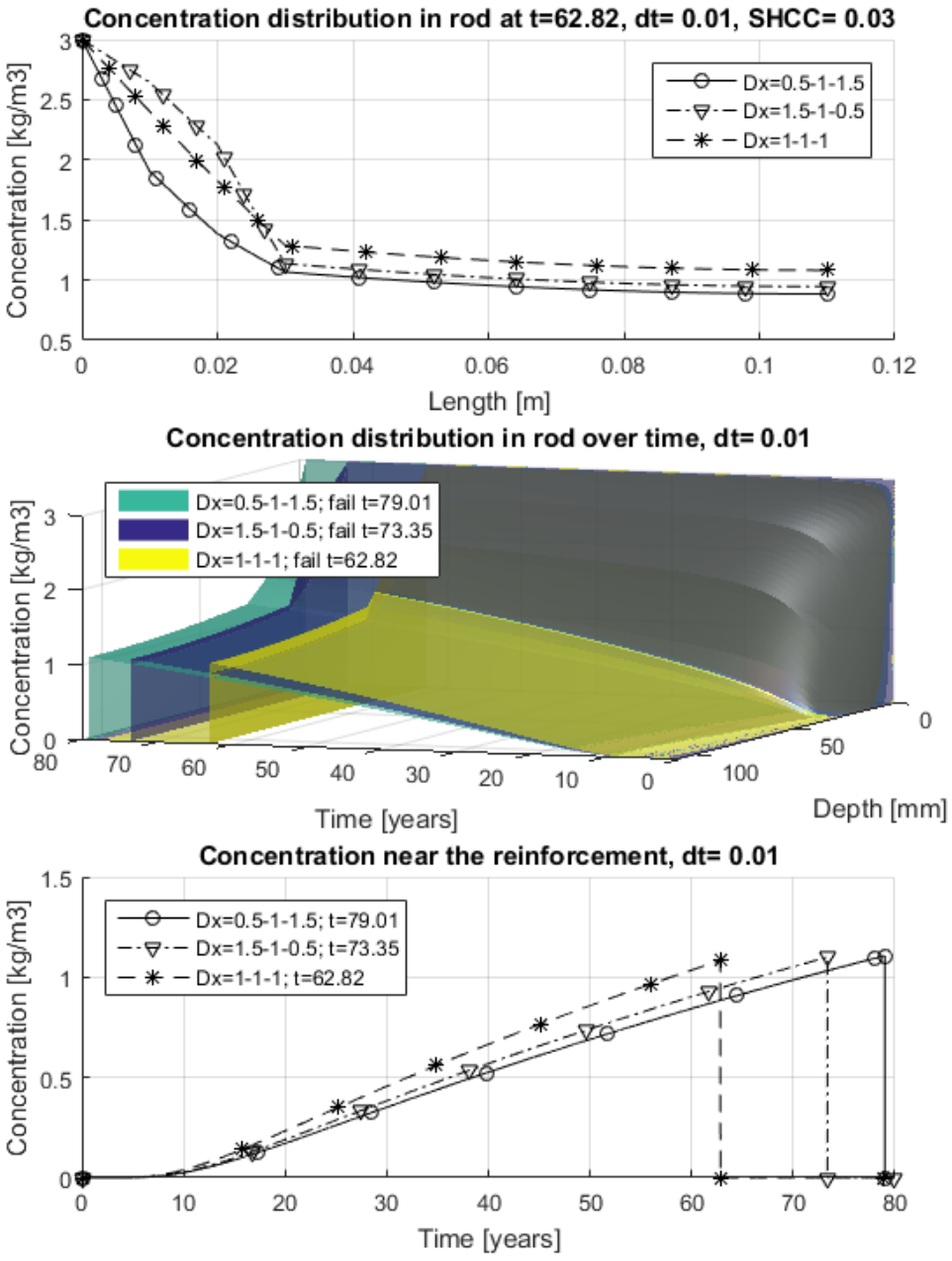

Fig. 4.1.10 Linear step wise function (Apparent diffusivity ratios 0.5:1.0:1.5)

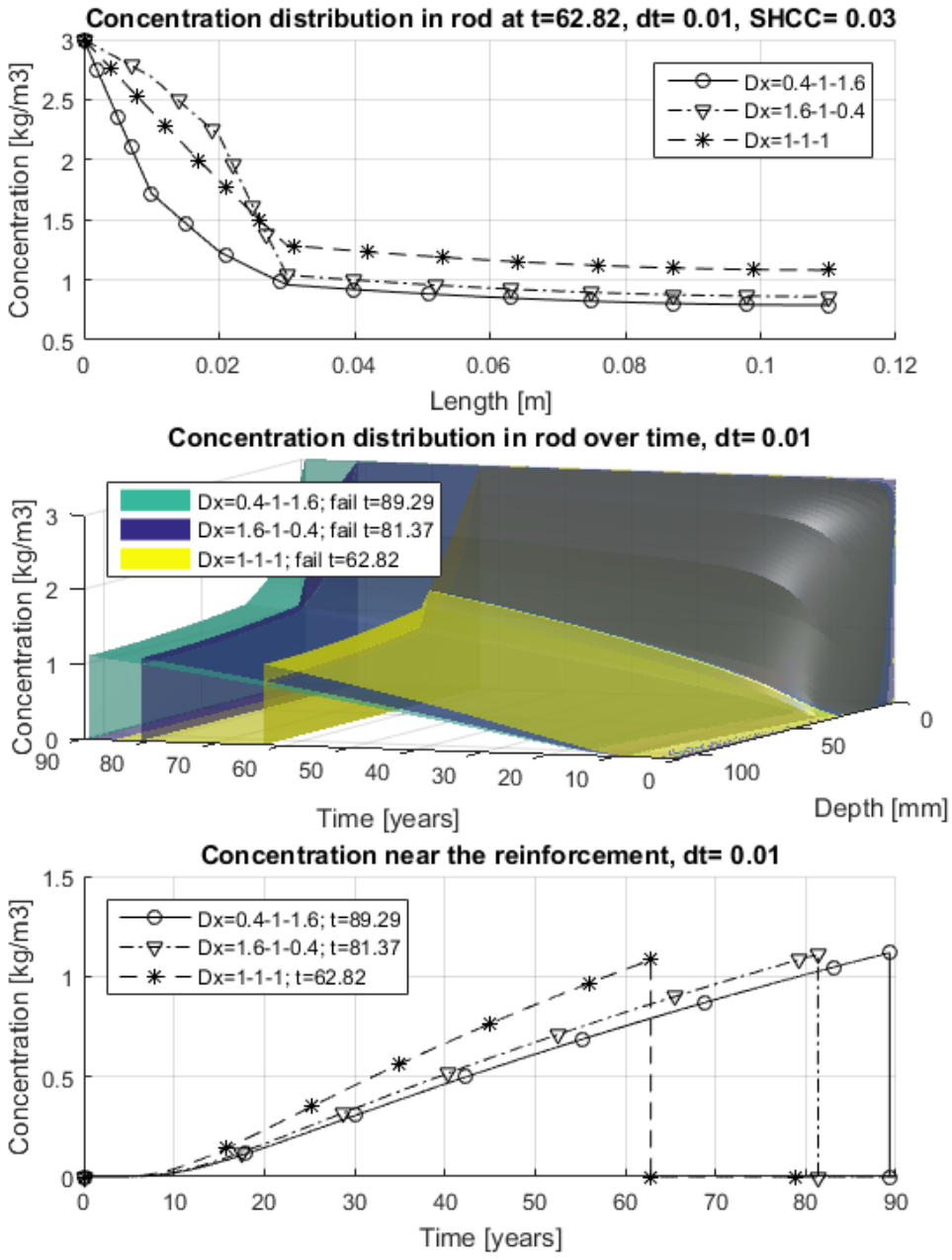

Fig. 4.1.11 Linear step wise function (Apparent diffusivity ratios 0.4:1.0:1.6)

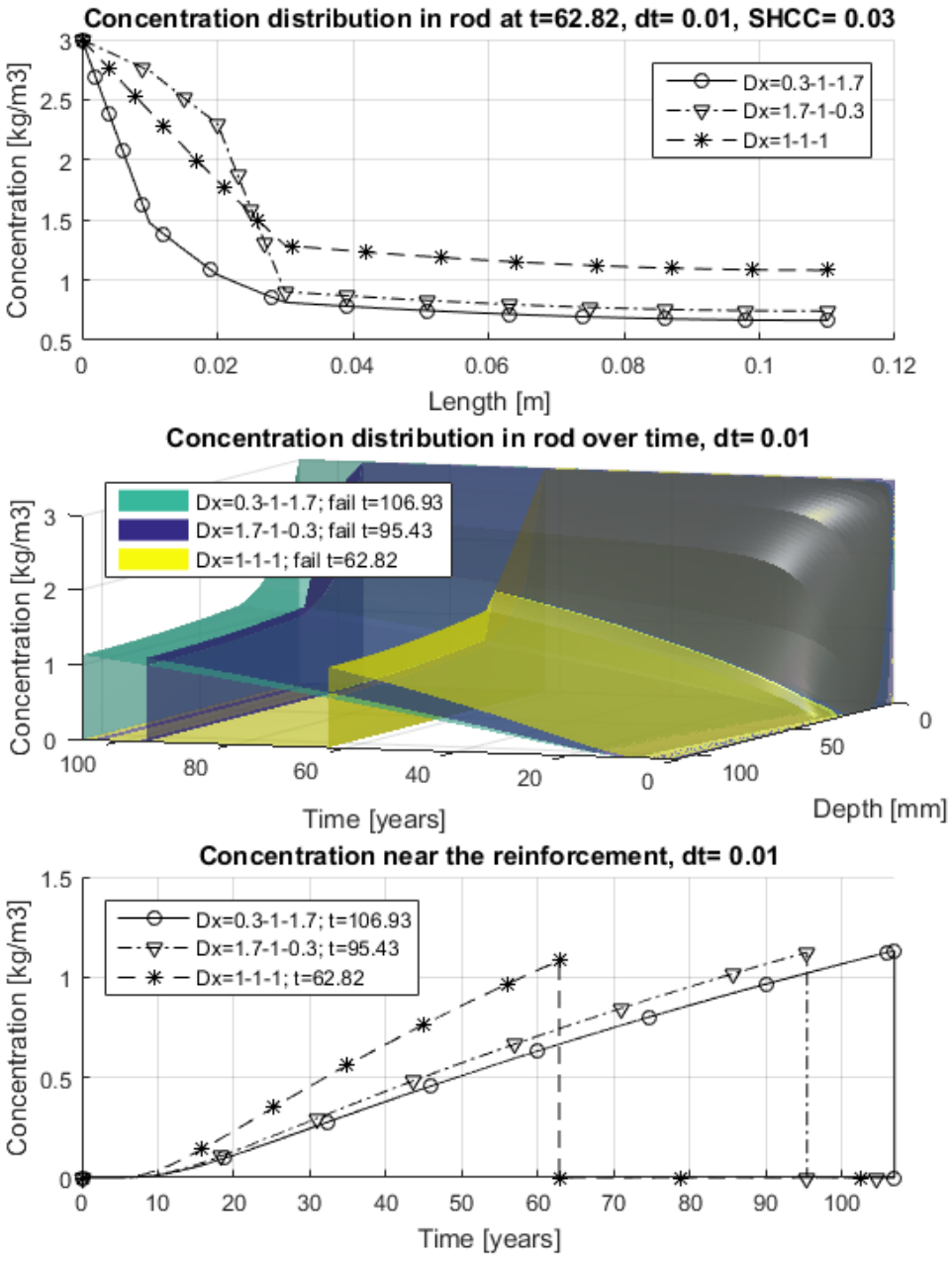

Fig. 4.1.12 Linear step wise function (Apparent diffusivity ratios 0.3:1.0:1.7)

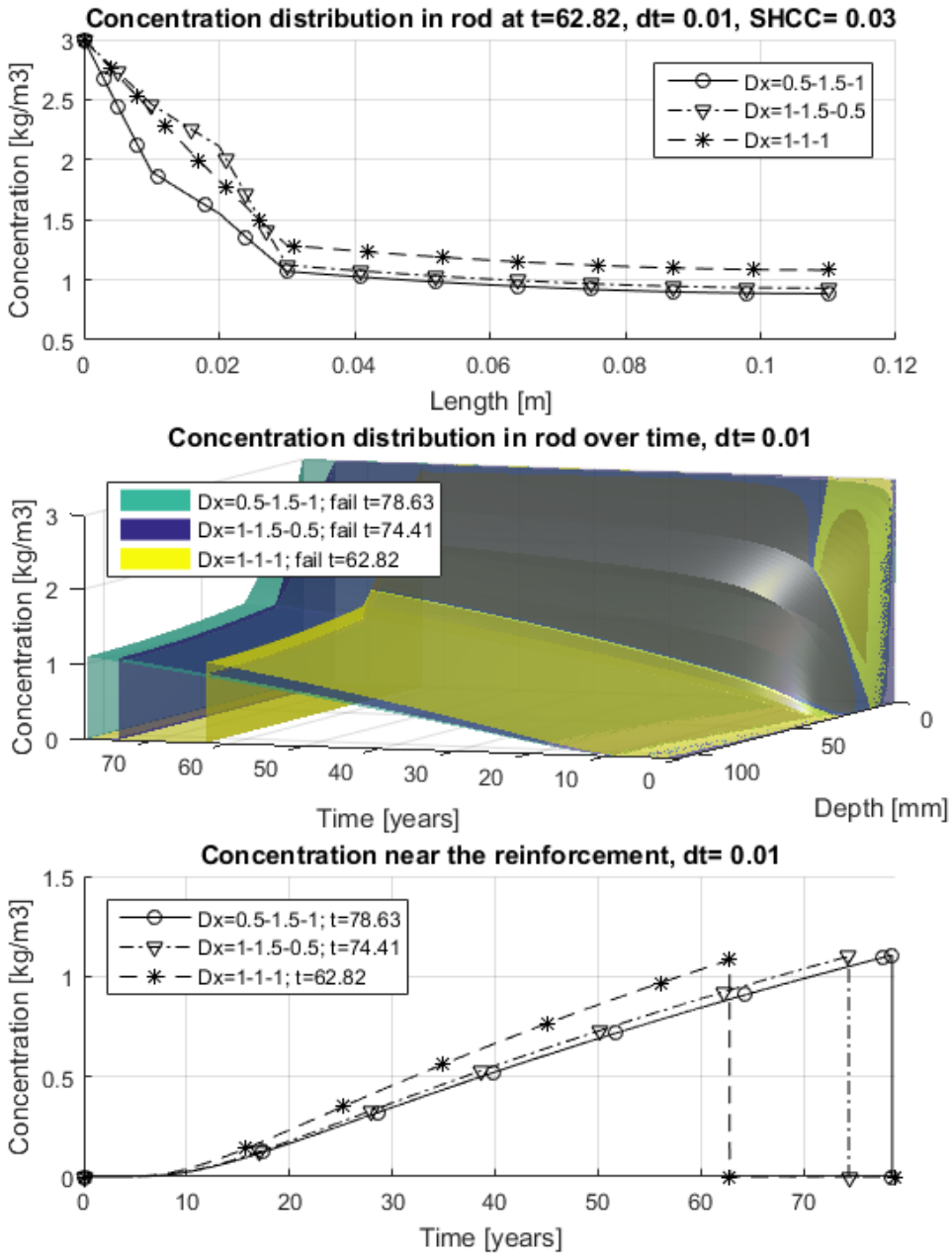

Fig. 4.1.13 Concave step wise function (Apparent diffusivity ratios 0.5:1.5:1.0)

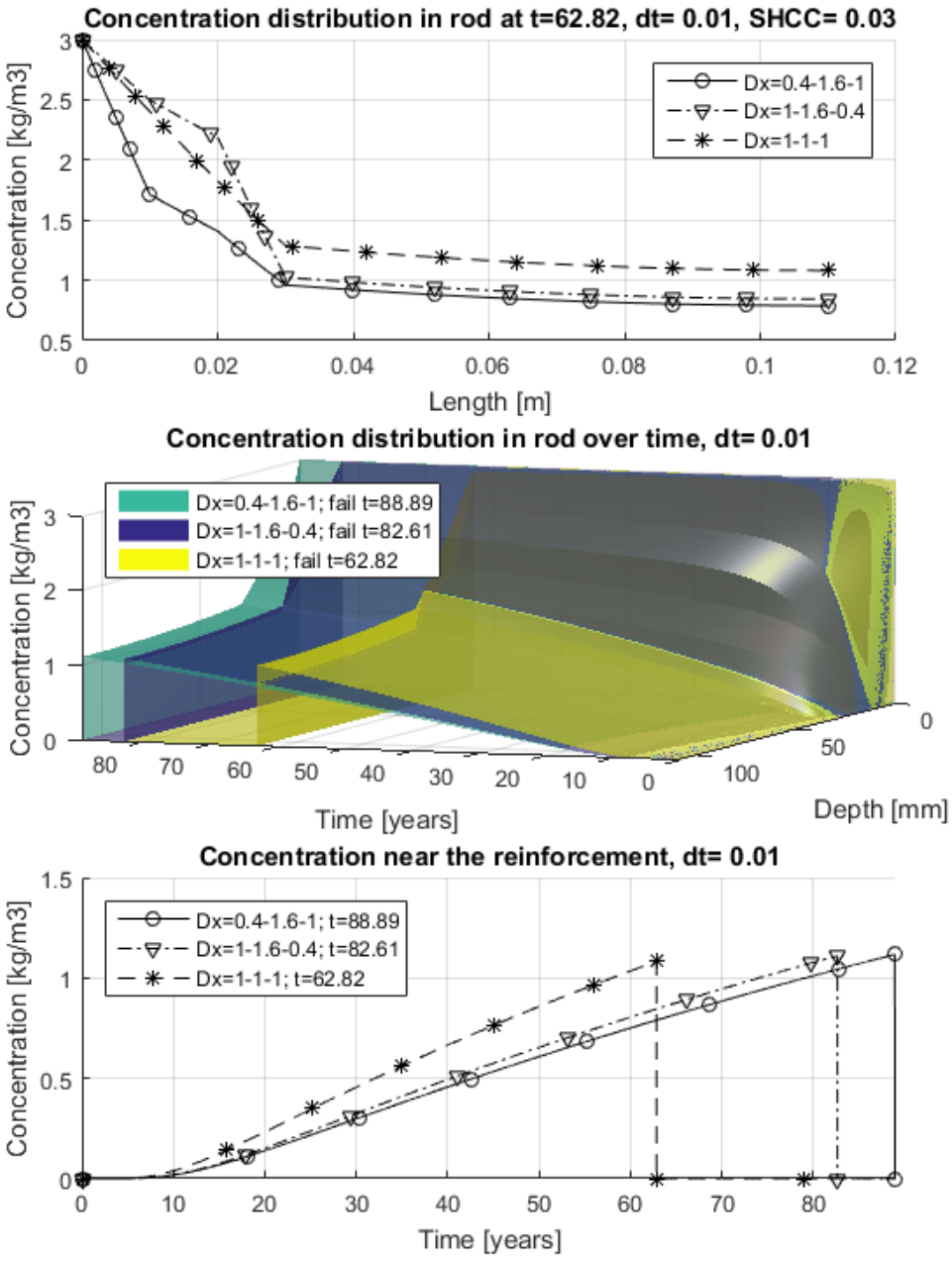

Fig. 4.1.14 Concave step wise function (Apparent diffusivity ratios 0.4:1.6:1.0)

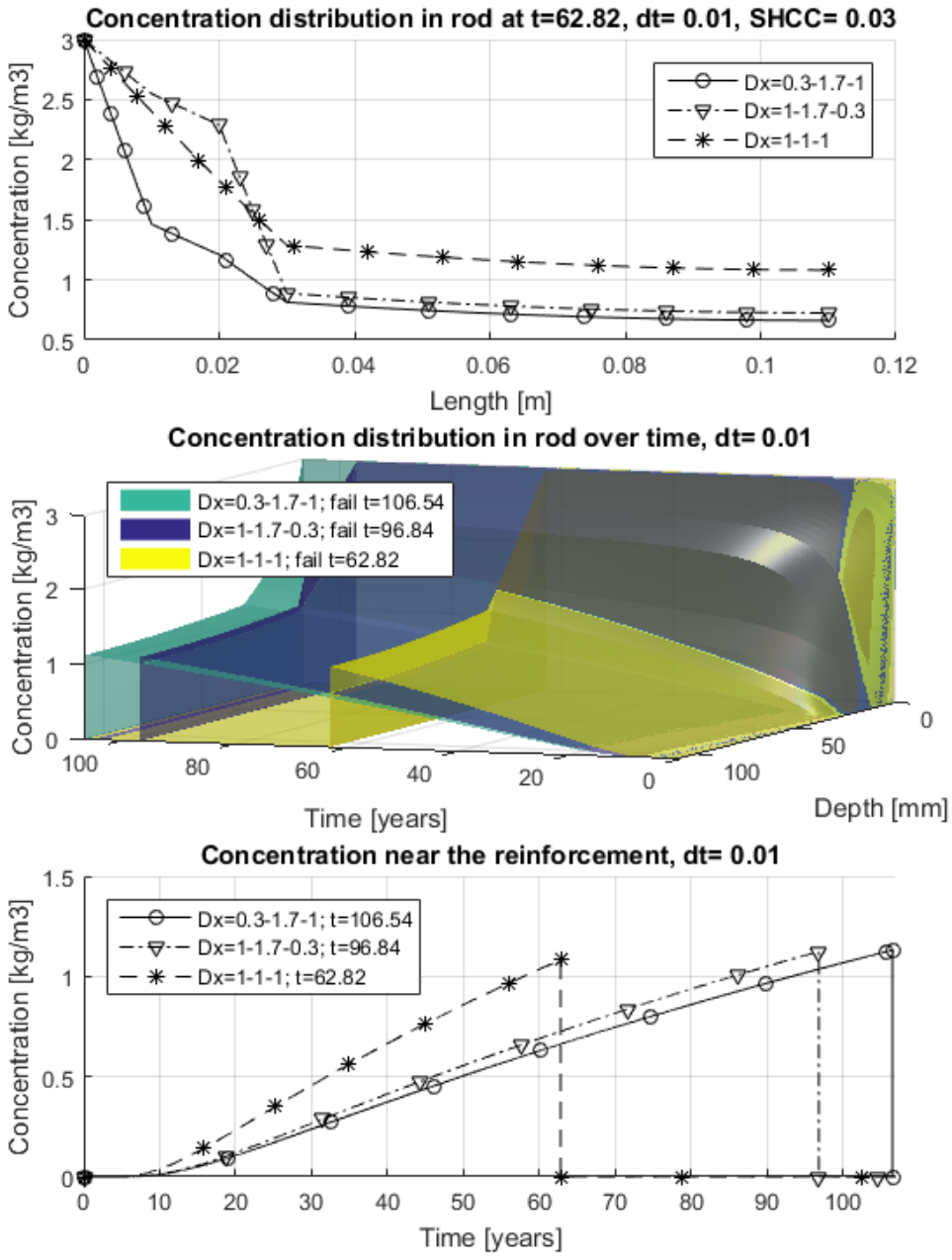

Fig. 4.1.15 Concave step wise function (Apparent diffusivity ratios 0.3:1.7:1.0)

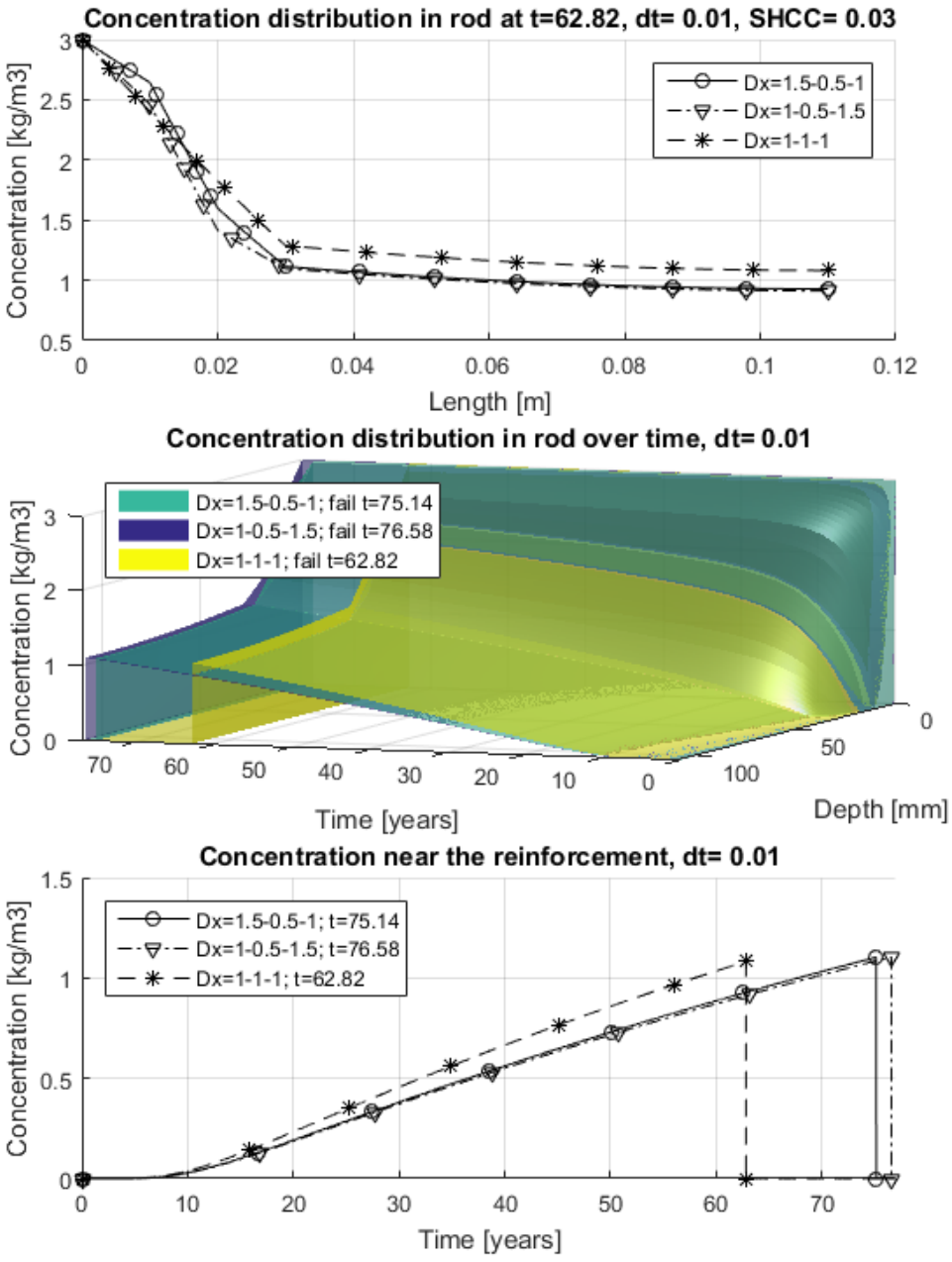

Fig. 4.1.16 Convex step wise function (Apparent diffusivity ratios 1.5:0.5:1.0)

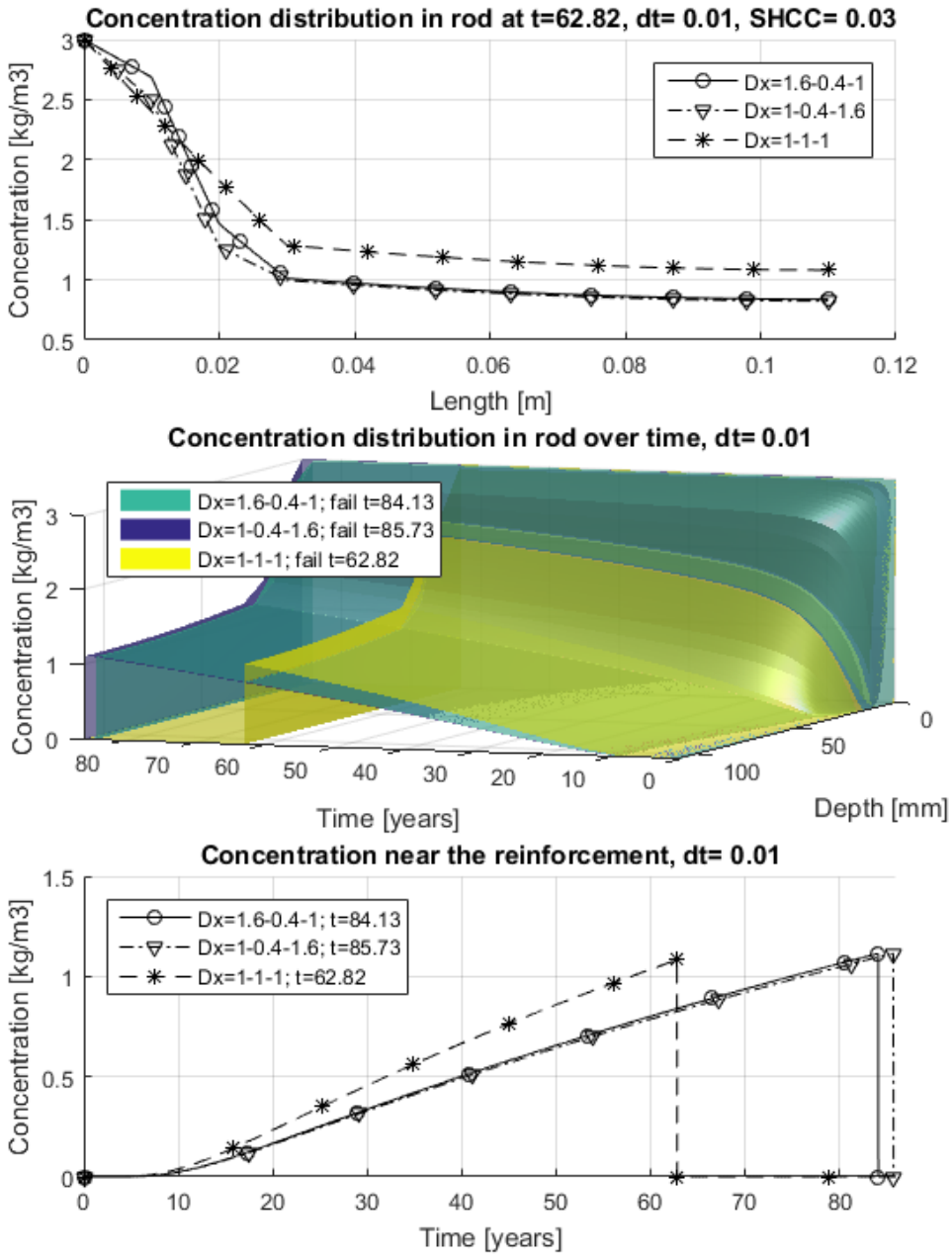

Fig. 4.1.17 Convex step wise function (Apparent diffusivity ratios 1.6:0.4:1.0)

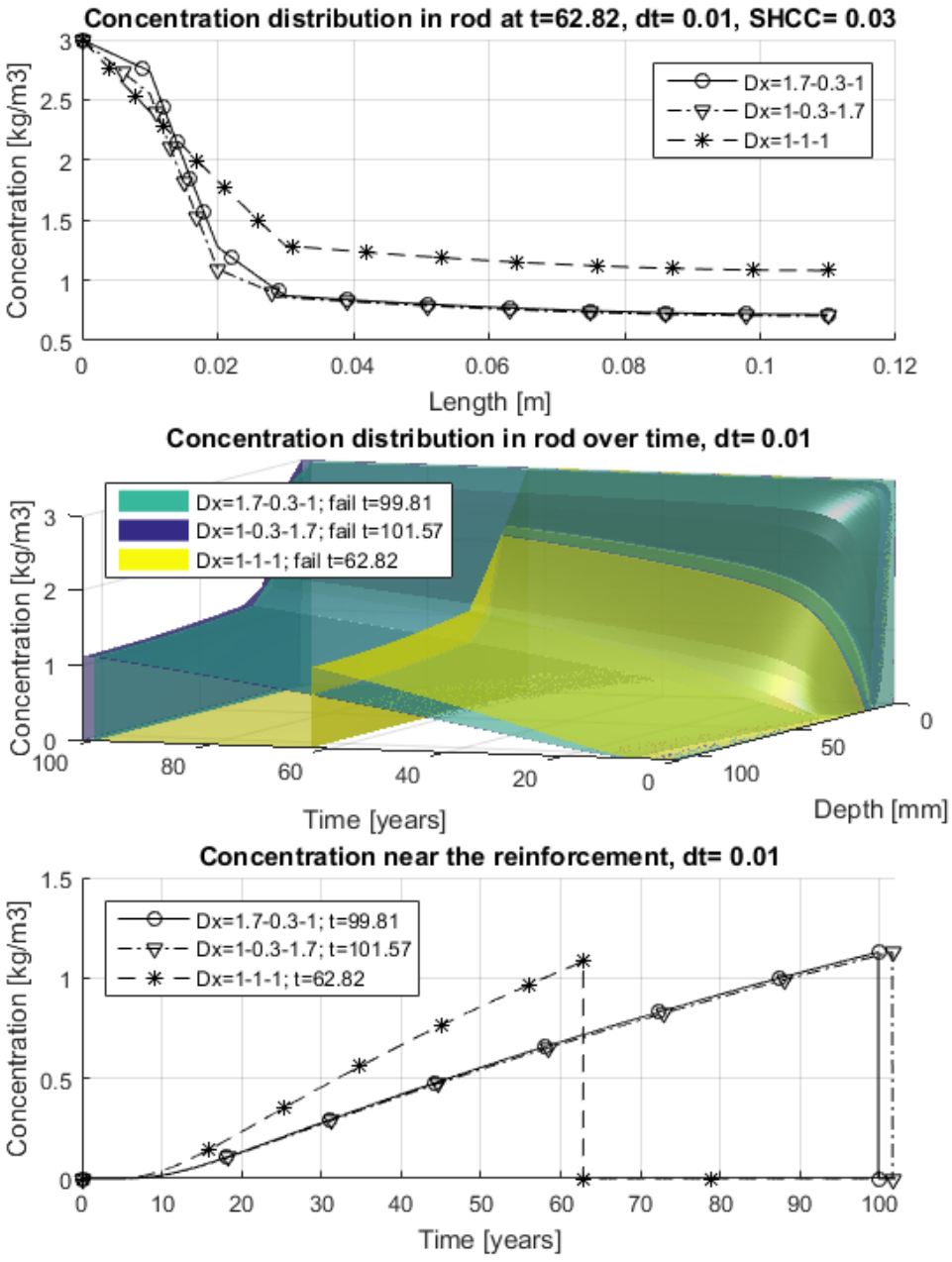

Fig. 4.1.18 Convex step wise function (Apparent diffusivity ratios 1.7:0.3:1.0)

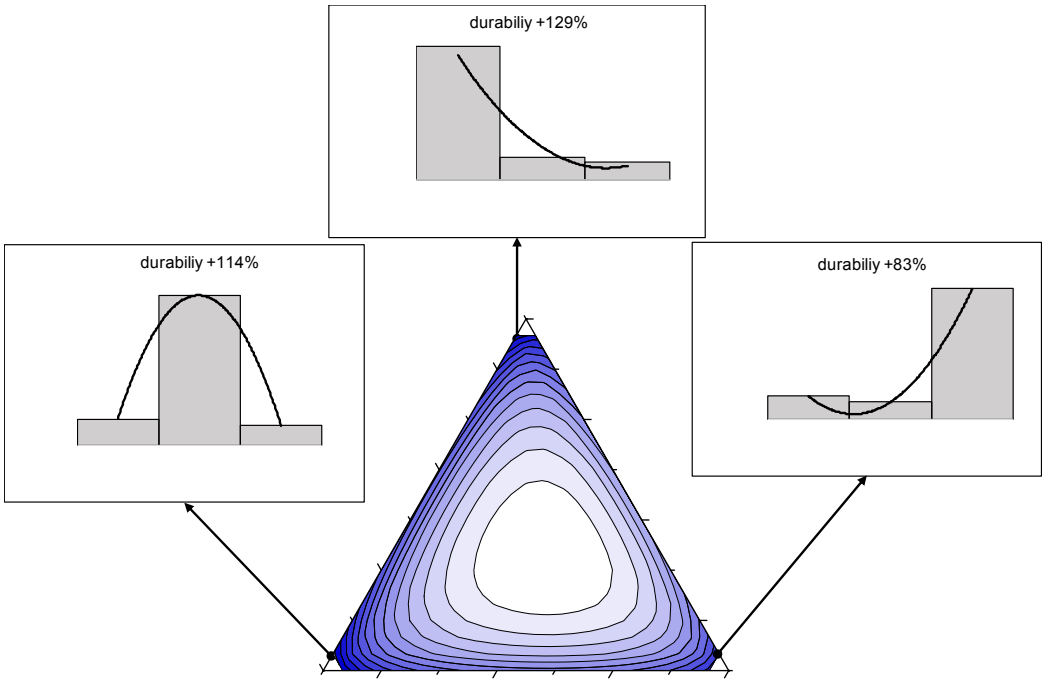

Fig. 4.1.19 Optimization for three layers of SHCC forming FGM, durability improvement for different diffusivity variations, centre is homogeneous.

ratio of 2.3 is equal to 0.575cm^2/year. From the figure it's clear, that high gradient can increase expected durability of a structure. This distribution suggest by a rather symmetric shape, that location of the layer with lowest diffusivity is of lower importance, but it was shown, that effect of cracks can magnify the importance of layer location, i.e. the best quality layer should be placed in the location with the lowest deterioration. In case of constant or no deterioration rate throughout the FGM structure, it is beneficial to place the best performing layer on the surface.

4.2 Crack distribution and layering

For this analysis, three kinds of SHCC materials, noted as H (high quality), N (normal quality) and L (low quality) were modelled. A constant crack width was assumed to penetrate from the exposed surface to the bar location. Three kinds of crack width are examined. First, a constant crack width of 100μm, i.e., average maximum crack width caused by applied service load (strain, $\epsilon = 5.0 \times 10^{-4}$); second, a constant crack width of 100μm; and last, a varied crack width ($50 - 100\mu$m, where smaller crack width is placed near the reinforcing steel bar) (see Fig 4.2.1).

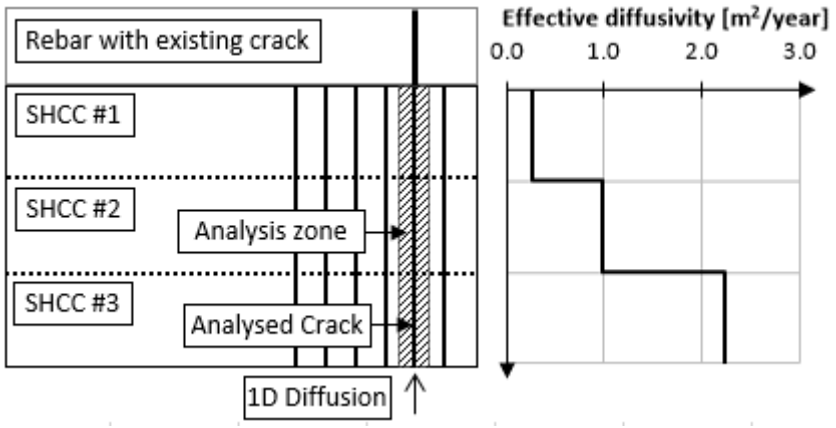

Fig. 4.2.1 The model for diffusion analysis and an example of the positive FG-SHCC

It is assumed, that crack width of SHCC subjected to an average strain value of $\epsilon = 5.0 \times 10^{-4}$ is different for each material due to different fibre content. Three different layering are examined: 30mm of homogeneous SHCC, i.e., three layers of material N. FG-SHCC layer is created by combining different quality layers to form a step-wise linear distribution function of apparent diffusivity. A positive gradient (see Fig 4.2.1) is formed by layers in order L-N-H, i.e., high quality on the surface, and a negative gradient is formed by layers in order H-N-L, i.e., high quality on near the reinforcing steel bar.

The size of the 1D analysed zone is defined by crack spacing in one direction and thickness of FG-SHCC in second direction. Each layer of SHCC is 10mm thick and the crack propagates straight through the layers to the reinforcement location. A reinforcement bar is not modelled and durability is calculated as the time needed for corrosion initiation. Diffusion analysis is governed by Fick's law, numerically solved using a Crank-Nicolson finite difference method in time and FEM in space. Boundary conditions are assumed as in a very severe environment, defined by allowable crack width $0.0035c$, where c is the cover thickness, i.e. 0.21mm.

4.3 Diffusion of chloride ions into cracked SHCC, 60mm FG-SHCC

Layer thickness in this model is increased to 60mm as a case of the maximum thickness, to study whether the effect of FGM will differ from the case of 15mm FG-SHCC

Table 4.1 Material parameters for chloride diffusion in SHCC

Quality	Chloride attack					
	H	N	L	H	N	L
Condition	Sound			Cracked		
w/c ratio [-]	0.30	0.45	0.60	0.30	0.45	0.60
D_0 crack coefficient [m^2/year]	1.47	1.91	2.23	1.47	1.91	2.23
Effective diffusivity [m^2/year]	0.50	1.92	4.26	4.45	7.07	10.27
Penetration depth [mm] [37]	*4.50*	8.85	*13.20*	13.50	17.00	*20.50*

thickness. Using assumed crack and strain values, chloride ion diffusion analysis of cracked SHCC is carried out. The diffusion parameter is defined as [44]

$$D_{eff} = D_k + D_0 log_{10}\left(\epsilon w^2\right) \tag{4.3.1}$$

where D_k [m^2/year] is diffusivity of uncracked SHCC, D_0 [m^2/year] is a parameter for cracks in SHCC, ϵ[%] is average strain of SHCC and w [μm] is an average crack width of SHCC.

Parameter D_0 is calculated by fitting the logarithmic relationship of equation Eq.4.3.1 between uncracked and cracked (max crack width 100μm) SHCC test data [37] presented in Table 4.1. Portland cement mixture has 1.5% by volume of PVA fibres, 12mm long and 12μm in diameter. Penetration depths measured at the crack location are presented by underlined italicized text. Apparent diffusivity of cracked and uncracked SHCC is obtained by carrying out diffusion analysis using constant chloride binding capacity, known boundary conditions of the test and duration of exposure. Penetration depth values not available from the test data were added by interpolation and extrapolation.

Design chloride ion permeability from equation 4.3.1 is presented in Fig. 4.3.1. It is assumed that at crack width larger than 100mm, the diffusivity of different materials is reaching an identical value, because the diffusion is driven mainly by the opened crack, and the material matrix effect is of low significance. Penetration of chloride ions in the crack, compared to the penetration of CO_2, is much smaller. It should be noted, that another researcher achieved much larger chloride penetration in cracked

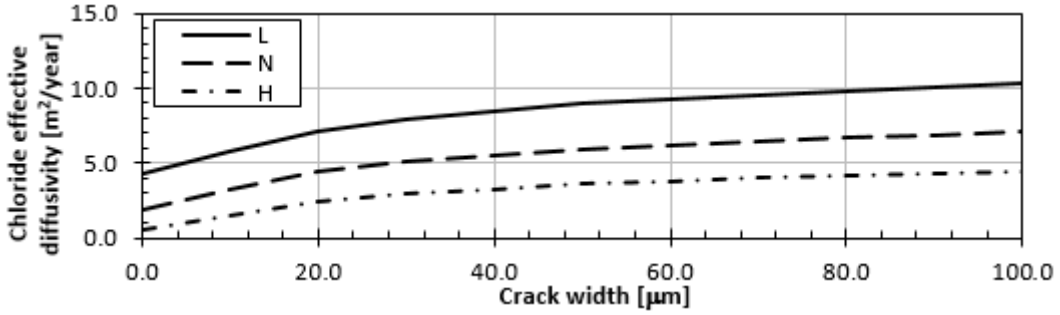

Fig. 4.3.1 Effect of crack width in SHCC on chloride apparent diffusivity

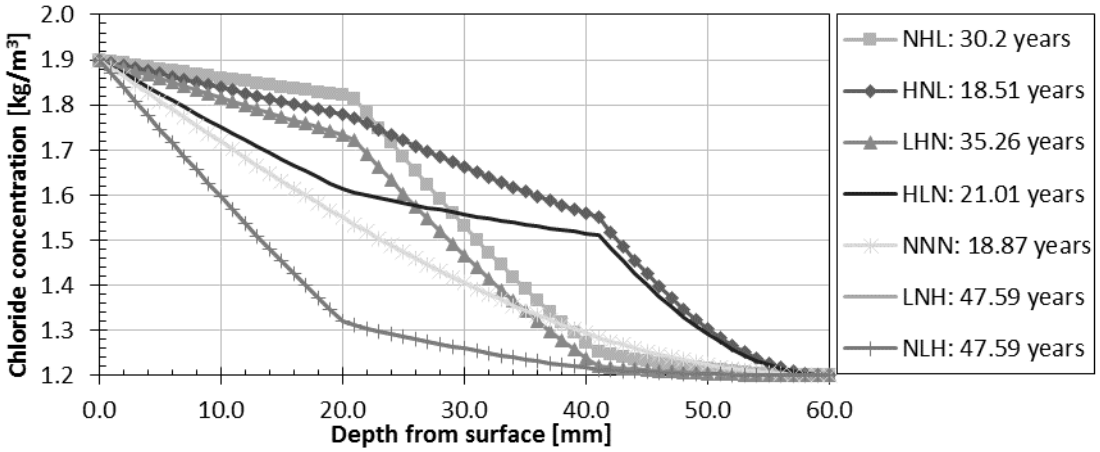

Fig. 4.3.2 Spatial distribution of chloride concentration in sound SHCC

area compared to uncracked area, e.g., 10.6 times larger penetration in crack width of less than 100μm, [11]. Data to use in this analysis are selected due to testing both chloride attack and carbonation, using the same material [37].

4.3.1 Chloride attack

Results of diffusion analysis of FG-SHCC are presented in Fig. 4.3.2, Fig. 4.3.3. and Fig. 4.3.4. Spatial distribution of chloride concentration in Fig. 4.3.2. shows the durability of different FG-SHCC layers order, including a homogeneous case. Highest durability time can be achieved mainly by placing the layer of the highest quality, i.e., layer H on the exposed surface, followed by layer N and lastly layer L. Same performance was shown by layering LNH, noted from the bar location to the exposed surface. Effect of FG material is for this case very high. Difference between the best and worst performing layering is 257%. When compared to the homogeneous layer, the performance increase is 252%.

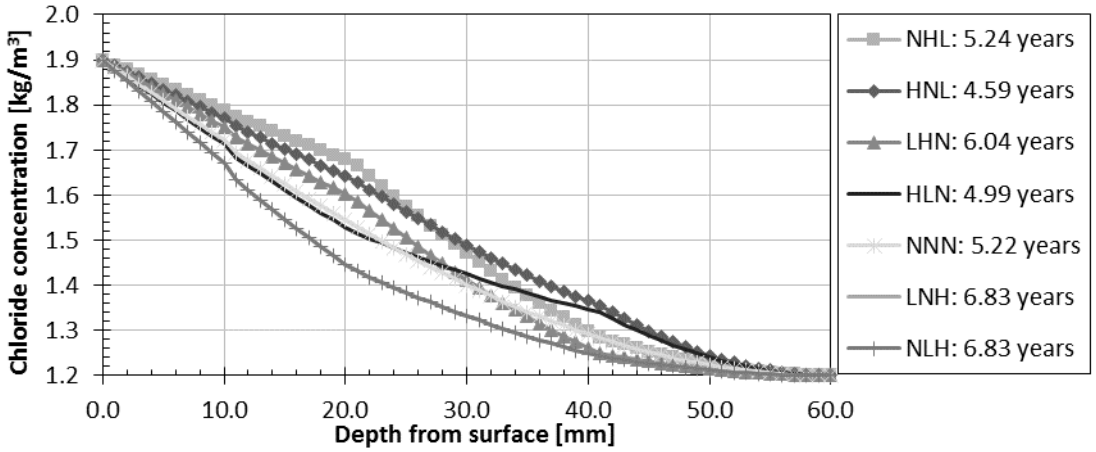

Fig. 4.3.3 Spatial distribution of chloride concentration in $0.05mm$ cracked SHCC

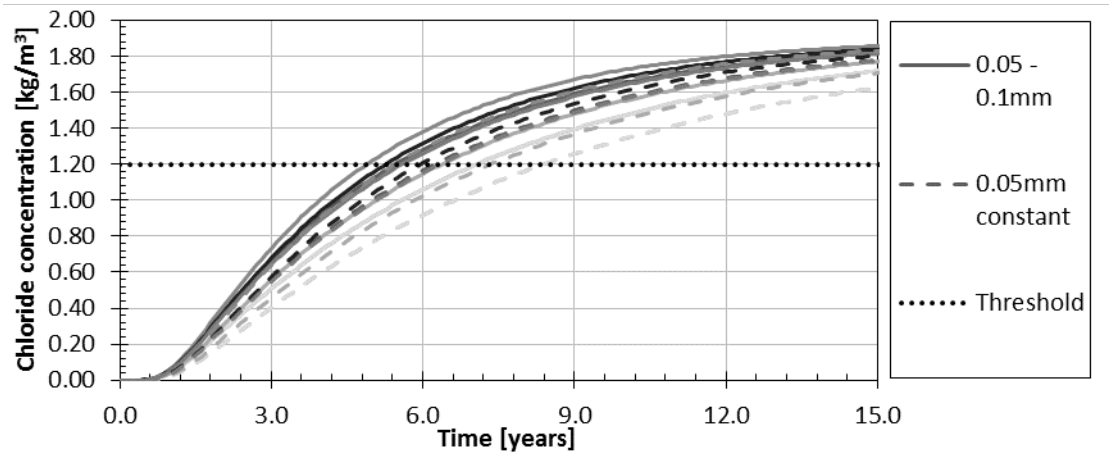

Fig. 4.3.4 Accumulation of Cl ions at the rebar location in cracked SHCC

In Fig. 4.3.3., distributions of chloride concentration in FG-SHCC with 100μm crack width are presented. Effect of FG-SHCC is compared to the effect of a much smaller crack. This effect can be observed as the size of the area between the top and bottom distribution. In some finite crack limit the effect of FG-SHCC will be zero, i.e., the area size will be zero as well. Highest durability is achieved by the same kind of layering as in the sound material, i.e. LNH offers the best durability. Difference between the best and worst performing layering is 61% and compared to homogeneous material the difference is 30. Even though the beneficial behaviour of FG-SHCC is highly reduced by cracks, the effect is not negligible.

Lastly, in Fig. 4.3.4., accumulation of chloride ions at the location of the rebar is presented. Two crack width options are compared, a constant crack width of 50μm and a variable crack width of 50μm to 100μm, with wider opening facing the environment. The effect of the crack width can be seen, as the constant crack width of 50μm shows better performance compared to the variable crack width. Order of best performing layers are for both crack width options identical to the constant 100μm and uncracked FG-SHCC.

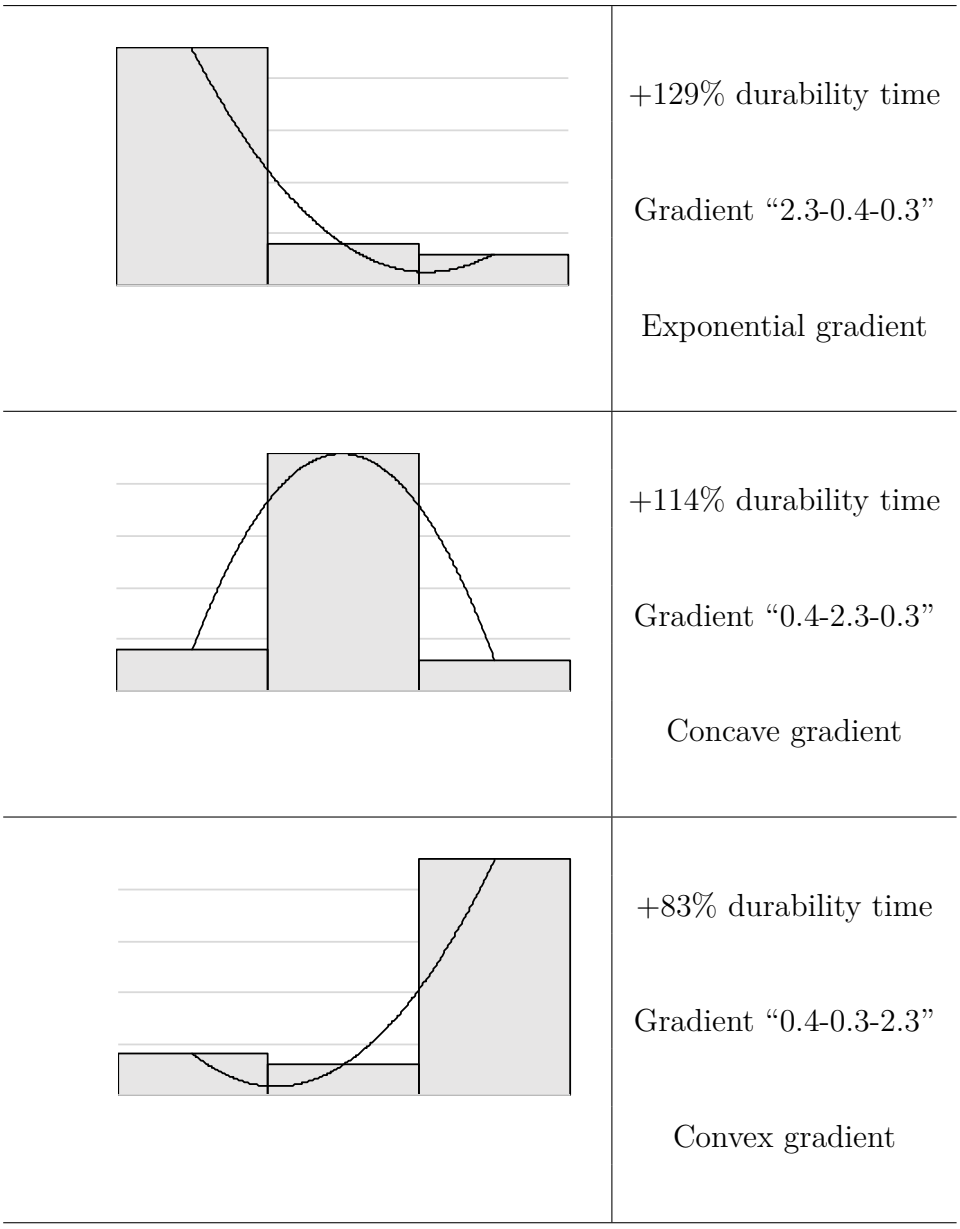

Fig. 4.4.1 FG-SHCC diffusivity steep gradients, use of the current best material

4.4 Remarks

As can be seen on Fig. 4.1.19, the rate of improvement is limited by the boundary condition itself, i.e. limited by the currently best achievable material. In all cases, higher gradient is providing the highest durability improvement. The exponential and convex gradient diffusivity distribution could be simplified into two layers of different thickness, Fig.4.4.1. The highest durability improvement is achieved by the exponential gradient with the best material on the surface.

Chapter 5

Optimized FG-SHCC multi-layer structure for chloride diffusion resistance

Use of the random trial and error method for optimization of FG-SHCC to increase durability or reduce cost of repair layer is studied. Compared to ordinary RC, formed micro-cracks increase resistance to moisture, gas and salt penetration. Scheme of optimized FG-SHCC is presented in Fig.5.0.1, studied at two strain levels, i.e., first linear distribution from 1.2% to 0.4% of average strain and second a uniform distribution at 1.2%.

5.1 Strain distribution under localized crack

The crack width in FG-SHCC is determined from fibre content and average strain values. FEM analysis is used to obtain average strain of specimen loaded by a live load value. Stress increase form a live load in a reinforcement is generally around 100MPa, i.e., with Young's modulus of a steel at 200GPa, expected strain from a live load is $\Delta u = 5.0 \times 10^{-4} m$. Strain at the prescribed displacement is presented in Fig.5.1.1 for three different order of layers consisted of three materials; H, N, L, i.e. high (2.5%),

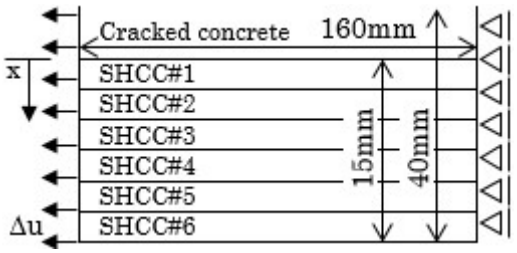

Fig. 5.0.1 Schematic representation of FG-SHCC repair material

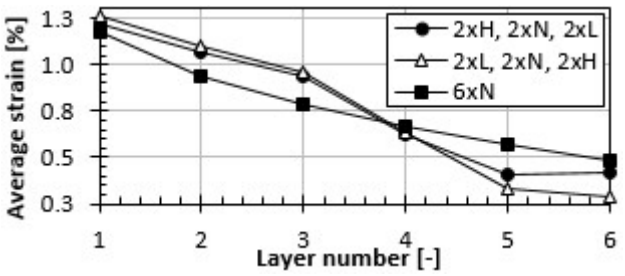

Fig. 5.1.1 FG-SHCC average strain from uniaxial tension

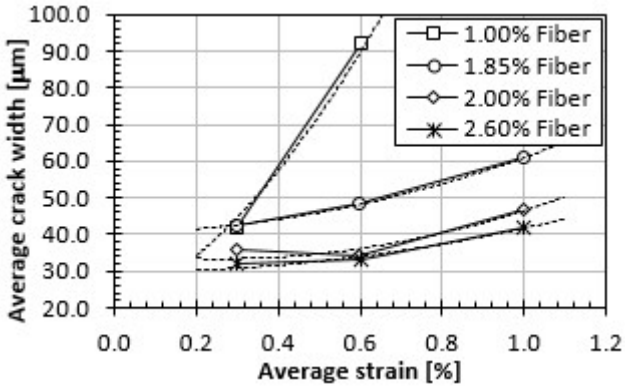

Fig. 5.1.2 Effect of fibres on crack width of SHCC [75]

normal (2.0%) and low (1.5%) fibre content, and the average values are used in further analysis. Because average crack width has a dominant effect on the diffusivity, it is assumed, that higher fibre content causes lower diffusivity due to finer cracking despite the higher porosity on ITZ (Interfacial Transition Zone) between a fibre and matrix.

Fig.5.1.2 shows the effect of fibres on SHCC cracking [75]. Low fibre content has very limited strain of 0.6%, and so using this material directly on the interface could lead to a crack localization before reaching a designed load. The amount of fibres in the SHCC layer near the crack was set so that the predicted average crack width would not be larger than 100μm, that is generally the upper limit of crack width formed in average SHCC.

5.2 Diffusion of chloride ions into cracked SHCC

From obtained strain values and fibre content of respective SHCC layer, average crack width and diffusivity of 15mm FG-SHCC are calculated. Using the test data [44, 53], a parameter D_0 (used range of 0.062 to 0.228) describing the effect of cracks in SHCC can be obtained using equation for apparent diffusivity defined in Eq. 4.3.1[44]. Crack

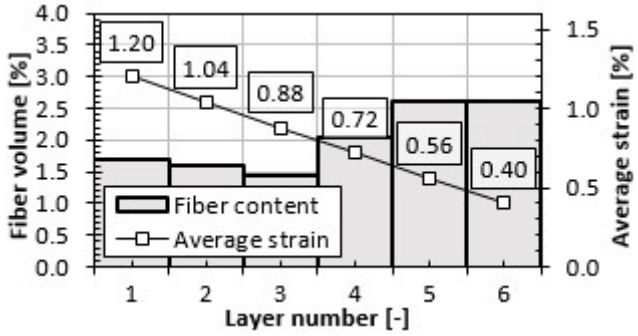

Fig. 5.2.1 Fibre distribution of SHCC layers optimized for the decreasing strain

width effect on diffusivity is presented in Fig.4.3.1.

Optimization of FG-SHCC layers, utilizing the random trial and error method, shows a beneficial behaviour compared to homogeneous SHCC. Highest durability (T_{dur}) is achieved by two layers of SHCC, one with low apparent diffusivity (0.24 cm^2/year, 2.6% fibre) on the surface and other with an average apparent diffusivity (1.44 cm^2/year, 1.4% fibre) on the concrete interface. This FG-SHCC shows 156% of durability of homogeneous SHCC, but with a risk of a localized crack due to the stress concentration near the crack.

Following the crack width limit of 100μm, fibre content near the interface is then set to 1.7%. Material with the lowest diffusivity is placed on the surface acting as a shield against environmental effects. Ideal FG-SHCC layer order, with respect to minimal fibre content on the interface is shown in Table 5.1 with the code S1. This layer shows 136% durability of homogeneous layer at identical strain distribution and total fibre content. Schematic representation of fibre distribution and average strain is shown in Fig.5.2.1. The same durability as with homogeneous layer, i.e., equal distribution of 2% of fibre and identical strain values, is achieved with 1.78% of fibre content using 2.5mm SHCC layers with 1.7%, 1.6%, 1.45%, 1.2%, 2.3 and 2.4% of fibre content respectively in direction of x.

FG-SHCC designed for high uniform average strain of 1.2% is shown in Table 5.1, code S2. This FGM shows even at larger strain 118% higher durability at the same fibre content. Schematic representation of fibre distribution and average strain is shown in Fig.5.2.2.

Table 5.1 Apparent diffusivity of SHCC and optimized FG-SHCC for different strain distributions S1 and S2

Function		Uniform		S1, Fig.5.2.1			S2, Fig.5.2.2	
Layer #	Strain ϵ [%]	Fibre [%]	D_{eff} [cm^2/year]	Fibre [%]	D_{eff} [cm^2/year]	Strain ϵ [%]	Fibre [%]	D_{eff} [cm^2/year]
1	1.20	2.00	0.698	1.70	1.061	1.2	1.70	1.061
2	1.04		0.666	1.60	1.149		1.70	1.061
3	0.88		0.644	1.45	1.284		1.70	1.061
4	0.72		0.628	2.05	0.605		1.70	1.061
5	0.56		0.614	2.60	0.251		2.60	0.290
6	0.40		0.602	2.60	0.239		2.60	0.290
T_{dur} :		10.30years		14.02years			12.12years	

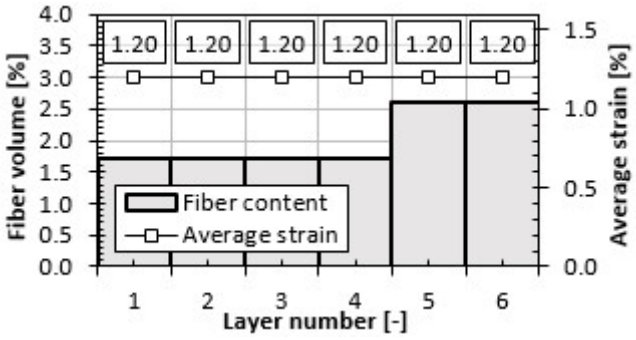

Fig. 5.2.2 Fibre distribution of SHCC layers optimized for the uniform strain

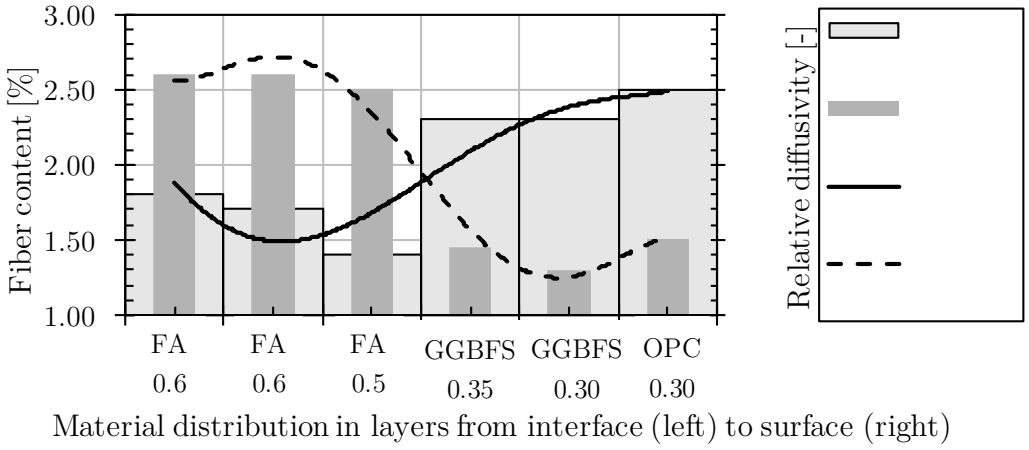

Fig. 5.3.1 Proposed FG-SHCC material for six layers

5.3 Function distribution

Proposed material distribution to form the FG-SHCC for high durability against scaling, diffusion and for a mechanical performance is presented in Fig.5.3.1. The surface layer use ordinary Portland cement for it's high resistance against salt scaling, followed by mixtures with additives, to reduce diffusivity. Fibre distribution followed same optimizing principle as in previous chapter.

5.4 Remarks

In the Chapter 3.8, it is suggested to use a material with high fracture energy on the interface to efficiently transfer stresses from crack. Here, to reduce a crack width on the surface, it's beneficial to use a material with high fibre content as a surface layer, because of narrower cracking, see Appendix E.1. Such a combination is possible, because a higher fibre content is not necessarily on its own a guarantee of high fracture energy, due to e.g. possibly low initial cracking strength, or low bond strength between fibres and matrix. The fibre content gradient formed by 3^{rd} order polynomial function is presented in Fig. 5.4.1.

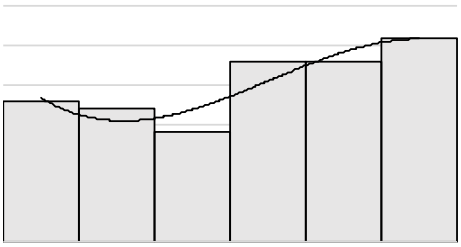

Variable strain 1.2-0.4%:
+36% durability time

Constant strain 1.2%:
+18% durability time

Fibre content layer 1∼6:
1.8-1.7-1.4-2.3-2.3-2.6 [%]

3^{rd} order polynomial gradient

Fig. 5.4.1 FG-SHCC gradient of fibre distribution

Chapter 6

FG-SHCC multi-layer structure for carbonation taking into account crack

Similar approach as in the case of chloride diffusion is used to calculate the apparent diffusivity of CO_2 in the SHCC. The relationship between the crack width in SHCC and apparent diffusivity is assumed to be linear. More test data is needed for detail relationship. Test data for the carbonation [37] reported zero carbonation penetration for the case of 30% W/C. Considering the analysis, a non-zero value must be used. Carbonation zone penetrated to almost the whole depth of a crack, compared to uncracked area, where penetration is very low. Relationship of crack width and apparent diffusivity for a crack location is presented in Fig. 6.0.1. apparent diffusivity values of uncracked SHCC are within the range of mortar samples [38]. Material parameters for carbonation of SHCC are summarized in Table 6.1.

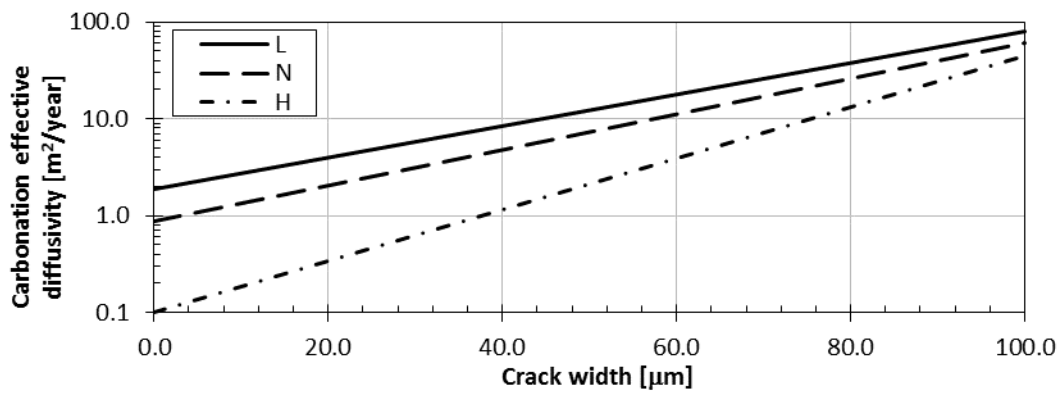

Fig. 6.0.1 Effect of crack width in SHCC on carbonation

Table 6.1 Material parameters for carbonation of SHCC

Quality	Carbonation					
	H	N	L	H	N	L
Condition	Sound			Cracked		
w/c ratio [-]	0.30	0.45	0.60	0.30	0.45	0.60
Effective diffusivity [m^2/year]	0.10	0.88	1.89	45.21	60.90	79.35
Penetration depth [mm] [37]	1.00	3.00	4.40	21.50	25.10	28.70

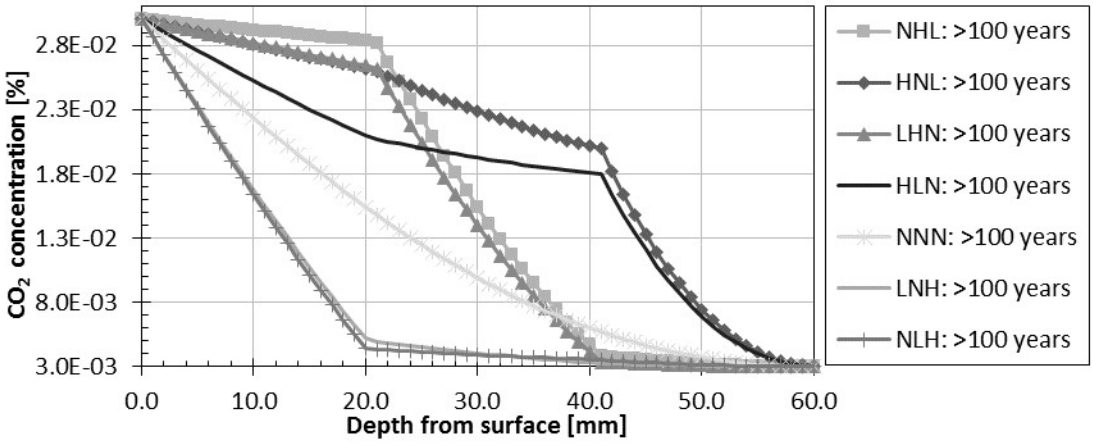

Fig. 6.1.1 Spatial distribution of CO_2 concentration in sound SHCC

6.1 Carbonation

Results of diffusion analysis of FG-SHCC are presented in Fig. 6.1.1., Fig. 6.1.2. and Fig. 6.1.3. Spatial distribution of CO_2 concentration in Fig. 6.1.1. shows the durability of different FG-SHCC layers order, including a homogeneous case. Highest durability time can be achieved mainly by placing the layer of the highest quality, i.e., layer H on the exposed surface, followed by layer N and lastly layer L. Same performance was shown by layering LNH, noted from the bar location to the exposed surface. The effect of FG material is for this case very high and achieved durability is over 100years. This high durability can be attributed to the used data, where carbonation depth is reported as zero.

In Fig. 6.1.2., distributions of CO_2 in FG-SHCC with 100μm crack width are presented. The effect of FG-SHCC is compared to the effect of a much smaller crack. This effect can be similarly as in the case of chloride attack observed as the size of

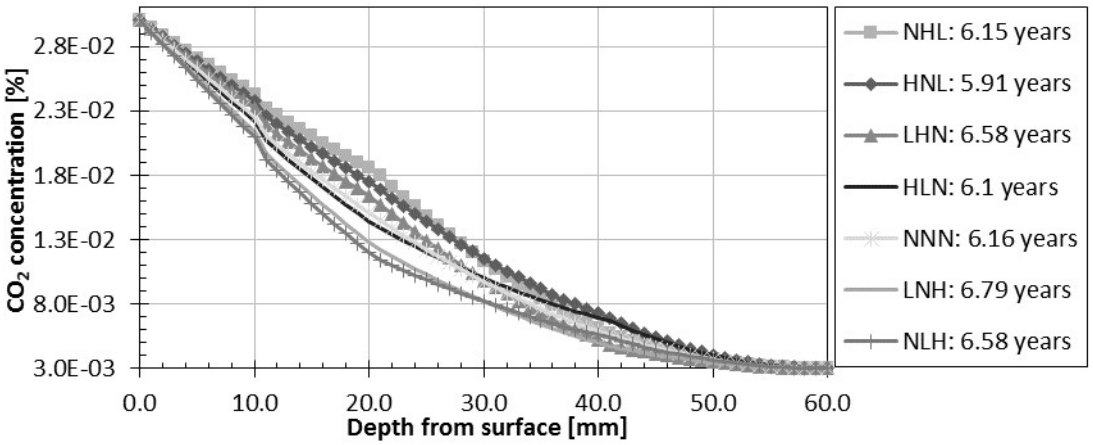

Fig. 6.1.2 Spatial distribution of CO_2 in $0.05mm$ cracked SHCC

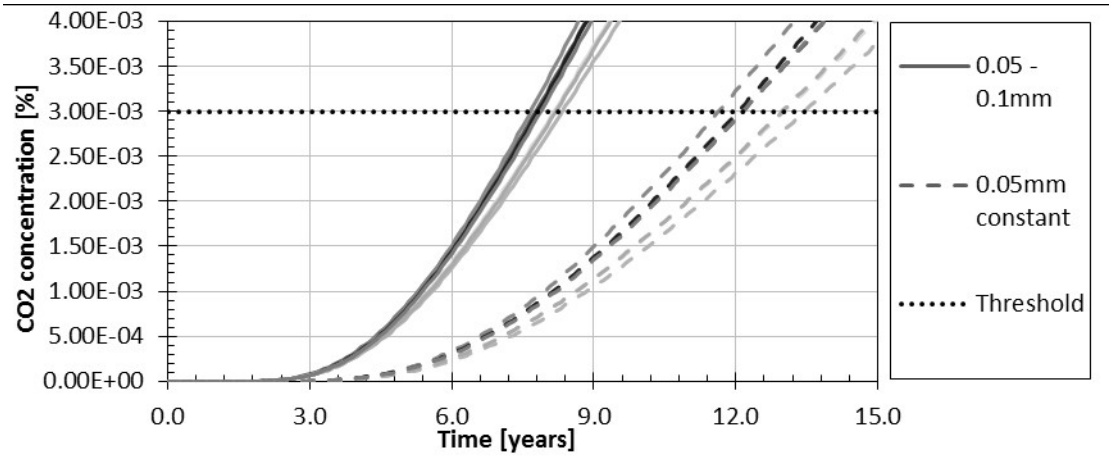

Fig. 6.1.3 Accumulation of CO_2 at the rebar location in cracked SHCC

the area between the top and bottom distribution. Highest durability is achieved by the same kind of layering as in the sound material, i.e. LNH offers the best durability. Difference between the best and worst performing layering is 14% and compared to homogeneous material the difference is 10%. The beneficial behaviour of FG-SHCC for this case of carbonation lower than for the chloride attack.

In both induced corrosion cases that are studied, layering of SHCC material is causing improved durability. The rate of improvement depends mainly on the diffusivity of cracked area compared to the area of sound material. When cracks penetrate through the whole layer up to the location of the reinforcement, durability can be substantially reduced, even if a layer of high quality material is used on the surface. FG-SHCC should be therefore designed, in a way, so that reflective cracking does not occur, e.g., possibly by reducing the bond around crack area, spreading the stress caused by the original crack in the repaired material. Another possibility to approach the problem of reflective cracking could be treated by using FG-SHCC not only within the thickness of the layer, but also by layering it along the repaired surface. Developing methods of 3D printed concrete could be in future utilized to create such material with high optimization.Studying the mechanical behaviour of strain hardening cementitious composites under various strain levels, crack width formation and number of cracks.

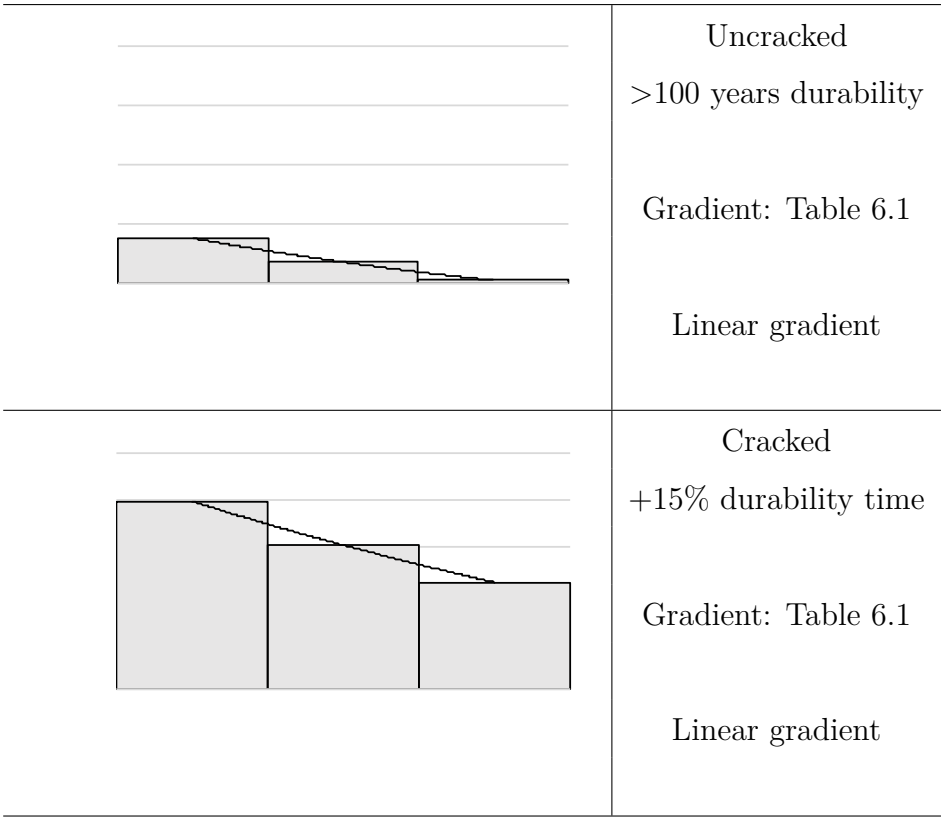

Fig. 6.2.1 Linear distribution of apparent diffusivity ratio, layer 1 on interface, layer 3 on surface

6.2 Remarks

Optimum FG multi-layer structure for carbonation is achieved by similar principle as for the chloride ion diffusion FGM. The best quality material should be placed on the surface, followed by lower quality materials. For carbonation, as optimum a step-wise linear function is used, Fig.6.2.1.

Chapter 7

Conclusions

The essence of this work is to find and present a function of a material distribution, i.e., create FGM, for improved durability. The beneficial behaviour is well presented. In this final chapter the summary of obtained results are presented in order of the set objectives in the first chapter. A diffusion FG-SHCC model along with finite element cracking model is here used to show the beneficial behaviour of this kind of material. FG-SHCC showed compared to homogeneous SHCC improved performance in both mechanical and chemical aspects. Layered structure can utilize specific beneficial behaviour of various material mixtures like use of highly scaling-resistant OPC as a surface layer, and a GGBFS material as a second layer for it's beneficial low diffusivity.

In total, three different layer thickness were tested. From a lower bound of 15mm, i.e., smallest from the fabrication point of view, to 30mm as a "median" value, up to 60mm as a maximum value at which durability time was reaching more than 100 years for the case of sound material. Total layer thickness is increasing the absolute value of durability time, but the relative effect of FGM is rather unchanged. Even a thin layer FG-SHCC of 15mm can improve durability time compared to homogeneous layer up to twice the performance. The rate of improvement is reduced with introduction of cracks, and therefore large cracks ($>100\mu$m) should be avoided.

The mechanical behaviour of FG-SHCC is shown and most common deterioration effects are examined showing greater durability performance.

Expected drawback of layered material like de-bonding of respective layers was studied experimentally, and it was found, that the bond between layers is sufficient even without applying a primer material and 24 hours of time gap between each new layer application.

With time, more and more structures will show a degradation, which can potentially when untreated or treated inefficiently cost not only money, but also endanger safety. It is therefore necessary to study good quality treatments. Presented durability improvement is applicable only up to the point of corrosion initiation, i.e., change of crack width due to corrosion products from reinforcement is not presented in the given analysis time scale.

7.1 Main conclusions

<table>
<tr><td colspan="2">Objective 1:</td></tr>
<tr><td colspan="2">Studying the mechanical behaviour of functionally graded strain hardening cementitious composites under various strain levels, crack width formation and number of cracks.</td></tr>
<tr><td>Chapter 3</td><td>In analysis done by finite element model of a repair layer consisted of FG-SHCC with best quality material as the surface surface layer showed similar crack width on the material surface and load capacity.
Number of cracks in FG-SHCC model is increased compared to homogeneous material. This suggested more ductile behaviour, and later was confirmed in the experiment.</td></tr>
<tr><td colspan="2">Objective 2:</td></tr>
<tr><td colspan="2">Studying how salts and carbon dioxide can penetrate inside the sound and cracked functionally graded strain hardening cementitious structures, and the rate of those processes.</td></tr>
<tr><td>Chapter 4</td><td>Diffusion analysis used to study the effect of different layer order and diffusivity distribution showed that the higher the gradient is, i.e., difference between the best and worst performing layer, the better durability structure we can obtain.
The concave step-wise diffusivity distribution function showed almost as good performance as the step-wise linear diffusivity distribution function. This means, that higher durability performance can be achieved by placing the best performing material further from the surface, so it can be protected by the external layer in case of a mechanical deterioration.</td></tr>
</table>

	3. Using the diffusion analysis, cracked FG-SHCC showed better performance compared to cracked homogeneous SHCC due to different cracking behaviour. Diffusion rate at the place of crack is highly increased compared to the uncracked area. High durability is kept due to small corrosion affected area.
Objective 3:	
Studying the physical behaviour of strain hardening cementitious composites, and how fibre content, water to binder ratio and matrix composition affects it's material properties, such as apparent diffusivity of chloride ions, carbonation and salt scaling.	
Chapter 2	1. In sound material, it is the diffusivity of material matrix, that limits the material durability. Densification of the material matrix is necessary to increase the matrix performance, and low water to binder ratio is one of the possibilities. Densification can be also done by using fly ash and ground granulated blast furnace slag, which both show reduced diffusivity compared to ordinary portland cement. Salt scaling durability on the other hand is achieved by use of OPC. This can be achieved using OPC material layer as the first, i.e., surface layer.
Chapter 5	2. In cracked material, it is the crack width and number of cracks limiting the diffusivity of aggressive chemicals, and larger fibre content offering higher fracture energy can offer this performance

Objective 4:	
Design different models of functionally graded material and optimize for a different deterioration by implied strain, see if the different type require a different kind of functionally graded material structure.	
Chapter 5	1. When mechanical limitation implied by the fibre content on the ultimate strain applied in the diffusion analysis together with increased number of layers, a higher order of optimization can be carried out. 2. With a given constant fibre content, optimization is carried out from two directions having a different condition. Optimized FG-SHCC for the linearly decreasing applied strain uses following fibre distribution: highest fibre content material layer is placed on the surface, largest strain values at the interface gives a limit to a minimum fibre content to avoid crack localization. Lowest fibre content is then used near the centre of the FG-SHCC. Optimized FG-SHCC for the constant strain value follows the same principle. 3. Almost 15% reduction in fibre content can be made in FG-SHCC while achieving comparable durability performance. 2% PVA fibre reinforcement can cost as much as $1m^3$ of concrete, making this an important possible saving.

Objective 5:	
Studying how FG-SHCC can be optimized for salt scaling phenomenon.	
Appendix D	1. Salt scaling material resistance is controlled mainly by matrix composition. FG-SHCC is then optimized by use of the fibre content to control cracking for diffusion resistance and cement type to control surface scaling resistance. OPC concrete due to it's scaling resistance is used as a surface layer, followed by layers of GGBFS and/or FA, which offers lower diffusivity due to the denser matrix.

7.2 Recommendations for future work

This work suggested layering of different kinds of SHCC to form a functionally graded material and used it's material parameters without considering the reciprocity effect of two neighbouring materials. FG-SHCC is a unique kind of material, that can benefit from developing 3D concrete printing techniques and perform optimization not only with respect to layers, but also with respect to length along the structure surface.

The model in this work would benefit with use of more test data on chemical attack on cracked SHCC materials progressively loaded to form different crack width and crack number to form better prediction of diffusivity. This would call for a large amount of experiments performed on one mixture type of different crack width.

From the short time behaviour, risk of de-bonding is not present, but bond degradation between layers and between the concrete surface and FG-SHCC over time of estimated durability must be examined. Insight into this behaviour would offer possible treatment of the surface in between each application, mechanical and/or chemical, if it is necessary.

Two dimensional model would be beneficial for better modelling of diffusion. To create such a model, it is necessary to handle diffusion in uncracked material and diffusion along and orthogonally in the cracks.

References

[1] American Concrete Institute Committee 201. Guide to Durable Concrete, Reported by ACI Committee 201. Tech. rep., ACI 201.2R-08, 2008.

[2] Bajer, Cz. Time integration methods - still questions. *Theoretical foundations of civil engineering 1* (2002), pp. 45–54.

[3] Bangert, F., Grasberger, S., Kuhl, D., and Meschke, G. Environmentally induced deterioration of concrete: Physical motivation and numerical modeling. *Engineering Fracture Mechanics vol. 70* (2003), pp. 891–910.

[4] Bary, B., Leterrier, N., Deville, E., and Le Bescop, P. Coupled chemo-transport-mechanical modelling and numerical simulation of external sulfate attack in mortar. *Cement and Concrete Composites vol. 49* (2014), pp. 70–83.

[5] Bažant, Z. P. Physical Model for Steel Corrosion in Concrete Sea Structures-Theory. *Journal of the Structural Division vol. 105* (1979), pp. 1137–1153.

[6] Beushausen, H., and Fernandez Luco, L., Eds. *Performance-Based Specifications and Control of Concrete Durability: State-of-the-Art Report RILEM TC 230-PSC*, vol. vol. 18. 2015.

[7] Boshoff, W. P., and Adendorff, C. J. Effect of sustained tensile loading on SHCC crack widths. *Cement and Concrete Composites 37*, 1 (2013), 119–125.

[8] Carslaw, H. J., and Jaeger, J. C. Conduction of heat in solids.

[9] Červenka, J., and Papanikolaou, V. K. Three dimensional combined fracture-plastic material model for concrete. *International Journal of Plasticity 24*, 12 (2008), 2192–2220.

[10] Červenka, V., Jendele, L., and Červenka, J. ATENA Program Documentation Part 1 Theory. *Atena* (2012), 1–282.

[11] Chandra Paul, S., and P. A. G. van Zijl, G. Crack Formation and Chloride Induced Corrosion in Reinforced Strain Hardening Cement-Based Composite (R/SHCC). *Journal of Advanced Concrete Technology vol. 12* (2014), pp. 340–351.

[12] Chang, C. F., and Chen, J. W. The experimental investigation of concrete carbonation depth. *Cement and Concrete Research vol. 36* (2006), pp. 1760–1767.

[13] Chen, X., Huang, W., and Zhou, J. Effect of moisture content on compressive and split tensile strength of concrete. *Indian Journal of Engineering & Materials Sciences vol. 19* (2012), pp. 427–435.

[14] Chen, Y., Gao, J., Tang, L., and Li, X. Resistance of concrete against combined attack of chloride and sulfate under drying-wetting cycles. *Construction and Building Materials vol. 106* (2016), pp. 650–658.

[15] Cheng-Feng, C., and Jing-Wen, C. Strength and elastic modulus of carbonated concrete. Tech. rep., 2005.

[16] Chisholm, D. H., and Lee, N. P. Actual and Effective Diffusion Coefficients of Concrete Under Marine Exposure Conditions. *20th Biennial Conference of the Concrete Institute of Australia vol. 96* (2001), pp. 1–11.

[17] Collepardi, M., Marcialis, A., and Turriziani, R. Penetration of chloride ions into cement pastes and concrete. *Journal of the American Ceramic Society 55*, 10 (1972), 534–535.

[18] Çopuroglu, O. *The characterisation, improvement and modelling aspects of frost salt scaling of cement-based materials with a high slag content.* 2006.

[19] Çopuroglu, O., and Schlangen, E. Modeling of frost salt scaling. *Cement and Concrete Research vol. 38* (2008), pp. 27–39.

[20] Costa, a., and Appleton, J. Concrete Carbonation and Chloride Penetration in a Marine Environment, 2001.

[21] Crank, J. *The mathematics of diffusion.* 1975.

[22] Crank, J. *Free and moving boundary problems.* 1984.

[23] Cui, H., Tang, W., Liu, W., Dong, Z., and Xing, F. Experimental study on effects of CO2 concentrations on concrete carbonation and diffusion mechanisms. *Construction and Building Materials vol. 93* (2015), pp. 522–527.

[24] de Vera, G., Climent, M. a., Viqueira, E., Antón, C., and López, M. P. Chloride Penetration Prediction in Concrete through an Empirical Model Based on Constant Flux Diffusion. *Journal of Materials in Civil Engineering vol. 27* (2015), 39.

[25] Delagrave, A., Marchand, J., Ollivier, J. P., Julien, S., and Hazrati, K. Chloride binding capacity of various hydrated cement paste systems. *Advanced Cement Based Materials vol. 6* (1997), pp. 28–35.

[26] Djerbi, A., Bonnet, S., Khelidj, A., and Baroghel-bouny, V. Influence of traversing crack on chloride diffusion into concrete. *Cement and Concrete Research vol. 38* (2008), pp. 877–883.

[27] Ekolu, S. O. A review on effects of curing, sheltering, and CO2 concentration upon natural carbonation of concrete. *Construction and Building Materials vol. 127* (2016), pp. 306–320.

[28] El-Hachem, R., Rozire, E., Grondin, F., and Loukili, A. New procedure to investigate external sulphate attack on cementitious materials. *Cement and Concrete Composites vol. 34* (2012), pp. 357–364.

[29] Endoh, H., Taguchi, F., Shimada, H., Atsumi, Y., Kubouchi, A., Hoshi, T., Oota, T., and Saeki, N. Investigation of Combine Deterioration with Breakwater Concrete in Cold Region which Passed from Construction for About 40 Years. pp. 17–27.

[30] Fachinotti, V. D., Cardona, A., and Huespe, a. E. A fast convergent and accurate temperature model for phase-change heat conduction. *International Journal for Numerical Methods in Engineering vol. 44* (1999), pp. 1863–1884.

[31] Fantilli, A., Kwon, S., Mihashi, H., and Nishiwaki, T. Tailoring high-strength SHCC. *Proceedings of the 8th International Conference on Fracture Mechanics of Concrete and Concrete Structures, FraMCoS 2013*, August 2015 (2013).

[32] FGM Study Group. Functionally gradient materials. *Kogyochosakai* (1993).

[33] Gaztanaga, T., Goñi, S., and Guerrero, A. Accelerated carbonation of calcium aluminate cement paste. *Calcium Aluminate Cements 2001 vol. 33* (2001), pp. 349–359.

[34] Glinicki, M. a., and Zielinski, M. Frost salt scaling resistance of concrete containing CFBC fly ash. *Materials and Structures vol. 42* (2009), pp. 993–1002.

[35] Halamickova, P., Detwiler, R. J., Bentz, D. P., and Garboczi, E. J. Water permeability and chloride ion diffusion in portland cement mortars: Relationship to sand content and critical pore diameter. *Cement and Concrete Research 25*, 4 (1995), 790–802.

[36] Hills, T. P., Gordon, F., Florin, N. H., and Fennell, P. S. Statistical analysis of the carbonation rate of concrete. *Cement and Concrete Research vol. 72* (2015), pp. 98–107.

[37] Hiraishi, Y., Honma, T., Hakoyama, M., and Miyazato, S. Steel Corrosion Induced by Chloride or Carbonation at Bending Crack in High Performance Fiber Reinforced Cementitious Composites. *Concrete Research and Technology vol. 16* (2005), pp. 31–38.

[38] Houst, Y. F., and Wittmann, F. H. Influence of porosity and water content on the diffusivity of CO2 and O2 through hydrated cement paste. *Cement and Concrete Research vol. 24* (1994), pp. 1165–1176.

[39] Hwang, J. P., Kim, M., and Ann, K. Y. Porosity generation arising from steel fibre in concrete. *Construction and Building Materials vol. 94* (2015), pp. 433–436.

[40] Ikumi, T., Cavalaro, S. H. P., Segura, I., and Aguado, A. Alternative methodology to consider damage and expansions in external sulfate attack modeling. *Cement and Concrete Research vol. 63* (2014), pp. 105–116.

[41] Ishida, T., Iqbal, P. O. N., and Anh, H. T. L. Modeling of chloride diffusivity coupled with non-linear binding capacity in sound and cracked concrete. *Cement and Concrete Research vol. 39* (2009), pp. 913–923.

[42] Janeiro, R. D., Wang, P.-g., Wittmann, F. H., Zhao, T.-j., and Huang, W.-l. Evolution of Crack Patterns on SHCC As Function of Imposed Strain. 217–224.

[43] Jang, S. Y., Kim, B. S., and Oh, B. H. Effect of crack width on chloride diffusion coefficients of concrete by steady-state migration tests. *Cement and Concrete Research vol. 41* (2011), pp. 9–19.

[44] Japan Society of Civil Engineers. *Recommendations for Design and Construction of High Performance Fiber Reinforced Cement Composites with Multiple Fine Cracks (HPFRCC)*, vol. 82. 2008.

[45] Jiang, C., Gu, X., Zhang, W., and Zou, W. Modeling of carbonation in tensile zone of plain concrete beams damaged by cyclic loading. *Construction and Building Materials vol. 77* (2015), pp. 479–488.

[46] Jin, W. L., Yan, Y. D., and Wang, H. L. Chloride diffusion in the cracked concrete. *Fracture Mechanics of Concrete and Concrete Structures-Assessment, Durability, Monitoring and Retrofitting* (2010), pp. 880–886.

[47] Jun, P., and Mechtcherine, V. Behaviour of strain-hardening cement-based composites (SHCC) under monotonic and cyclic tensile loading: Part 1 - Experimental investigations. *Cement and Concrete Composites 32*, 10 (2010), 801–809.

[48] Kabele, P. Stochastic finite element modeling of multiple vracking in fiber reinforced cementitious composites. *Fracture and Damage of Advanced Fibre-reinforced Cement-based Materials* (2010), 155–163.

[49] Kabele, P., Novák, L., Nemecek, J., and Kopecký, L. Effects of chemical exposure on bond between synthetic fiber and cementitious matrix. *ICTRC'2006 - 1st International RILEM Conference on Textile Reinforced Concrete* (2006), 91–99.

[50] Kang, Y. *Surface scaling mechanism and prediction for concrete*. 2010.

[51] Khan, M. U., Ahmad, S., and Al-gahtani, H. J. Chloride-Induced Corrosion of Steel in Concrete : An Overview on Chloride Diffusion and Prediction of Corrosion Initiation Time. *International Journal of Corrosion vol. 2017* (2017), pp. 1–9.

[52] Kim, Y. Y., Lee, K. M., Bang, J. W., and Kwon, S. J. Effect of W/C ratio on durability and porosity in cement mortar with constant cement amount. *Advances in Materials Science and Engineering vol. 2014* (2014).

[53] Kobayashi, K., Le Ahn, D., and Rokugo, K. Effects of crack properties and water-cement ratio on the chloride proofing performance of cracked SHCC suffering from chloride attack. *Cement and Concrete Composites 69* (2016), 18–27.

[54] Kürschner, P., Mäki-Marttunen, T., Vestergaard, S., and Wandl, S. *Modelling and simulation of ice / snow melting*. 2008.

[55] Lagerblad, B. *Carbon dioxide uptake during concrete life cycle - State of the art*. 2005.

[56] Lepech, M., and Li, V. C. Water Permeability of Cracked Cementitious Composites. *11th International Conference on Fracture (ICF11), Paper 4539* (2005).

[57] Li, K. *Durability Design of Concrete Structures, Phenomena, Modeling and Practice*. 2016.

[58] Liang, M. T., Qu, W., and C-H, L. Mathematical modeling and prediction of concrete carbonation and its applications. *Marine and Science Technology vol. 10* (2002), pp. 128–135.

[59] Litvan, G., and Meyer, A. Carbonation of granulated blast furnace slag cement concrete during twenty years of field exposure. *NRC Publications Archive Archives des publications du CNRC vol. 2* (1986), pp. 1445–1462.

[60] Liu, Z., and Hansen, W. Freeze-thaw durability of high strength concrete under deicer salt exposure. *Construction and Building Materials vol. 102* (2016), pp. 478–485.

[61] Luković, M., Dong, H., Šavija, B., Schlangen, E., Ye, G., and Breugel, K. V. Tailoring strain-hardening cementitious composite repair systems through numerical experimentation. *Cement and Concrete Composites vol. 53* (2014), pp. 200–213.

[62] Lund university, D. o. B. M. L. T. H. CONTECVET : A validated Users Manual for assessing the residual service life of concrete structures. 202.

[63] Maekawa, K., Ishida, T., and Kishi, T. *Multi-scale modeling of structural concrete.* 2009.

[64] Magalhaes, M. Influence of local raw materials on the mechanical behaviour and fracture process of PVA-SHCC. *Materials Research 17*, 1 (2013), 146–156.

[65] MLIT. Report of Technical Research Development for Quality Improvement of Highway Policy, Report No. 20-5. Tech. rep., 2011.

[66] Muigai, R., Alexander, M., and Moyo, P. A novel framework towards the design of more sustainable concrete infrastructure. *Materials and Structures/Materiaux et Constructions 49*, 4 (2016), 1127–1141.

[67] Nallathambi, A. K., Specht, E., and Bertram, A. Finite Element Technique for Phase-Change Heat Conduction Problem. *Volume 2: Theory and Fundamental Research; Aerospace Heat Transfer; Gas Turbine Heat Transfer; Computational Heat Transfer* (2009), pp. 667–674.

[68] Nieuwoudt, P. D. Quantifying the Cracking Behaviour of Strain Hardening Cement-based Composites by Masters of Science in Engineering.

[69] Nowak-Michta, A. Water-binder ratio influence on de-icing salt scaling of fly ash concretes. *Procedia Engineering vol. 57* (2013), pp. 823–829.

[70] Otsuki, N., Nagataki, S., and Nakashita, K. Evaluation of the AgNO3 solution spray method for measurement of chloride penetration into hardened cementitious matrix materials. *Construction and Building Materials 7*, 4 (1993), 195–201.

[71] Papadakis, V., Vayenas, C., and Fardis, M. Physical and chemical characteristics affecting the durability of concrete. *ACI Materials Journal vol. 8* (1991), pp. 186–196.

[72] Papadakis, V. G., Vayenas, C. G., and Fardis, M. N. Experimental Investigation and Mathematical-Modeling of the Concrete Carbonation Problem. *Chemical Engineering Science vol. 46* (1991), pp. 1333–1338.

[73] Papadakis, V. G., Vayenas, C. G., and Fardis, M. N. Fundamental modeling and experimental investigation of concrete carbonation. *ACI Materials Journal vol. 88* (1991), pp. 363–373.

[74] Paper, T., Yun, H. D., Kim, S. H., Han, S. J., and Yang, H. J. Effects of freeze-thaw action on themechanical properties of strain-hardening cement composite.

[75] Paul, S., Pirskawetz, S., van Zijl, G., and Schmidt, W. Acoustic emission for characterising the crack propagation in strain-hardening cement-based composites (SHCC). *Cement and Concrete Research 69*, December (2015), 19–24.

[76] Paul, S. C., and van Zijl, G. P. A. G. Chloride-induced corrosion modelling of cracked reinforced SHCC. *Archives of Civil and Mechanical Engineering 16*, 4 (2016), 734–742.

[77] Paul, S. C., Van Zijl, G. P. A. G., Babafemi, A. J., and Tan, M. J. Chloride ingress in cracked and uncracked SHCC under cyclic wetting-drying exposure. *Construction and Building Materials 114* (2016), 232–240.

[78] Portland Cement Association. Concrete slab surface defects: Causes, Prevention, Repair. Tech. rep., 2001.

[79] Pryl, D., and Červenka, J. ATENA Program Documentation Part 11 Troubleshooting Manual. *Cervenka Consulting* (2016).

[80] Puatatsananon, W., and Saouma, V. E. Nonlinear Coupling of Carbonation and Chloride Diffusion in Concrete. *Journal of Materials in Civil Engineering vol. 17* (2005), pp. 264–275.

[81] Qian, S., and Li, V. C. Simplified Inverse Method for Determining the Tensile Strain Capacity of Strain Hardening Cementitious Composites. *Journal of Advanced Concrete Technology 5*, 2 (2007), 235–246.

[82] Rapoport, J., Aldea, C.-M., Shah, S. P., Bruce, A., and Karr, A. Permeability of Cracked Steel Fiber-Reinforced Concrete. *National Institute of Statistical Sciences vol. 115* (2001), pp. 1–10.

[83] Rilem. *Frost Resistance of Concrete*. 1997.

[84] Rilem. *Freeze- Thaw Durability of Concrete*. 2005.

[85] Sahmaran, M., and Li, V. C. De-icing salt scaling resistance of mechanically loaded engineered cementitious composites. *Cement and Concrete Research 37*, 7 (2007), 1035–1046.

[86] Sahmaran, M., Li, V. C., and Li, M. Transport Properties of Engineered Cementitious Composites under Chloride Exposure-2007.pdf. *Aci Materials Journal vol. 104* (2007), pp. 604–611.

[87] Shen, B., Hubler, M., Paulino, G. H., and Struble, L. J. Functionally-graded fiber-reinforced cement composite: Processing, microstructure, and properties. *Cement and Concrete Composites 30*, 8 (2008), 663–673.

[88] Smith, T. C. A finite difference method for a Stefan problem. *Calcolo vol. 18* (1981), pp. 131–154.

[89] Song, W. L., Li, X. F., and Ma, K. F. The Effect of Freeze-Thaw Cycles on Mechanical Properties of Concrete. *Advanced Materials Research vol. 2014* (2014), pp. 1–7.

[90] Tai, R. *Upscaling of strain-hardening cementitioust, The effect of upscaling element size on the composite performance*. PhD thesis, Delft university of technology.

[91] Tang, S. W., Yao, Y., Andrade, C., and Li, Z. J. Recent durability studies on concrete structure. *Cement and Concrete Research vol. 78* (2015), pp. 143–154.

[92] Truex, M. *Numerical Simulation of Liquid-Solid , Solid-Liquid Phase Change Using Finite Element Method in h, p, k Framework with Space-Time Variationally Consistent Integral Forms*. PhD thesis, University of Kansas, 2010.

[93] Umbreen-Us-Sahar. Micromechanical modelling for deformational behavior of strain hardening cement-based composites. *PhD dissertation, Dept. of Civil Engineering, Yokohama National University* (2015), p.163.

[94] Val, D. V., and Stewart, M. G. Life-cycle cost analysis of reinforced concrete structures in marine environments. *Structural Safety 25*, 4 (2003), 343–362.

[95] Valenza, J. J., and Scherer, G. W. A review of salt scaling: I. Phenomenology. *Cement and Concrete Research vol. 37* (2007), pp. 1007–1021.

[96] Valenza, J. J., and Scherer, G. W. A review of salt scaling: II. Mechanisms. *Cement and Concrete Research vol. 37* (2007), pp. 1022–1034.

[97] Valenza II, J. J., and Scherer, G. W. Mechanisms of salt scaling. *Materials and Structures vol. 38* (2005), pp. 479–488.

[98] Van Den Heede, P., Furniere, J., and De Belie, N. Influence of air entraining agents on deicing salt scaling resistance and transport properties of

high-volume fly ash concrete. *Cement and Concrete Composites vol. 37* (2013), pp. 293–303.

[99] Van Zijl, G., Wittmann, F., Oh, B., Kabele, P., Toledo Filho, R., Fairbairn, E., Slowik, V., Ogawa, A., Hoshiro, H., Mechtcherine, V., Altmann, F., and Lepech, M. Durability of strain-hardening cement-based composites (SHCC). *Materials and Structures/Materiaux et Constructions 45*, 10 (2012), 1447–1463.

[100] van Zijl, G. P. A. G., Slowik, V., Toledo Filho, R. D., Wittmann, F. H., and Mihashi, H. Comparative testing of crack formation in strain-hardening cement-based composites (SHCC). *Materials and Structures 49*, 4 (2016), 1175–1189.

[101] van Zijl, G. P. A. G., and Wittmann, F. H. *Durability of strain-hardening fibre-reinforced cement-based composites (SHCC)*. Rilem, 2011.

[102] Vassilev, D. G. *Evaluation of Test Methods for De-Icer Scaling Resistance of Concrete*. 2012.

[103] Wang, B., Xu, S., and Liu, F. Evaluation of tensile bonding strength between UHTCC repair materials and concrete substrate. *Construction and Building Materials 112* (2016), 595–606.

[104] Wang, X. Y., and Zhang, L. N. Simulation of Chloride Diffusion in Cracked Concrete with Different Crack Patterns. *Advances in Materials Science and Engineering vol. 2016* (2016), pp. 1–11.

[105] Watanabe, H., and Koga, H. General Information on Deterioration of Existing Concrete Structures and Recent Research Topics on the Maintenance Techniques in PWR. *Maintenance and Management Strategy of Infrastructures in Japan and Korea* (2006).

[106] Weimann, M. B., and Li, V. C. Hygral behavior of engineered cementitious composites (ECC). *IInternational Journal for Restoration of Buildings and Monuments 9*, 5 (2003), 513–534.

[107] Winslow, D. The Pore Size Distribution of Portland Cement Paste. Tech. rep., 1968.

[108] Wittmann, F. H., and Ash, F. Capillary absorption and chloride penetration into neat and water repellent shcc under imposed strain. 165–172.

[109] Wittmann, F. H., Zhang, P., and Zhao, T. J. Water and chloride penetration into strain hardening cement-based composites under and after imposed strain. *Symposium on Fracture and Damage of Advanced Fibre-reinforced Cement-based Materials* (2010), 51–58.

[110] Xiao-gang, W., Wittmann, F. H., and Tie-jun, Z. Comparative Study of Test Methods to Determine Fracture Energy and Strain Hardening of Cement-based Composites (SHCC). *Restoration of Buildings and Monuments 12* (2006), 169–178.

[111] Ye, H., Tian, Y., Jin, N., Jin, X., and Fu, C. Influence of cracking on chloride diffusivity and moisture influential depth in concrete subjected to simulated environmental conditions. *Construction and Building Materials vol. 47* (2013), pp. 66–79.

[112] Yun, H. D. Effect of accelerated freeze-thaw cycling on mechanical properties of hybrid PVA and PE fiber-reinforced strain-hardening cement-based composites (SHCCs). *Composites Part B: Engineering 52* (2013), 11–20.

[113] Zhou, J., Qian, S., Sierra Beltran, M. G., Ye, G., Breugel, K., and Li, V. C. Development of engineered cementitious composites with limestone powder and blast furnace slag. *Materials and Structures 43*, 6 (2010), 803–814.

[114] Zhu, X., Zi, G., Cao, Z., and Cheng, X. Combined effect of carbonation and chloride ingress in concrete. *Construction and Building Materials vol. 110* (2016), pp. 369–380.

[115] Zijl, G. P. A. G. V. Crack distribution characterisation towards a framework for durability design of SHCC. *2nd International RILEM conference on strain hardening cementitious composites*, December (2011).

[116] Zofia, S., and Adam, Z. Theoretical model and experimental tests on chloride diffusion and migration processes in concrete. *Procedia Engineering 57* (2013), 1121–1130.

Appendix A

Previous works

Problem of diffusion in composite solids, also addressed as "skin effect", is addressed by work of Carslaw and Jaeger [8], J. Crank, and CONTECVET. Chloride profile in real structures does not fit well with the theoretical distribution obtained by Eq.B.0.2. The reason for this discrepancy can be the surface layer carbonation causing lower chlorides binding capacity and higher chloride diffusion coefficient.

The solution for case of semi-infinite medium of two different diffusion parameters is given. In the assumed semi-infinite region $-l < x < \infty$, the D_1 diffusion coefficient and concentration c_1 are used in the region $-l < x < 0$, and the D_2 diffusion coefficient and concentration c_2 are used in the region $x > 0$. Interface conditions are assumed to be

$$\begin{aligned} c_1 &= c_2 \quad , \quad x = 0 \\ D_1 \frac{\partial c_1}{\partial x} &= D_2 \frac{\partial c_2}{\partial x} \quad , \quad x = 0 \end{aligned}$$

The problem of zero initial concentration and the surface $x = -l$ maintained at constant concentration C_0 is given by Carslaw and Jaeger, and Crank as

$$\begin{aligned} c_1 &= C_0 \sum_{n=0}^{\infty} \alpha^n \left\{ erfc \frac{(2n+1)\, l + x}{2\sqrt{(D_1 t)}} - \alpha\, erfc \frac{(2n+1)\, l - x}{2\sqrt{(D_1 t)}} \right\} \\ c_2 &= \frac{2kC_0}{k+1} \sum_{n=0}^{\infty} \alpha^n \left\{ erfc \frac{(2n+1)\, l + kx}{2\sqrt{(D_1 t)}} \right\} \end{aligned}$$

where $k = (D_1/D_2)^{\frac{1}{2}}$, and $\alpha = (1-k)\,/\,(1+k)$. Skin effect solution is represented in Fig.(A.0.1) along with the numerical solution, where the skin layer is $2mm$ thick. The same problem is solved by CONTECVET as

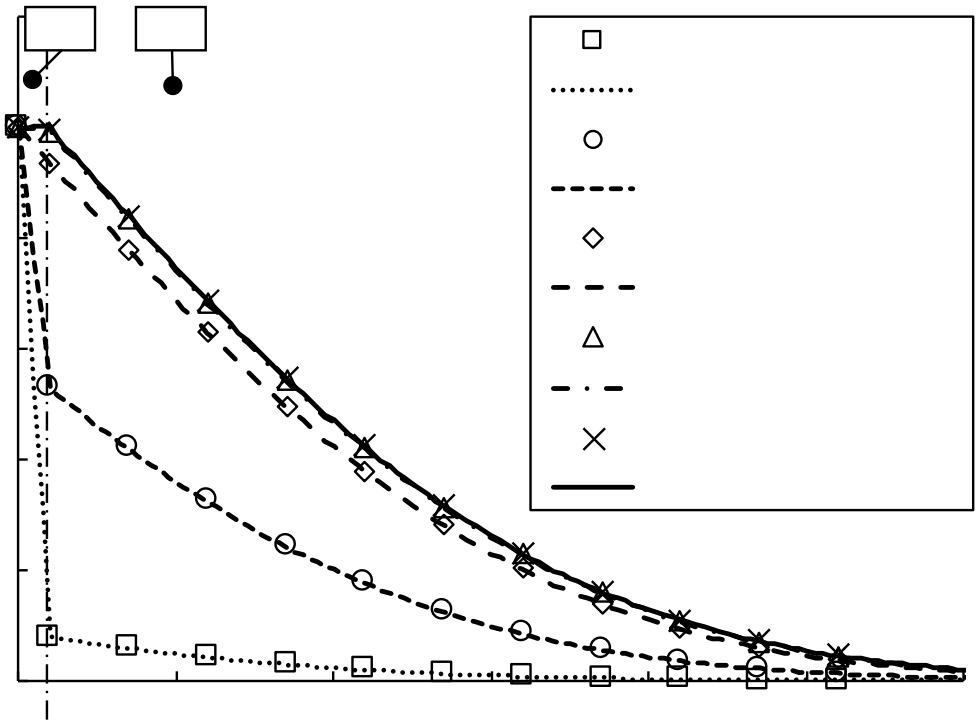

Fig. A.0.1 Skin effect

$$
\begin{aligned}
c_1(x,t) &= C_0 \sum_{n=0}^{\infty} \alpha^n \left\{ erfc\frac{2nl+x}{2\sqrt{(D_1 t)}} - \alpha\, erfc\frac{(2n+2)\,l-x}{2\sqrt{(D_1 t)}} \right\} \\
c_2(x,t) &= \frac{2kC_0}{k+1} \sum_{n=0}^{\infty} \alpha^n \left\{ erfc\frac{(2n+1)\,l+kx}{2\sqrt{(D_1 t)}} \right\}
\end{aligned}
$$

where $k = (D_1/D_2)^{\frac{1}{2}}$, and $\alpha = (1-k)\,/\,(1+k)$.

Previous work done by Lukovic et. al, and Bin Shen et. al [61, 87], showed possible application of SHCC as a repair layer, and effect of fibre content distribution. Effect of interface was studied, and it was observed, that rougher surface providing better mechanical connection with the repaired layer shows crack propagation through the interface, i.e. crack doesn't propagate along the interface. Functionally graded FRCC consisted of 4 layers with fibre content varied from surface at 2%, 1.33%, 0.67% and 0%, i.e. 1% average fibre content. In a flexural test, FGFRCC showed only 5% increase in fracture energy compared to 1% of homogeneous distribution, but 80% increase in load capacity at the same displacement. Failure of FGFRCC showed more brittle failure.

Appendix B

Prediction of chloride ion diffusion

Chloride ion penetration into concrete can be predicted by four different methods.

1. Apparent diffusion coefficient obtained by a diffusion equation
2. Diffusion coefficient from accelerated test
3. From numerical analysis considering the reaction of chloride of ions or the movement of chloride ions at the boundary with the environment

Here only apparent diffusion coefficient obtained by a diffusion equation is presented. To obtain apparent diffusion coefficient, one can solve a diffusion equation (B.0.1) known as a Fick's second law with appropriate boundary condition. In this method, transfer of chloride ions in concrete is understand as a simple diffusion process.

$$\frac{\partial C}{\partial t} = D_{cl}(t)\frac{\partial^2 C}{\partial x^2} \tag{B.0.1}$$

where C is chloride ion concentration in liquid phase D_{cl} is chloride ion diffusion coefficient, x is depth from concrete surface and t is time. Equation (B.0.2) is a solution obtained based on the assumption of constant concentration of chloride on the surface.

$$C(x,t) = \gamma_{cl} \cdot C_0 \left(1 - erf\frac{x}{2\sqrt{D_{ap} \cdot t}}\right) \tag{B.0.2}$$

where $C(x,t)$ is chloride ion concentration [kg/m^3] at depth x[cm] and time t[years], C_0 is chloride ion concentration at the surface [kg/m^3], D_{ap} is apparent chloride ion

Table B.1 Surface chloride ion concentration $C_0[kg/m^3]$

	Splash zone	Distance from seashore $[km]$				
		Near the shoreline	0.1	0.25	0.5	1.0
Areas with a high volume of air-born salt (Hokkaido, Tohoku, Hokuriku, Okinawa...)	13	9.0	4.5	3.0	2.0	1.5
Areas with low volume of air-born salt (Kanto, Tokai, Kinki...)	13	4.5	2.5	2.0	1.5	1.0

diffusion coefficient [cm^2/year], γ_{cl} is safety factor for prediction precision, generally 1.0 can be used. Boundary concentration values for surface chloride ion concentration may be used from Table B.1.

Appendix C

Models for carbonation of concrete

All models are based on Fick's second law of diffusion equation, just as for chloride ion diffusion, but with different physical meaning.

$$\frac{\partial C}{\partial t} = D_{CO_2}(t)\frac{\partial^2 C}{\partial x^2} \tag{C.0.1}$$

where C is CO_2 concentration, D_{CO_2} is CO_2 diffusion coefficient, x is depth from concrete surface, t is time. Fick's law is presented in unidimensional form as

$$x_c = \alpha\sqrt{t} \tag{C.0.2}$$

where x_c is carbonation depth, α is coefficient of carbonation rate different from each model, and t is time [58, 36, 55]. Coefficient α can be varied even within one structure in a rather broad range, Fig. C.0.1.

C.1 Schiessl's model of the parameter α

In Schiessl's model parameter α from Eq.C.0.2 is described as

$$\alpha = \sqrt{\frac{2D_{CO_2}C_{CO_2}}{m_c C_{CO_{2,tot}}/100}} \tag{C.1.1}$$

where D_{CO_2} is CO_2 diffusion coefficient into concrete [m^2/s], m_t is amount of cement in 1m^{3}of finished concrete [kg/m^3], C_{CO_2} is CO_2 concentration in air [kg/m^3], $C_{CO_2,tot}$ is CO_2 content needed for complete carbonation [%].

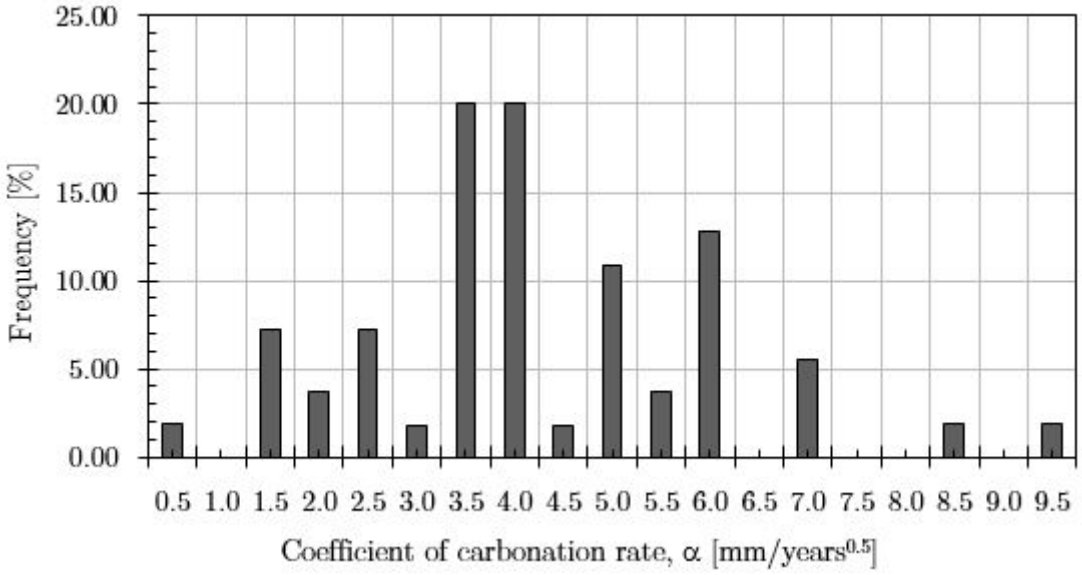

Fig. C.0.1 Frequency distribution of the coefficient of carbonation rate in a single structure (Gaang-shi viaduct in Taiwan)

C.2 Bob's model of the parameter α

In Bob's model parameter α from Eq.C.0.2 is described as

$$\alpha = \sqrt{\frac{150 \cdot C \cdot k \cdot d}{f_c}} \tag{C.2.1}$$

where C is 1.0 for Romanian Portland cement class $P40$ and $P45$; 1.2 for Portland cement with 15% slag; 1.4 for Portland cement with max. 30% slag; 2.0 for Portland cement with max. 50% slag. Parameter k is 1.0 under indoor conditions; 0.7 under protected outdoor conditions; 0.5 under average outdoor conditions; 0.3 for wet concrete, d is 1.0 for $CO_2 = 0.03\%$; 2.0 for $CO_2 = 0.1\%$ f_c is compressive strength of concrete [N/mm^2].

C.3 De Sittera's model of the parameter α

In De Sittera's model parameter α from Eq.C.0.2 is described as

$$\alpha = \sqrt{\frac{46w - 17.6}{2.7} \cdot R \cdot k} \tag{C.3.1}$$

Table C.1 Effect of relative humidity on the carbonation rate

Relative humidity RH [%]	0	7	50	93	100
Value of function f_{RH} [−]	0	0	0.425	0.5	0

where w is water to cement ratio, condition $w < 0.6$. The parameter R is describing the effect of cement type, recommended values are$< 0.6; 2.2 >$ and k is effect of ambient humidity, recommended values $< 1.0; 0.3 >$, where 1.0 is for a closed space and 0.3 is permanently wet.

C.4 Papadakis & Matouška's Model for Portland cement without additives

Papadakis and Matouška are presenting a more complex evaluation of the parameter, taking into consideration the type of a cement [72]. The parameter is described as

$$\alpha = 350 \frac{\rho_c \left(wc - 0.3\right)}{\rho_v \left(1 + \frac{\rho_c}{\rho_v} \cdot wc\right)} f_{RH} \sqrt{\left(1 + \frac{\rho_c}{\rho_v} wc + \frac{\rho_c}{\rho_a} \frac{m_a}{m_c}\right) C_{CO_2}} \qquad \text{(C.4.1)}$$

where ρ_c, ρ_v, ρ_a is density of cement, water and aggregate respectively [kg/m^3], wc is water to cement ratio [−], $\frac{m_a}{m_c}$ is weight ratio of aggregate and cement [−], C_{CO_2} is CO_2 concentration in air [kg/m^3] and f_{RH} is semi-linear function (Fig.C.4.1) of relative ambient humidity [%], Table C.1. Extensive experiments on effect of carbonation on blast furnace slag cement showed higher vulnerability when compared to OPC concretes [59].

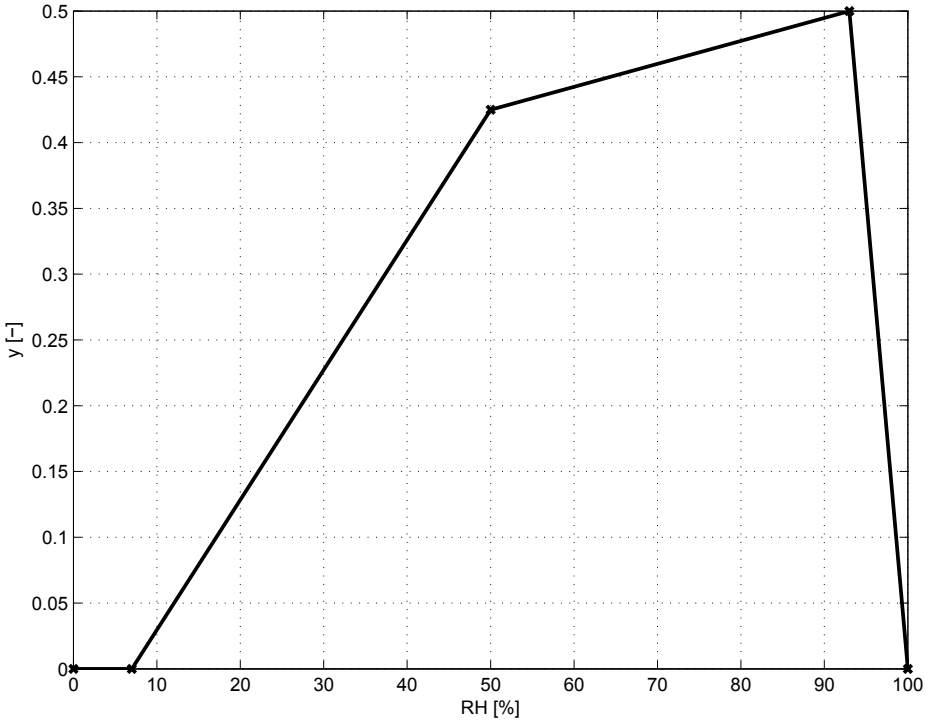

Fig. C.4.1 Semi-linear function f_{RH}

Appendix D

Diffusion analysis of FG-SHCC with effect of salt scaling

Salt scaling is introduced into the diffusion analysis by re-mashing of the model, or solving an analogical model of ice melting [54, 88, 92, 67], i.e., the scaled-off part of the structure is removed and the analysis zone is reduced. Analysis domain is update within each time step. Example of 5mm scaled of layer is shown in Fig.D.0.1. Such a scaling can be expected when slag cement is used, especially at the carbonated zone. On the other hand, OPC shows high scaling resistance, and carbonation has positive effect by densification of the material. Scaled of thickness then has to be decided based upon the experimental data of used material mixture. Fibres are generally expected to have very low to none benefit in increasing the scaling resistance. Matlab code is presented in Appendix J.

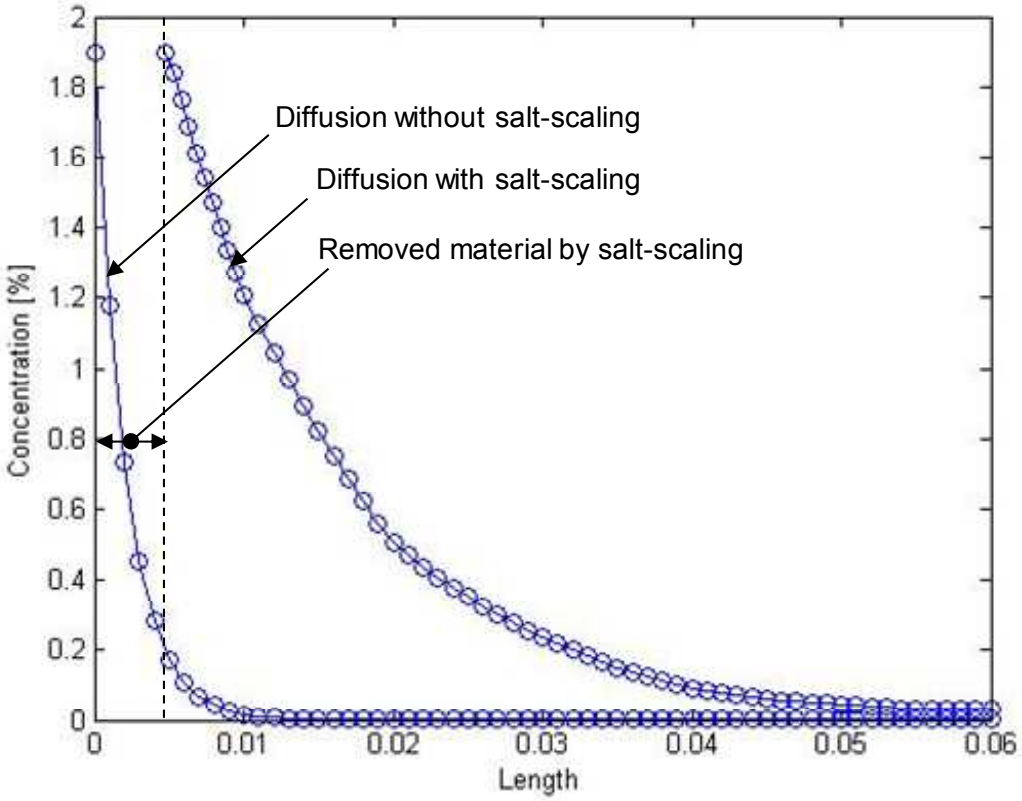

Fig. D.0.1 Chloride ion diffusion with effect of scaling

Appendix E

Coupling of chloride diffusion, carbonation and cracking of FG-SHCC taking into account the change of material properties

Concrete structures exposed to atmosphere will eventually show signs of carbonation, i.e., lowered pH level, which will depasivate the carbon steel reinforcement and initiate corrosion, or at least break the approximately 10000Å thick surface film of ferric oxide, Fe_2O_3 [5]. Based on experimental evidence, its is well established, that carbonation reduces rate of chloride diffusion [80]. On the other hand, even though the durability would be generally increased by lower diffusivity, results show that the time for corrosion initiation can be reduced about 40% by this combined mechanism [114].

E.1 Fibre content effect on fracture energy of SHCC

Fibre content with respective relative fracture energy of each layer is presented in the Table E.1. Fracture energy depends not only on the fibre content, but also on the fibre properties, i.e., length, coating and orientation in the mixture, and lastly matrix mixture composition itself. Ratios of chloride ion diffusivity are defined by a ratio to an average diffusivity of SHCC material mixture at value of 0.25cm^2/year. The constraining condition is an average ratio to be equal to 1. Different diffusivity is squired mainly by modification of water to cement ratio. Diffusivity of unreinforced mortar of different w/c is given in Fig.E.1.1. It has been found, that diffusivity of sound SHCC is very close to that of mortar, i.e., the effect of fibres is not as significant as

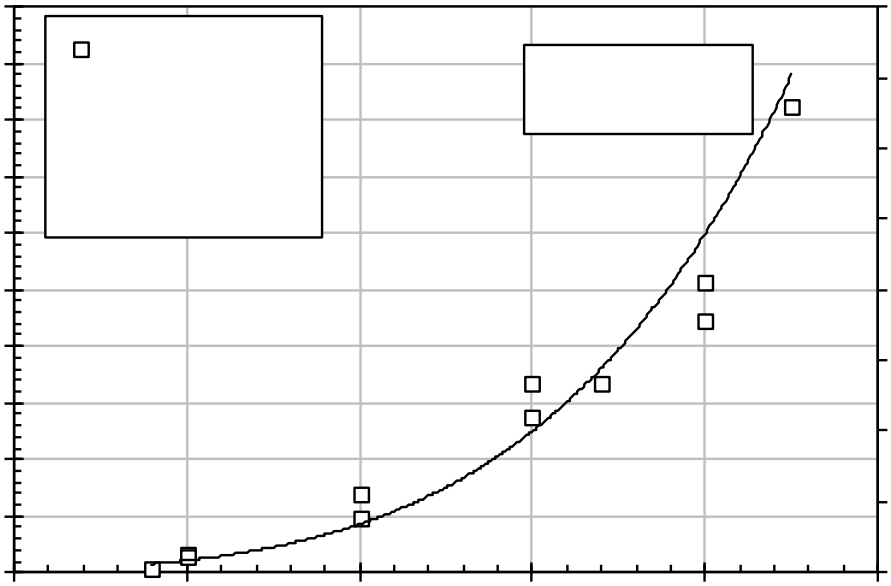

Fig. E.1.1 w/c ratio vs chloride diffusivity

Table E.1 Fibre content and fracture energy

Layer type	Relative fracture energy [-]	Fibre volume [%]
High performance	1.50	2.00
Normal performance	1.00	1.5
Low performance	0.50	1.10

the effect of w/c. Other parameters affecting the diffusivity of SHCC are for example degree of hydration, which is considered to be a constant (100%), aggregate ratio, admixtures etc.

By using the available data [104, 53], relationship between the fibre content and fracture energy can be established in Fig.E.1 where estimated function is drawn with the available data points. Base relative fracture energy was set at fibre content of 1.5%. Using more data [113] with same principle of base fracture energy at 2% of fibre volume, established relationship was accepted and fibre content for relative fracture energy of other layers, i.e. layer with high performance and layer with low performance was calculated.

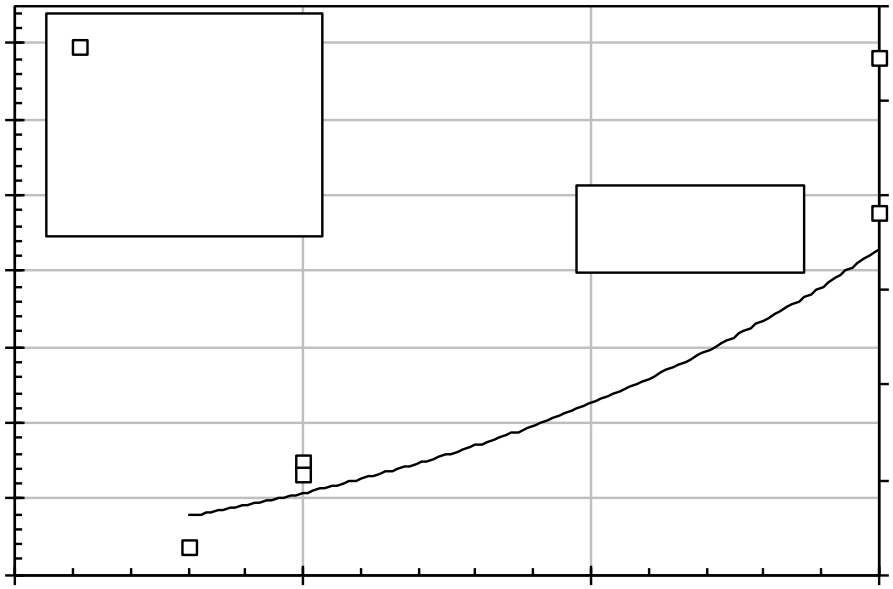

Fig. E.1.2 w/c ratio vs chloride diffusivity, detail

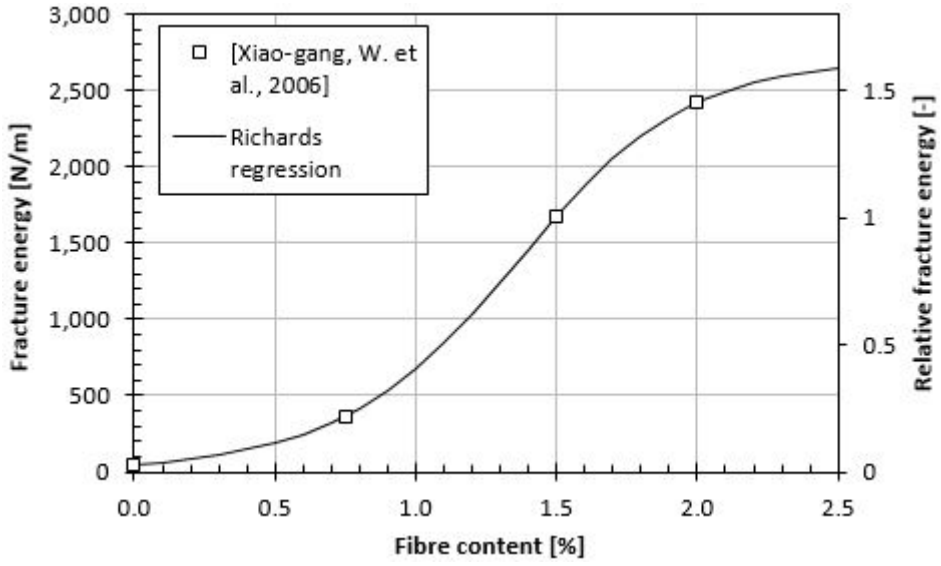

Fig. E.1.3 Effect of fibre content on fracture energy

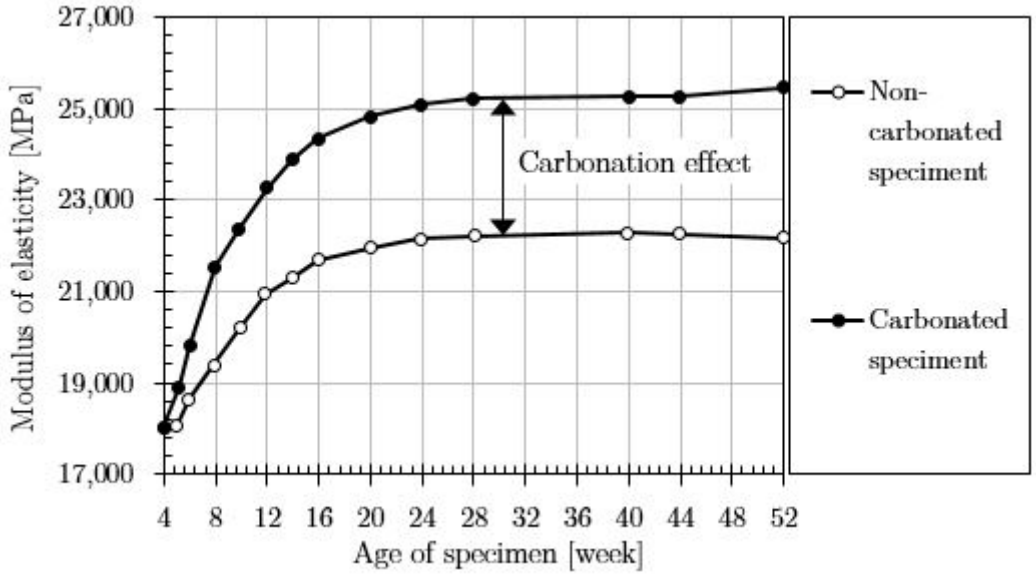

Fig. E.2.1 Carbonation effect on modulus of elasticity

E.2 Change of mechanical properties by carbonation and effect on crack width in SHCC

Carbonated concrete shows more brittle failure with higher elastic modulus, which is partly attributed to densification of the pore structure [107], and this effect can be also observed on the SHCC, where fracture energy is reduced. The rate of changes of material properties, such as density and strength, is reported to be proportional to the cement content of a mixture. Modulus of elasticity is increased during carbonation partly also because of the still ongoing hydration of the cement paste, it is then necessary to isolate those two effects by comparing modulus of elasticity of carbonated and non-carbonated samples, where modulus of elasticity increased by carbonation can be seen as a difference of those two E.2.1 [15, 45].

E.3 Chloride diffusivity vs carbonation

Simultaneous ingress of chloride and carbonation often occurs in a marine atmospheric environment and in areas where de-icing salts are used during winter. The influence of of carbonated concrete on diffusivity of chloride ions is rather complicated, as it's difficult to establish if carbonation reduce or increase the concrete resistance. This behaviour is depended on the mixture composition and has to be established experi-

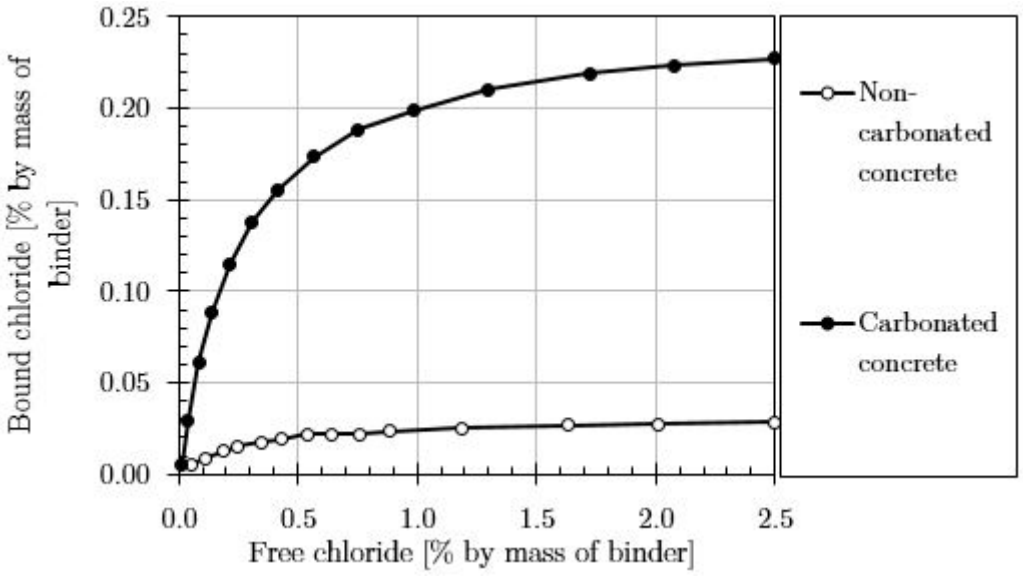

Fig. E.3.1 Chloride binding capacity of carbonated and non-carbonated concrete

mentally [114]. Carbonation in aforementioned environments usually occurs in concrete with already high chloride content, because the rate of chloride ions diffusion is faster than the carbonation. Carbonation of concrete is reducing the chloride binding capacity up to 20% of initial binding capacity, i.e., amount of free chlorides is increased and can cause earlier corrosion .

Appendix F

Calculation method of crack width in ATENA

The biaxial stress state is used to describe the non-linear behaviour of concrete materials. A main focus here is on the tensile performance. The complete uniaxial stress-strain law for concrete is shown in Fig. F.0.1, describing the relationship between the effective stress $\sigma_c^{ef} = E_c \epsilon^{eq}$, and the equivalent uniaxial strain ϵ^{eq}. Unloading is a linear function to the origin, and subsequent reloading if applied is following the unloading path, until the last loading point is reached again, resuming the initial loading function.

Poisson's effect in plane stress state is eliminated by introduction of equivalent uniaxial strain $\epsilon^{eq} = \sigma_{ci}/E_{ci}$. The equivalent uniaxial strain is produced by the stress σ_{ci} in a uniaxial test with Young's modulus E_{ci} in the direction i.

The behaviour of concrete in tension up to cracking is considered as linear elastic, described by the initial elastic modulus of concrete E_c, and the effective tensile strength $f_t^{'ef}$ derived from the biaxial failure function. In the tension-tension state, the tensile strength is equal to the uniaxial tensile strength $f_t^{'}$. When compression is present, i.e. the state of tension-compression, the tensile strength must be reduced by the reduction factor $r_{et} = 1 - 0.95\left(\sigma_{c2}/f_c^{'}\right)$ for the linear decrease of the tensile strength. For hyperbolic decrease the reduction factor is calculated as $r_{et} = \frac{A+(A-1)B}{AB}$, where $B = Kx + A$ and $x = \sigma_{c2}/f_c^{'}$.

Crack formation is divided into uncracked, process, and cracked zones. Tensile strength is separating the uncracked and process zone, and complete release of stress is followed by cracked zone. The crack width is calculated as

$$w = \epsilon_{cr} L_t^{'}$$

where ϵ_{cr} is the crack opening strain and $L_t^{'}$ is the failure band for tension.

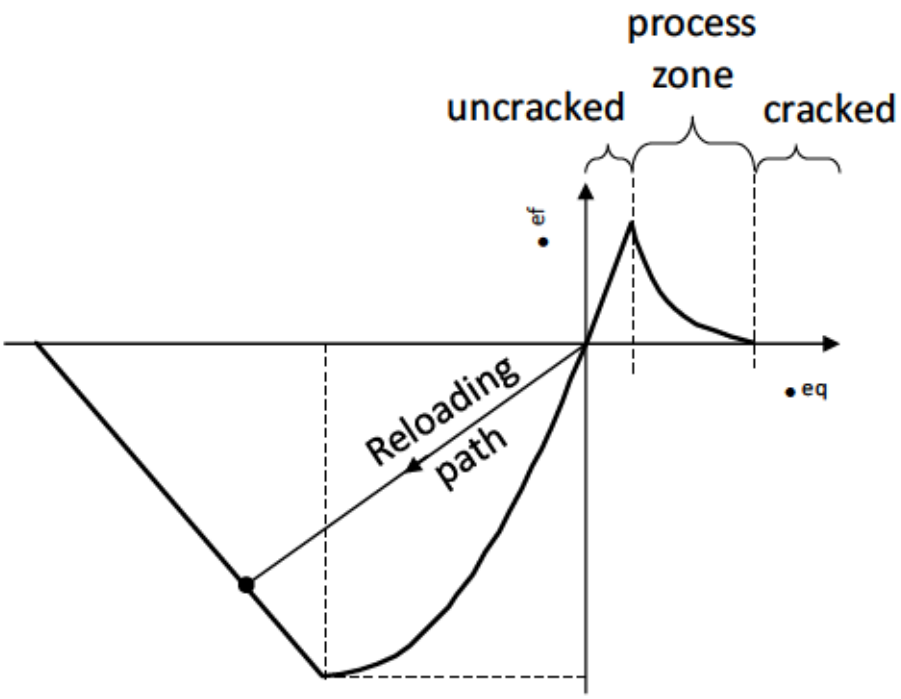

Fig. F.0.1 Uniaxial stress-strain law for concrete

F.1 Tension after cracking

Tension after cracking is handled by a fictitious crack model based on a fracture energy and crack-opening law with combination of the crack band. SBETA material model includes five different softening models for concrete, which are (1) exponential crack opening law, (2) linear crack opening law, (3) linear softening based on local strain, (4) SFRC based on fracture energy, and (5) SFRC based on strain.

F.2 Localization limiters

Deformations in the cracked condition is controlled by localization limiter controls. Crack in tension is represented by discrete failure plane in the finite element analysis. This approach is known as a crack band theory, and the purpose of the failure band is to eliminate the effect of element size and element orientation. The orientation of the failure plane in an element is assumed to be normal to the principal tensile stresses. The failure band for tension L_t is defined in Fig.F.2.1. An angle θ is the minimal angle of θ_1 and θ_2 between the direction of the normal to the failure plane and element sides, which for the case of general quadrilateral element are calculated as average for

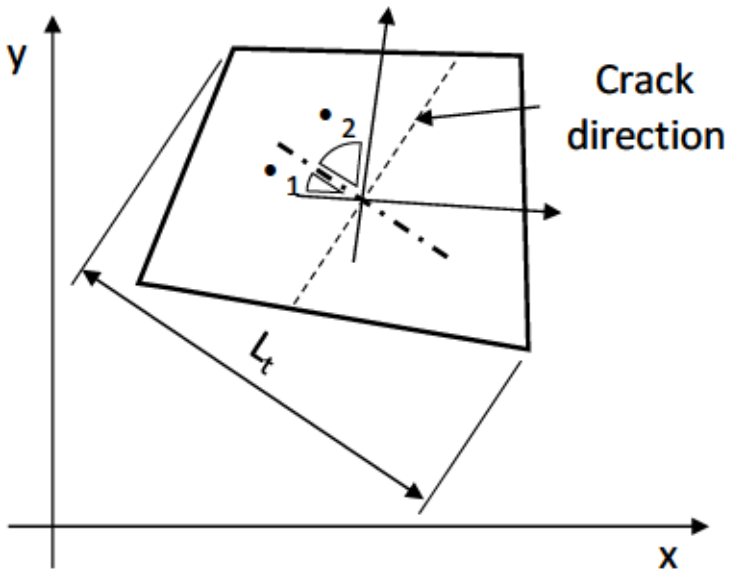

Fig. F.2.1 Definition of tensile localization band on 4 noded element

two opposite edges. The effect of element orientation is further reduced by increasing the failure band for skew meshes using $L_t^{'} = \gamma L_t$, where $\gamma = 1 + (\gamma^{max} - 1)\,\theta/45$, and $\theta \in < 0; 45 >$. The recommended value of $\gamma^{max} = 1.5$.

Appendix G

Experimental work: Bond and flexure tests of FG-SHCC applied as a repair layer

Anisotropic, strain hardening cementitious composites (SHCC) are used as a repair material on mortar beams (40x25x160mm) with a crack in the centre of the span formed by a sheet of foil, repaired by 15mm of SHCC. To avoid size effect, the dimensions of the experimental model are identical to the numerical model. Thicker material can lead to a different fibre arrangement and overestimation or underestimation of the fracture energy [90].

Analytical model is then created and analysed using non-linear finite element method, which combines fracture-plastic model for concrete. Tension is handled by a fracture model based on the classical orthotropic smeared crack formulation and the crack band approach. The model employs the Rankine failure criterion, exponential softening, and fixed crack model [9].

Adopted SHCC material mixture [81] is applied on mortar surface for the bond test, Fig.G.0.1, and on a pre-cracked mortar beam, Fig.G.0.2, with thickness of 15mm. Bond is tested by a hydraulic jack bolt on a mortar cylinder ϕ50mm glued by epoxy resin to the SHCC surface with loading capacity of up to 7.3kN. Half of cross section of the damaged surface is shown in Fig. G.0.3. Diameter of damaged surface is up to 60mm. Formed cracks of tested beam, reaching up to 9kN load, are presented in Fig. G.0.4.

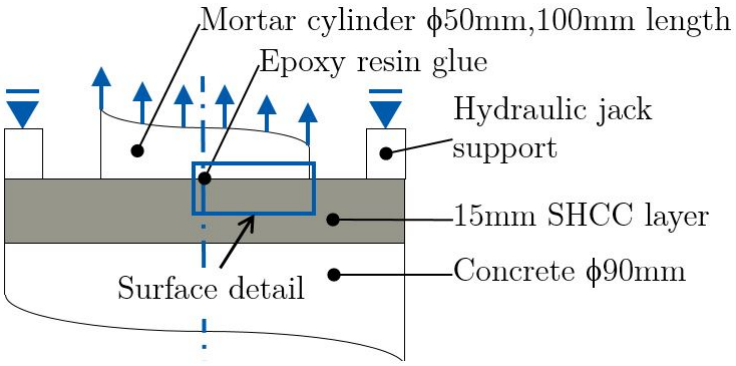

Fig. G.0.1 Scheme of the bond test

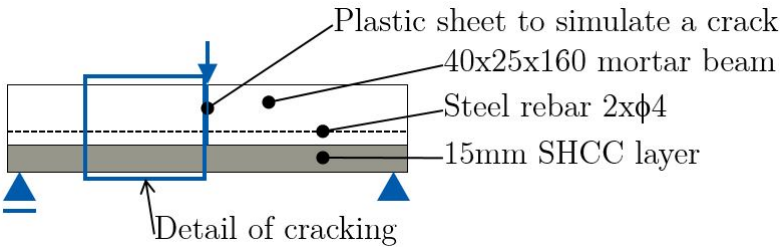

Fig. G.0.2 Scheme of the flexural test

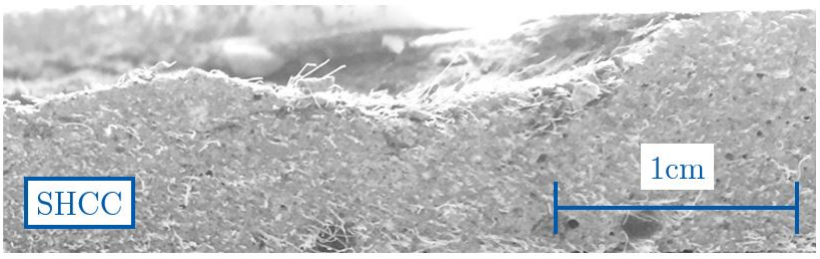

Fig. G.0.3 Failure of the SHCC layer of the bond specimen

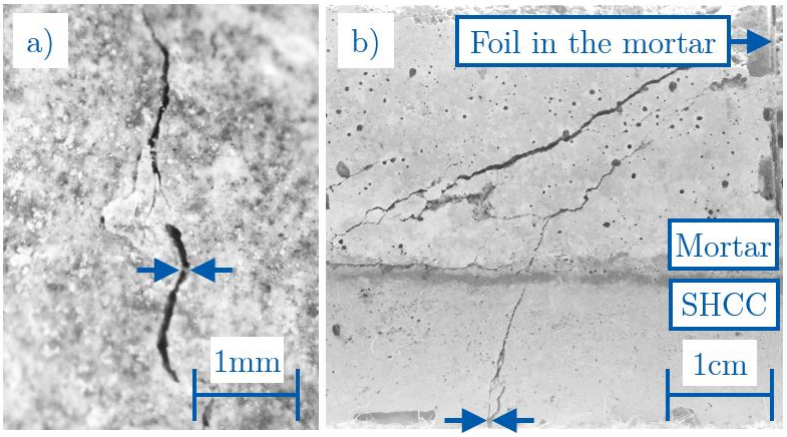

Fig. G.0.4 a) MCW=49μmat peak load of 8.82kN b)MCW=120μm peak load (localized cracking)

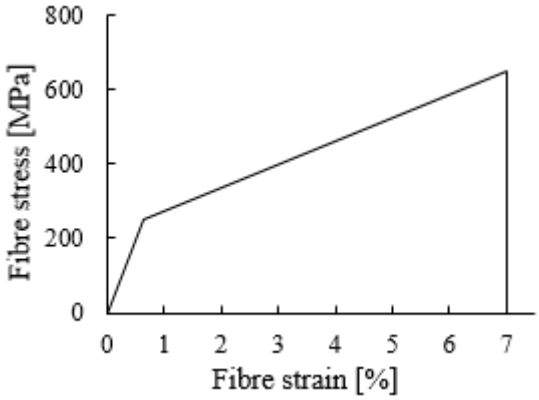

Fig. G.1.1 Stress-strain law of smeared fibre reinforcement

G.1 Analytical model taking into account anisotropy of FG-SHCC

The SHCC material model is a combination of a constitutive model for concrete and smeared reinforcement. This gives us the option to create an anisotropic material model based on the fibre reinforcement ratio and its orientation. Total fracture energy of the model is then created as a combination of the homogeneous fixed crack model with prescribed fracture energy of 45N/m and exponential tension softening, and reinforcement with elastic modulus of 40GPa for PVA fibres, following the bilinear stress-strain law (Fig.G.1.1). The benefit of above described approach is that the model under tension shows gradual crack opening, compared to use of only a non-linear model with prescribed tension law function. The tension test of created material model is presented in Fig.G.1.2, where grey colour represents an elastic loading plate through which a displacement is introduced. ACW (average crack width) area is 30μm, and MCW (maximum crack width) is 45μm. White area has no visible cracks, i.e., cracks are smaller than $1\mu m$. The crack width is computed as a multiplication of the characteristic length of an element size with the total value of fracturing strain in the direction of crack opening, plus the current increment of fracturing strain. Finite element mesh size of 2.5x2.5mm is then selected as an optimal value for crack width representation. This element size is used in all presented models.

The stress-strain relationship of the tensile test is shown in Fig.G.1.3. Models for tensile test are loaded in the direction of fibre orientation and second, orthogonally to fibres. As is expected, the latter load orientation has fracture energy of plain concrete.

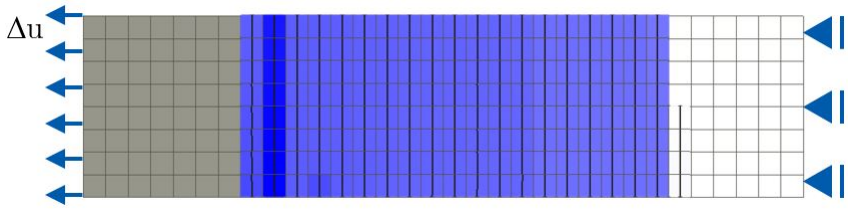

Fig. G.1.2 Tension test of the SHCC model. $\Delta u = 3.4 \times 10^{-4} m$; $\epsilon = 0.005$; $ACW = 30\mu m$; $MCW = 45\mu m$; Grey: Loading plate, White: uncracked

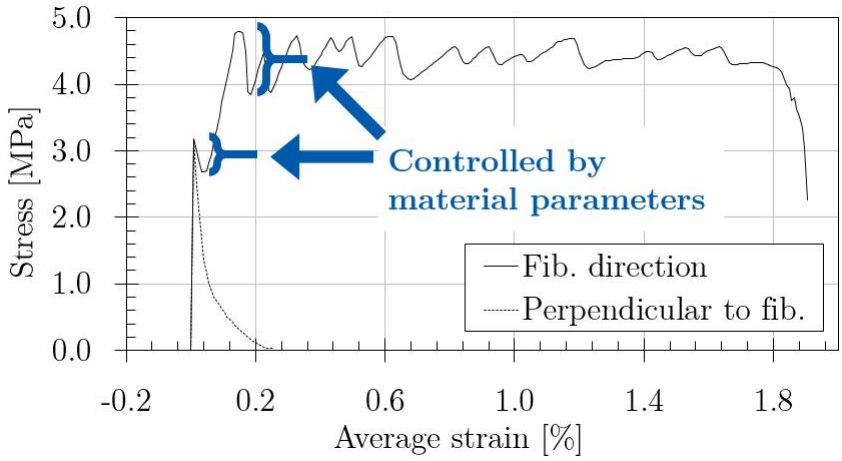

Fig. G.1.3 Stress-strain relationship of the anisotropic SHCC model

The drop in stress after first cracking of the tension model can be effectively controlled mainly by three parameters, fracture energy, elastic modulus of the smeared fibre reinforcement, and strength of the smeared fibre reinforcement also used to control the ultimate strain.

G.2 Application and remarks

Axial symmetry model of a bond test was created to simulate a bond performance between different casting technique and fibre content on the surface. Homogeneous mixture assumes random orientation of fibres, whereas anisotropic model has fibres oriented predominantly in one direction at the angle theta, Fig.G.2.1. Proposed SHCC model is using in total 2% of fibres, where in case of homogeneous SHCC, even distribution in two orthogonal directions is applied, Fig.G.2.5. For the bond test, it is assumed, that the surface layer has fibres predominantly oriented along the surface, and all fibres are therefore aligned in such a way in the material model.

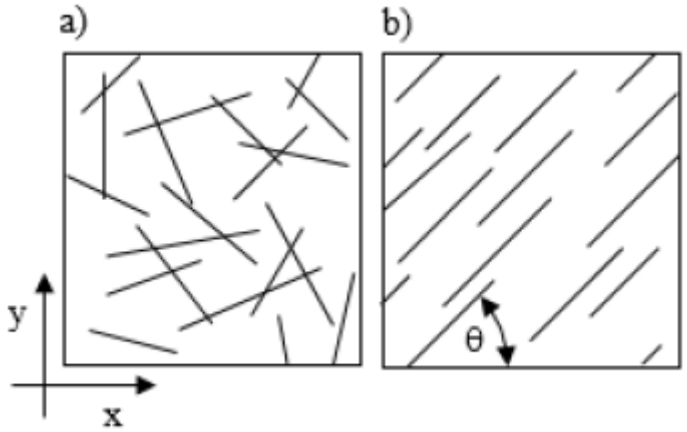

Fig. G.2.1 Fibre orientation of SHCC: a) Random, b) Aligned

Gradual cracking sequence can be observed. At the first loading step of applied displacement at 5microns, each element in the model develops a narrow crack width smaller than 1micron. Fig.G.2.2-a) is showing cracking at applied displacement of 0.5mm. At this displacement, 4 cracks of around 110 micron width each are created, whilst rest of the initial cracks are kept at values lower than 1 micron. Fig.G.2.2-b) is showing cracking at applied displacement of 2.5mm. At this displacement, 12 cracks of around 110 micron width each are created, whilst rest of the initial cracks are kept at values lower than 1micron. Fig.G.2.2-c) is showing cracking at applied displacement of 4.0mm. At this displacement, most of the cracks are having width of up to 110 micron, with only last 6 elements remaining at crack width around 1 micron. Fig.G.2.2-d) is showing cracking at applied displacement of 7.2mm. At this displacement, all elements developed crack width of up to 110 micron. Crack localization occurred at applied displacement of 7.4mm, see Fig.G.2.2-e). Crack localization is characterized as wide crack width opening followed by complete failure. This gradual cracking sequence is beneficial for further application in the flexure test. If this gradual crack with formation would not be introduced, all cracks width in the tensile test would develop simultaneously, and cracked area of the repair layer would tend to be larger, i.e., more narrow cracks over n elements, rather than the observed single crack width development.

Number of cracks created during applied displacement is presented in Fig.G.2.3. Crack formation shows a step-wise evolution, as can be deducted from the presented cracking sequence. This is showing sudden cracking, just as is observed in real SHCC behaviour. At the ultimate average strain, all elements are cracked. As can be seen,

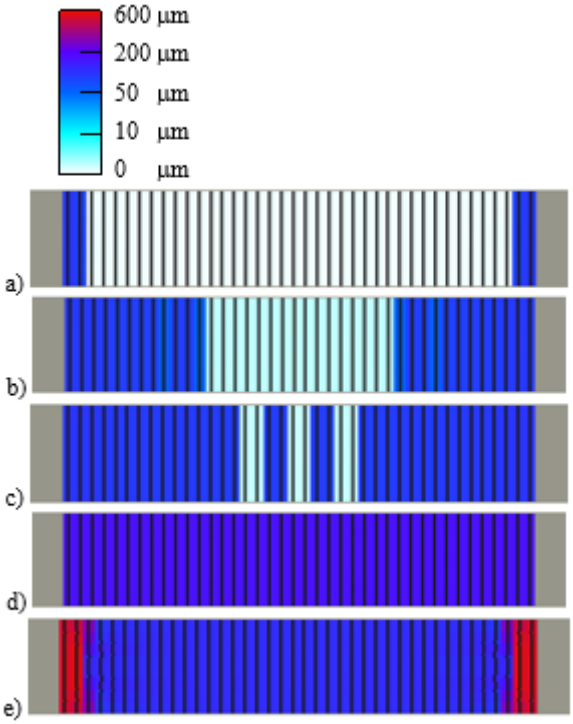

Fig. G.2.2 Cracking sequence of the simulated uniaxial tension test at displacement of: a) 0.5mm, b) 2.5mm, c) 4.0mm, d) 7.2mm, e) 7.4mm

some steps are larger than others, showing different number of cracked elements in a cracking group. It must be noted, that crack width smaller than 2microns is here ignored. Total crack width is linearly increasing during the imposed displacement, see Fig.G.2.4.

Failure surface occurred up to 5mm thickness of surface layer and no de-lamination between layers occurred. Connection between layers is then modelled as perfectly rigid. After reaching the maximum load capacity, sudden failure occurred. This kind of failure is due to fibre orientation mostly parallel to the surface, so the anisotropic model with fibres oriented only parallel to the surface is used. The load-displacement diagram is presented in Fig.G.2.6 and failure surface in Fig.G.2.7.

Three-point bending is used for the flexural test of a mortar specimen repaired by one 15mm layer of SHCC with 2% of fibre. Mechanism of cracking is as follows, firstly, a crack is formed on the bottom surface of SHCC, secondly, a crack propagates diagonally from the loading point up to reaching the embedded reinforcement and cracking along its position. The analysis model boundary conditions presented in Fig.G.2.8 are showing how the pre-cracked elements are introduced. One option is

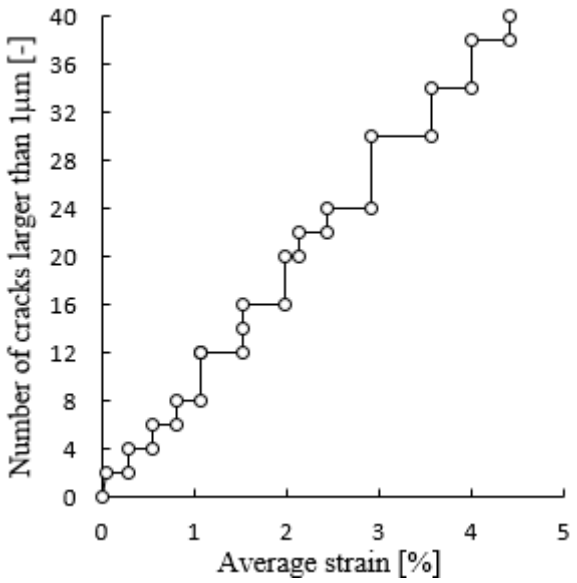

Fig. G.2.3 Number of cracks and average strain of the tensile test

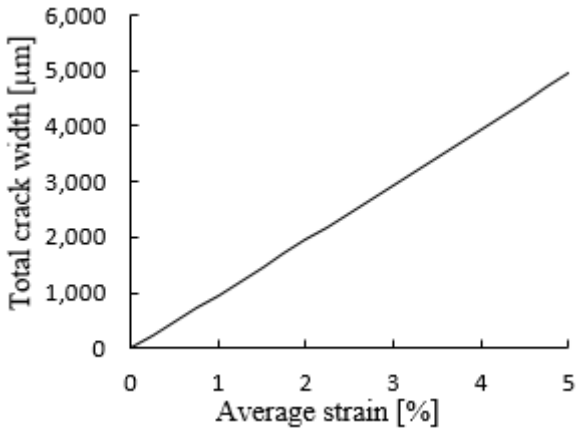

Fig. G.2.4 Total crack width and average strain of the tensile test

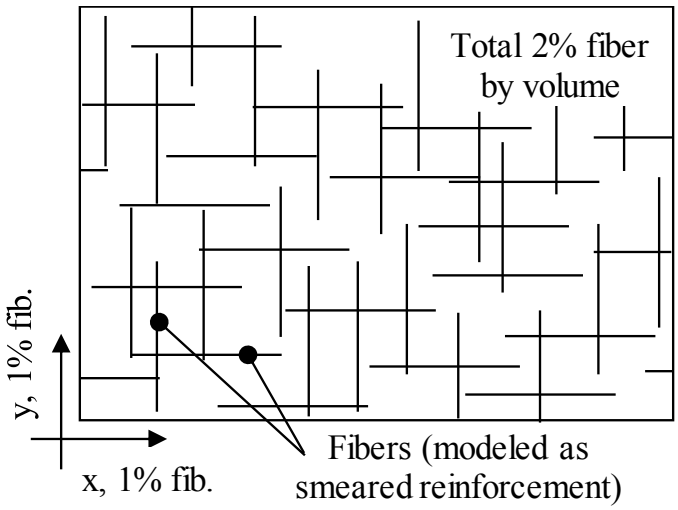

Fig. G.2.5 Orthogonal fibre orientation for homogeneous material modelling

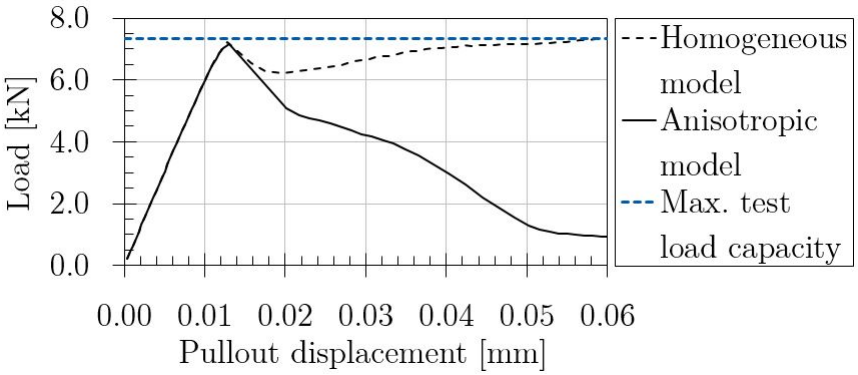

Fig. G.2.6 Load/stress - displacement of the bond test

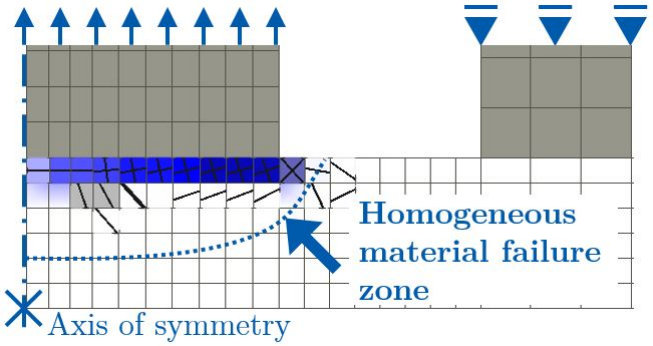

Fig. G.2.7 Surface failure of the SHCC layer. Depth of cracking: 3.8mm, $\Delta u = 5.4 \times 10^{-5} m$

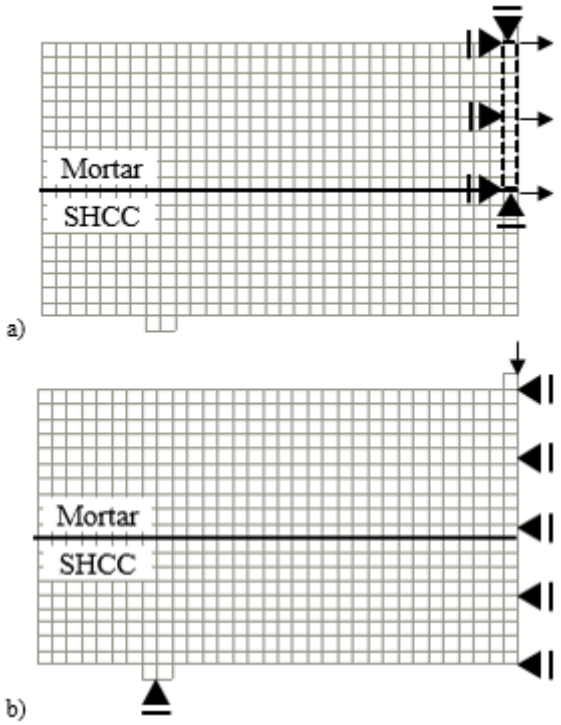

Fig. G.2.8 Boundary condition of the flexure test: a) Pre-cracking of the mortar elements, b) Applied displacement in the centre

to create elements with lower thickness, or reduced material quality, or as in this model, a special initial loading step can be introduced, at which the crack is created by applied displacement of 1micron and given boundary conditions, Fig.G.2.8-a). Next loading steps are using usual boundary conditions of 3-point bending test set-up with an introduced symmetry in the centre.

Load up to 3kN causes no cracking on the SHCC surface, as is observed in the experiment, beam is at this load fully elastic. Loading up to 6kN caused crack width of 81microns. To obtain the residual crack width, load was after reaching 6kN removed. Loading and unloading of the beam is shown in Fig.G.2.9. The residual crack width is 19microns, that is very close to 21microns measured in the experiment. The cracked analysis model from the pre-cracking is in Fig.G.2.10-a), using the same color range for cracks as for the tensile test, Fig.G.2.2. As expected, elements in the location of the foil are cracked by a single load step. Loading up to 6kN caused mainly a single crack, penetrating from the SHCC repair surface, to the initial crack. Secondary cracking is observed spreading diagonally from the point of the introduced dis-placement into the mortar and from the interface between the mortar and SHCC into the SHCC.

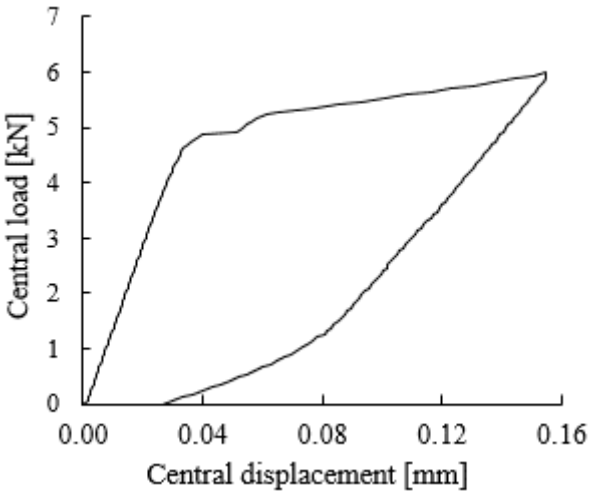

Fig. G.2.9 Loading and unloading of the beam model for residual crack width

Secondary crack width is lower than 1micron, and are mostly closed in the unloaded case, Fig.G.2.10-c).

This cracking behaviour is well represented by the analytical model. During crack width opening on the SHCC surface, load reaches up to 9kN followed by opening of the diagonal crack in the pre-cracked mortar sample causing a reduction of load capacity followed by slow increase (Fig.G.2.11). Further loading causes cracking along the reinforcement in the mortar alongside with progressive crack width opening (Fig.G.2.12). Measured cracks are presented in Fig.G.2.13 to Fig.G.2.26.

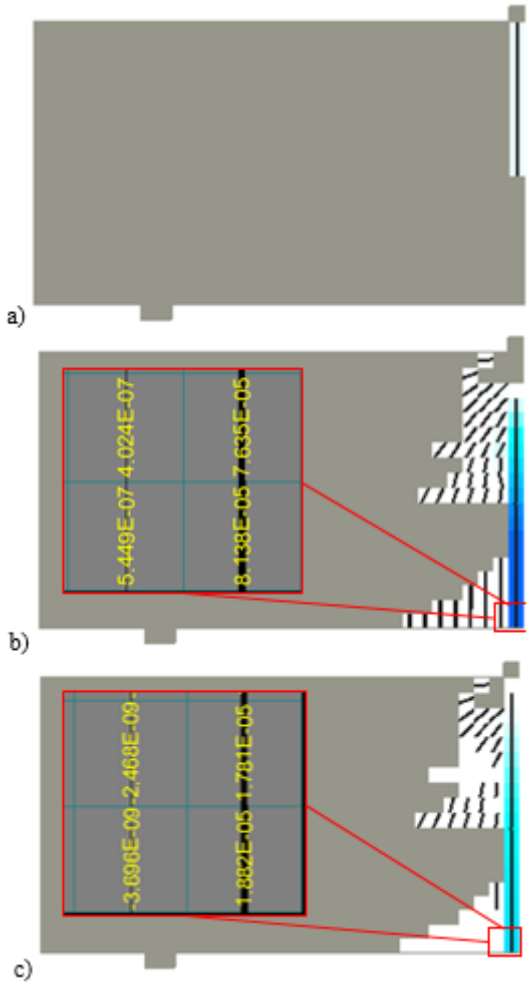

Fig. G.2.10 Cracking of the flexure model. a) Pre-cracking, b) Cracking at 6kN, c) Residual cracking

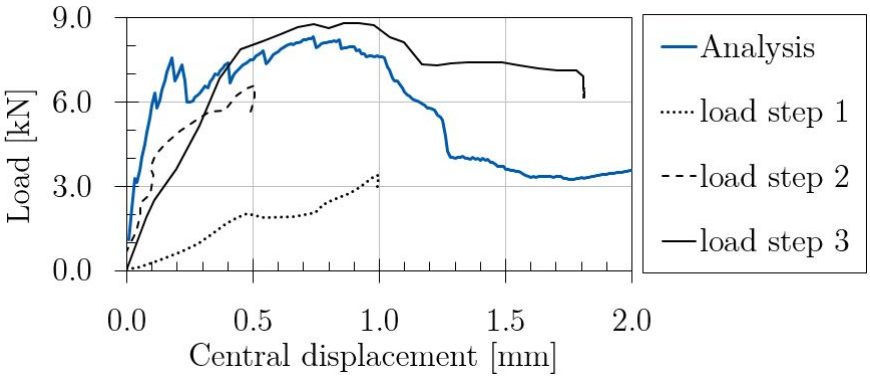

Fig. G.2.11 Load - displacement of the flexural test

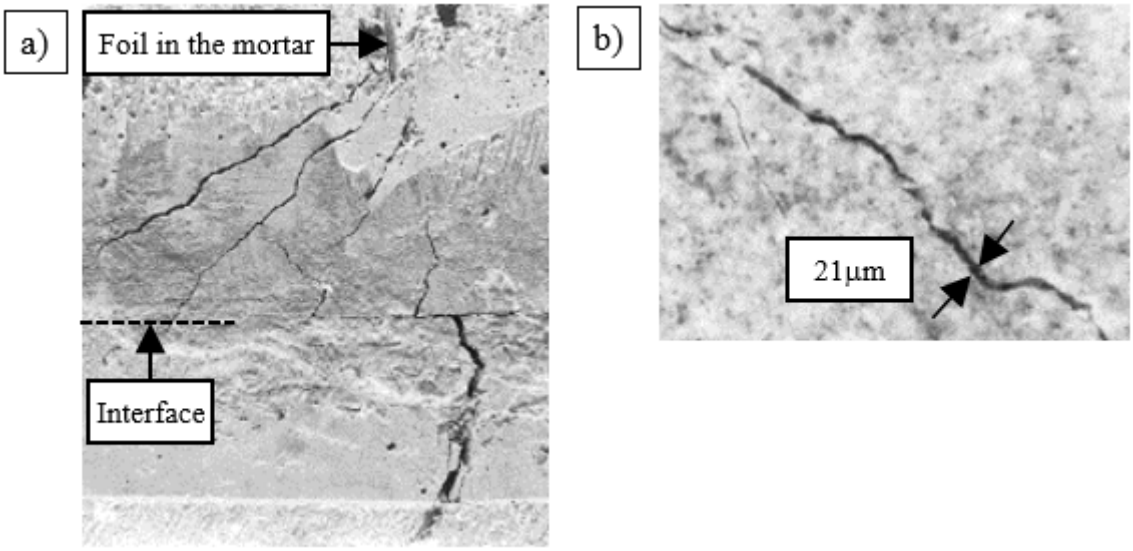

Fig. G.2.12 Flexure test: a) Crack pattern at the ultimate load capacity (10.02kN), top mortar, bottom SHCC; b) Residual crack width on the surface at 6kN load

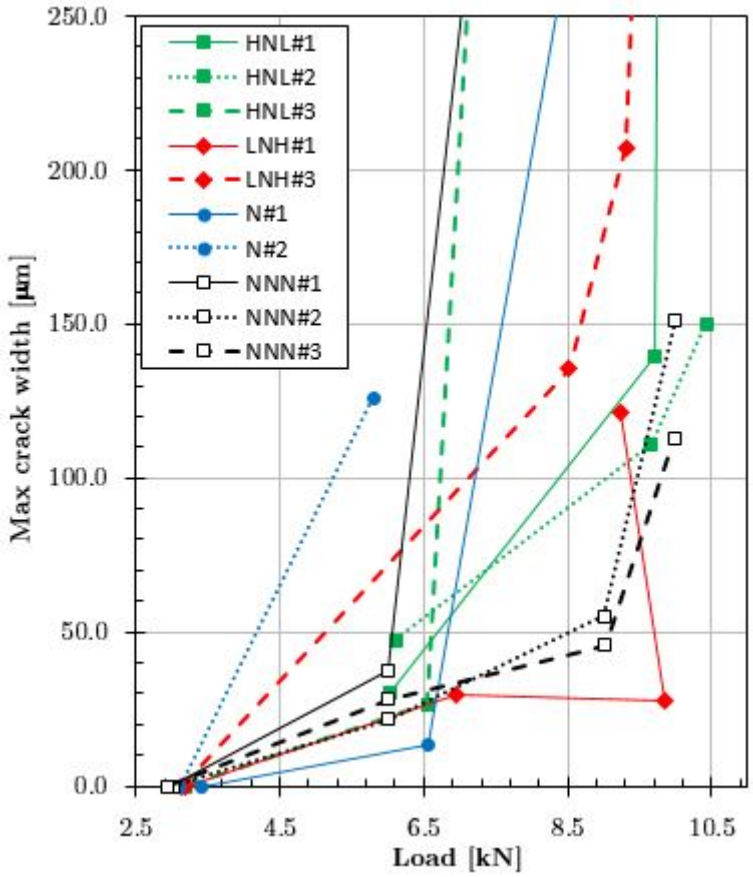

Fig. G.2.13 Maximum crack width VS load of the 3-point bending test

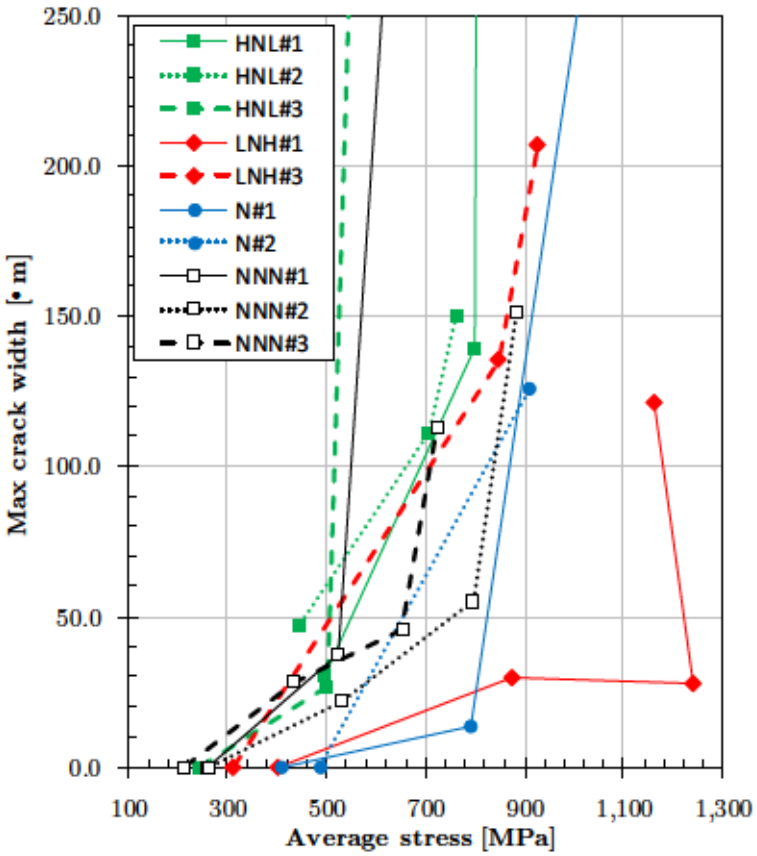

Fig. G.2.14 Maximum crack width VS average stress of the 3-point bending test

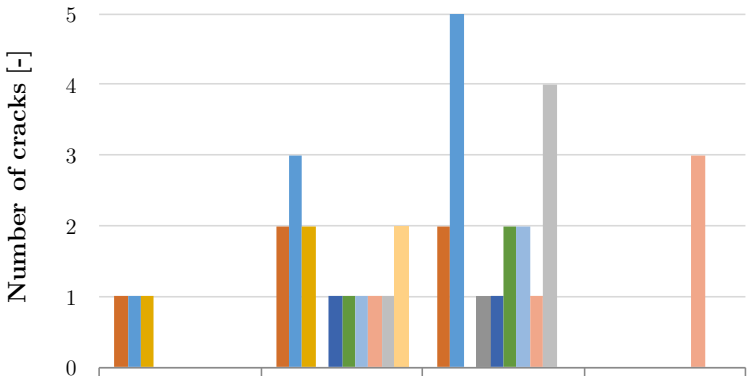

Load step:	1	2	3	4
HNL#1	1	2	2	
HNL#2	1	3	5	
HNL#3	1	2		
LNH#1	0	0	1	
LNH#3	0	1	1	
NNN#1	0	1	2	
NNN#2	0	1	2	
NNN#3	0	1	1	3
N#1	0	1	4	
N#2	0	2		

Fig. G.2.15 Number of cracks on the SHCC surface VS load step

Step before crack localization	Step after peak load/ crack localization
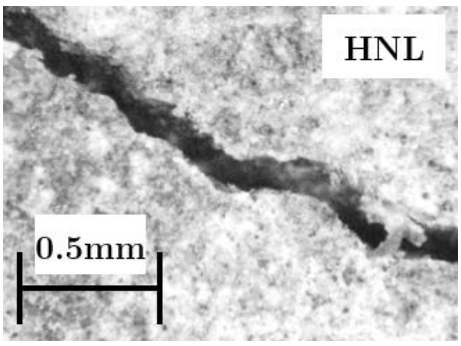	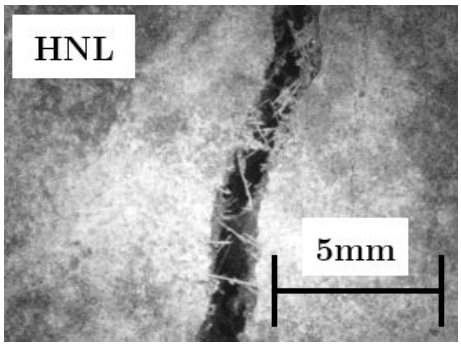

Fig. G.2.16 Cracking localization of layering HNL#1

Step before crack localization	Step after peak load/ crack localization
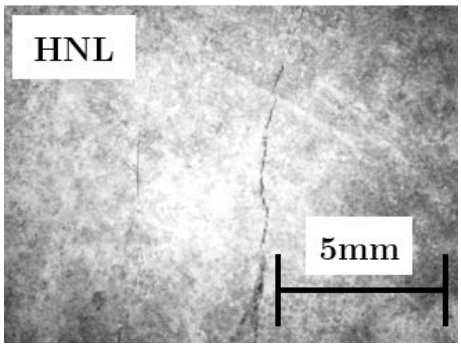	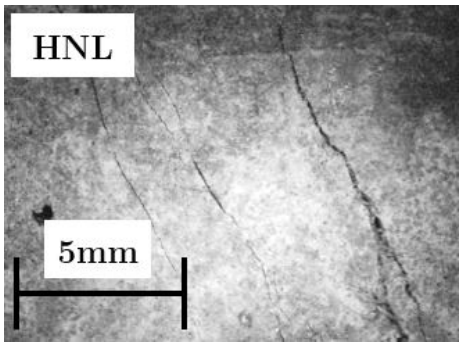

Fig. G.2.17 Formation of new cracks in layering HNL#2

Step before crack localization	Step after peak load/ crack localization
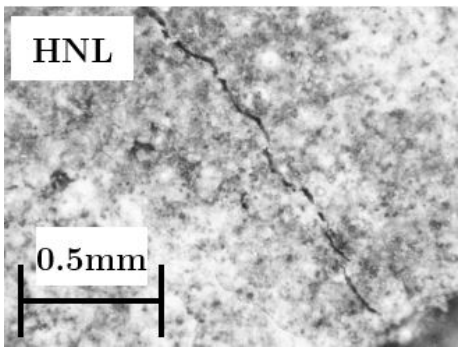	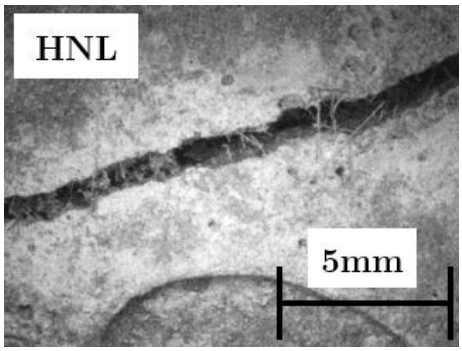

Fig. G.2.18 Cracking localization of layering HNL#3

Step before crack localization	Step after peak load/ crack localization
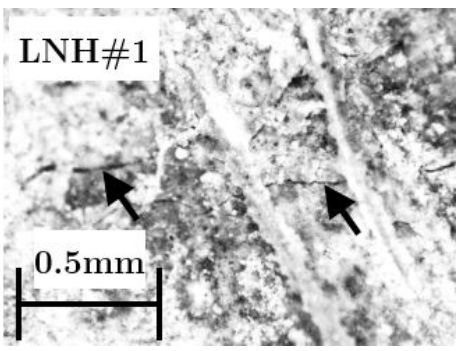	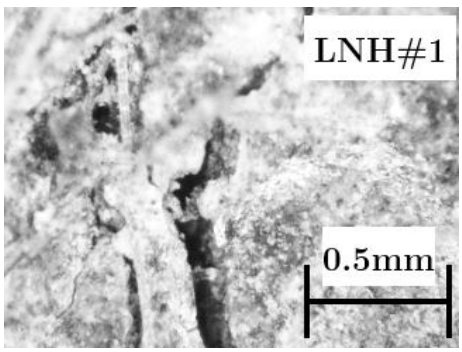

Fig. G.2.19 Cracking localization of layering LNH#1

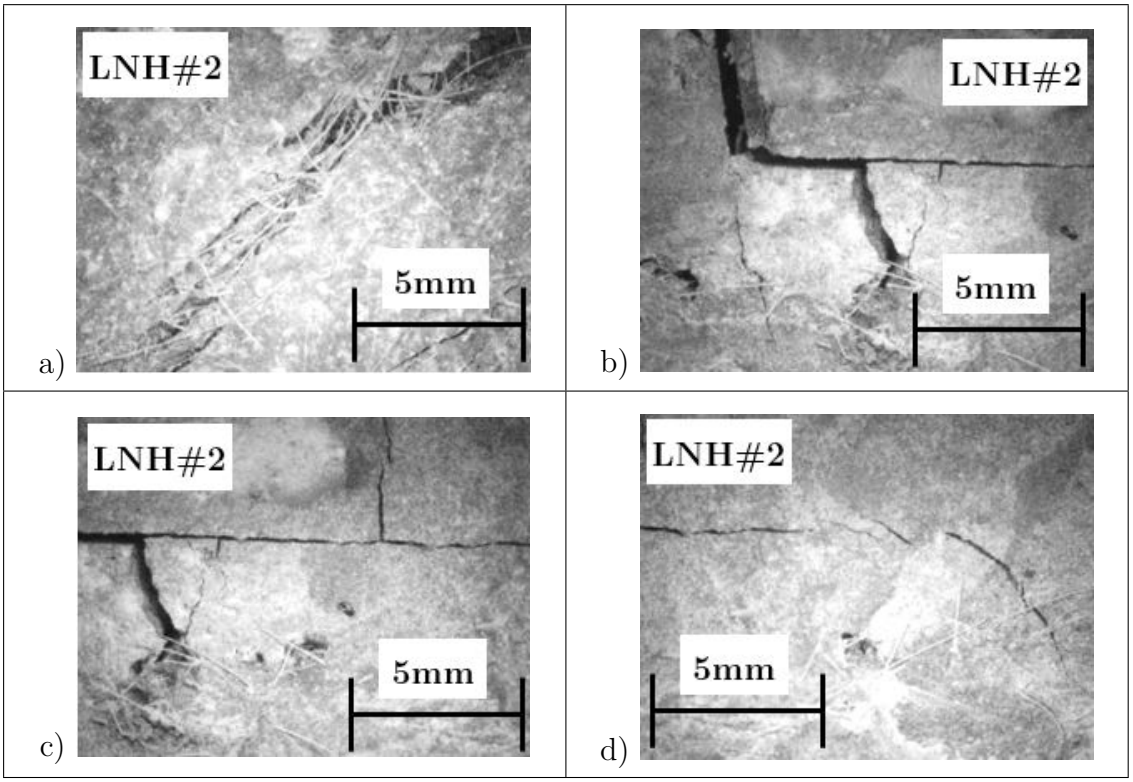

Fig. G.2.20 LNH#2: a) Surface crack localization of layering, b) Interface- SHCC layer is down, c) Interface- SHCC layer is down, d) Interface crack propagates into SHCC layer

Step before crack localization	Step after peak load/ crack localization
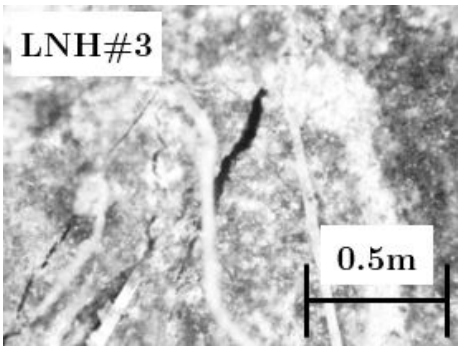	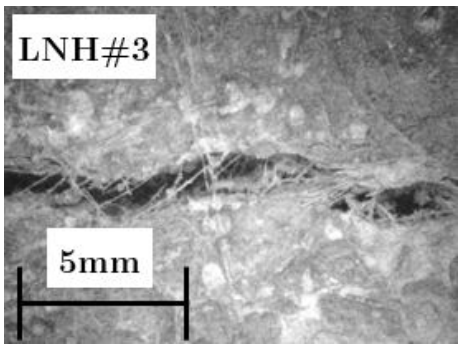

Fig. G.2.21 Cracking localization of layering LNH#3

Step before crack localization	Step after peak load/ crack localization
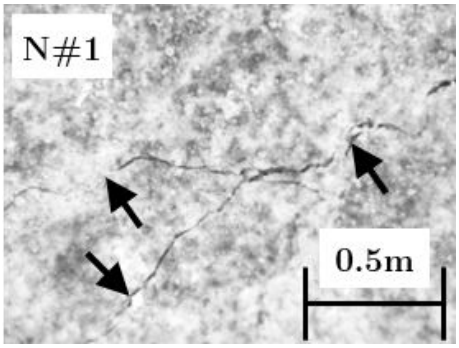	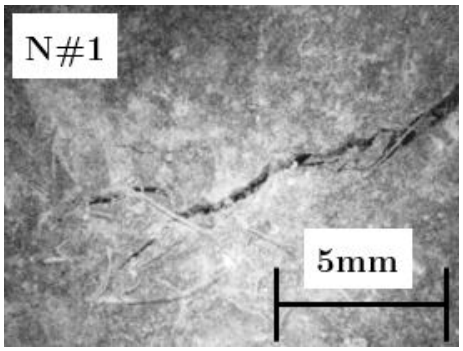

Fig. G.2.22 Cracking localization of a single SHCC layer N#1

Step before crack localization	Step after peak load/ crack localization
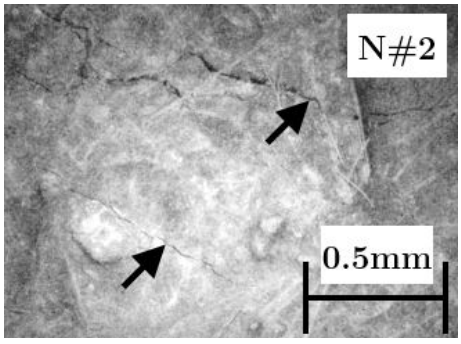	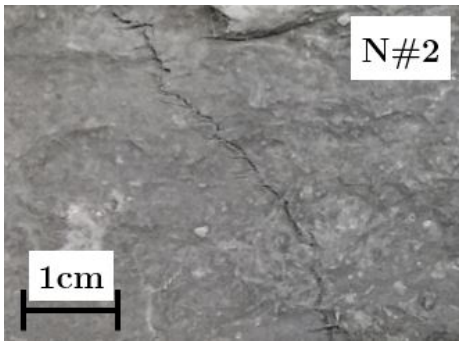

Fig. G.2.23 Cracking localization of a single SHCC layer N#2

Step before crack localization	Step after peak load/ crack localization
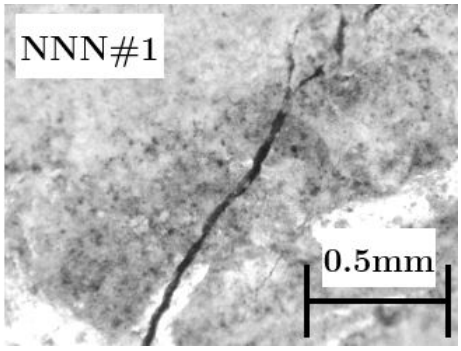	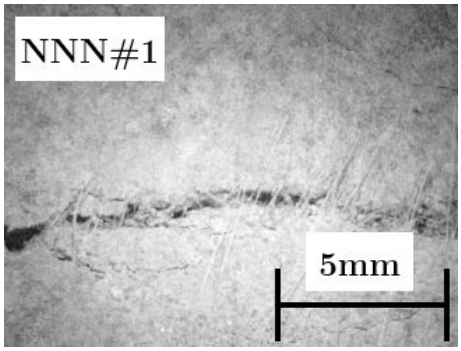

Fig. G.2.24 Cracking localization of a layered SHCC, NNN#1

Step before crack localization	Step after peak load/ crack localization
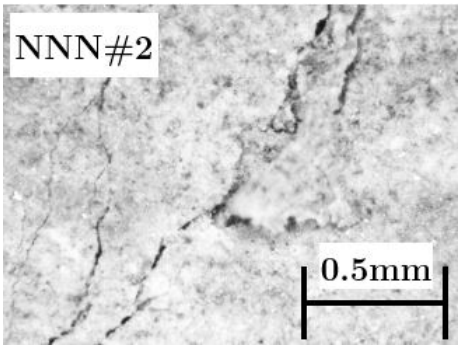	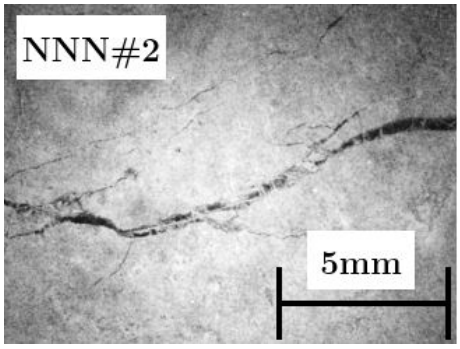

Fig. G.2.25 Cracking localization of a layered SHCC NNN#2

Step before crack localization	Step after peak load/ crack localization
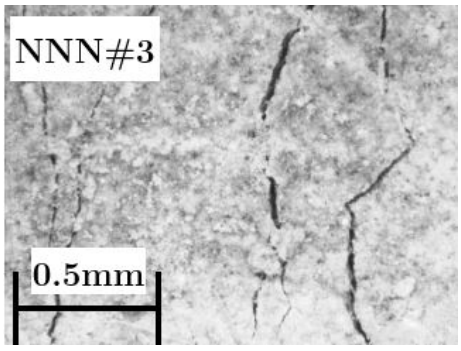	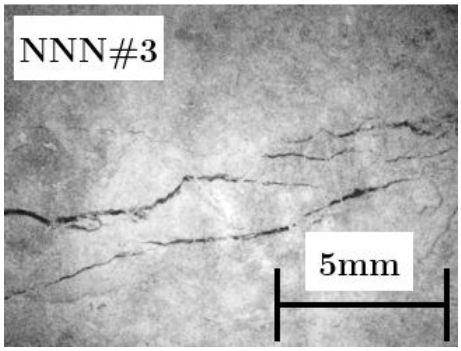

Fig. G.2.26 Cracking localization of a layered SHCC NNN#3

Appendix H

Numerical error of FEM diffusion analysis

Numerical error of diffusion analysis is examined on two different analytical solutions. First, semi-infinite domain of constant diffusivity with constant boundary concentration and secondly a two-layer semi-infinite domain. It has been found, that for accurate modelling of semi-infinite concentration distribution, a certain "backyard" domain is necessary to model infinite "backyard". Error size with respect of size and time steps for homogeneous solution is presented in Table H.1 and Fig H.0.1, followed by errors of the multi-layer solution in Table H.2 and FigH.0.2. As an optimal thickness of the backyard domain to simulate the semi-infinite solution, the $\alpha = 1.5$ is selected at time step of 0.01year and size step 0.001m, where $backyard = \alpha \cdot cover$.

Cover [mm]	Time step [year]	Size step [m]	Maximal error [%]							Maximal error [%]						
			10	5	1	0.5	0.1	0.05	0.01	10	5	1	0.5	0.1	0.05	0.01
			Backyard thickness to achieve the error [mm]							α, backyard thickness to achieve the error [mm]						
40	1	0.001	x	x	x	x	x	x	x	x	x	x	x	x	x	x
	0.1	0.001	40	40	50	50	x	x	x	1	1	1.25	1.25	x	x	x
	0.01	0.001	40	40	60	60	70	70	x	1	1	1.5	1.5	1.75	1.75	x
	0.001	0.005	40	40	60	60	60	80	x	1	1	1.5	1.5	1.5	2	x
	0.001	0.001	40	40	60	60	70	80	80	1	1	1.5	1.5	1.75	2	2
	0.001	0.0005	40	40	60	80	80	80	80	1	1	1.5	2	2	2	2
x...error is larger than the maximal error																

Table H.1 Estimated error, approximation of homogeneous semi-infinite solution by FEM

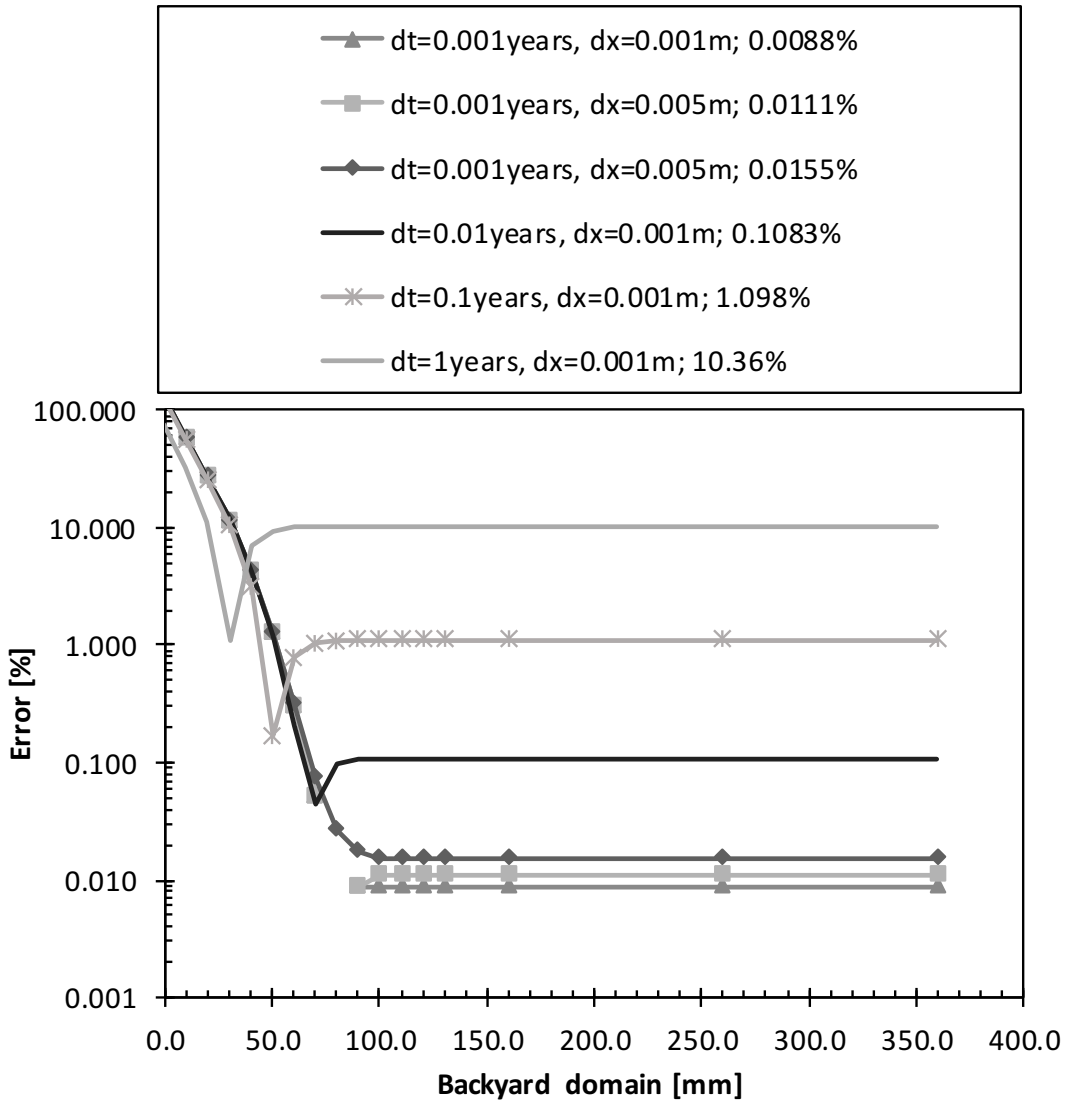

Fig. H.0.1 Estimated error, approximation of homogeneous semi-infinite solution by FEM

Cover [mm]	Time step [year]	Size step [m]	Maximal error [%]							Maximal error [%]						
			10	5	1	0.5	0.1	0.05	0.01	10	5	1	0.5	0.1	0.05	0.01
			Backyard thickness to achieve the error [mm]							α, backyard thickness to achieve the error [mm]						
52	1	0.001	x	x	x	x	x	x	x	x	x	x	x	x	x	x
	0.1	0.001	10	20	20	20	x	x	x	0.19	0.38	0.38	0.38	x	x	x
	0.01	0.001	20	20	20	30	30	30	30	0.38	0.38	0.38	0.58	0.58	0.58	0.58
	0.001	0.002	20	20	20	20	30	x	x	0.38	0.38	0.38	0.38	0.58	x	x
	0.001	0.001	20	20	20	30	30	30	30	0.38	0.38	0.38	0.58	0.58	0.58	0.58
	0.001	0.0005	20	20	20	20	30	30	30	0.38	0.38	0.38	0.58	0.58	0.58	0.58
x...error is larger than the maximal error																

Table H.2 Estimated error, approximation of multi-layer semi-infinite solution by FEM

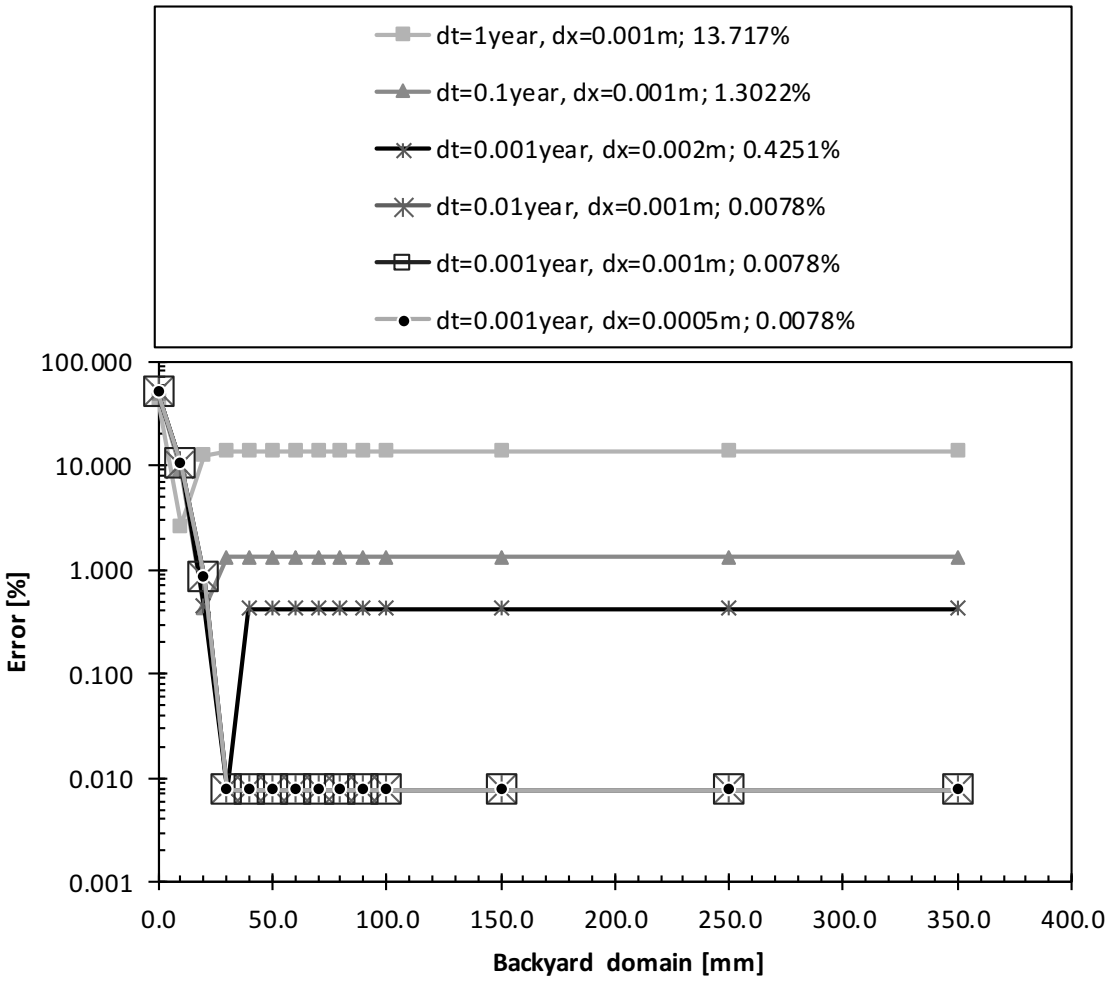

Fig. H.0.2 Estimated error, approximation of multi-layer semi-infinite solution by FEM

Appendix I

Mechanism of durability improvement by FG-SHCC

The mechanism behind the FGM is explained on three layer material. In Fig.I.0.1 is shown a multi-layer structure of three different material diffusivities d_1, d_2, and d_3. In the layer #2, the diffusivity ratio d_1/d_2 is being changed from 0.01 to 10. For SHCC, diffusivity ratio between the best and low quality material can be up to an order of magnitude. Diffusivity of material $d_3$has 10 times higher diffusivity and is understood as a layer of mortar. Material of high diffusivity located at layer #2 is having low resistance compared to the rest of the layers, and diffused substance can penetrate much easier. On the other hand, layer of high resistivity will slow down the penetration, and the diffused substance is accumulated in the layer #1. This mechanism suggest that placing a layer of low diffusivity should be placed close to the surface layer. Direct position on the surface as an external layer might increase a risk of mechanical damage of the good quality layer, so from this point of view it is better to use a lower quality material as a protection. This protective layer would have two goals, firstly the protection, and secondly it could be designed for reduction of the chloride content by a wash-away mechanism, further increasing the durability.

Flux at the position of rebar for the case of homogeneous material is 5.6x larger than for the case of $D_1/D_2 = 0.1$, i.e. the layer D_1 having 10 times lower diffusivity. For the case of suggested optimum FG-SHCC diffusivity ratio (0.3-0.4-2.3), the flux of the homogeneous layer (1.0-1.0-1.0) is 4.3 times larger. This is also showing, that with a higher function gradient the effect is rising.

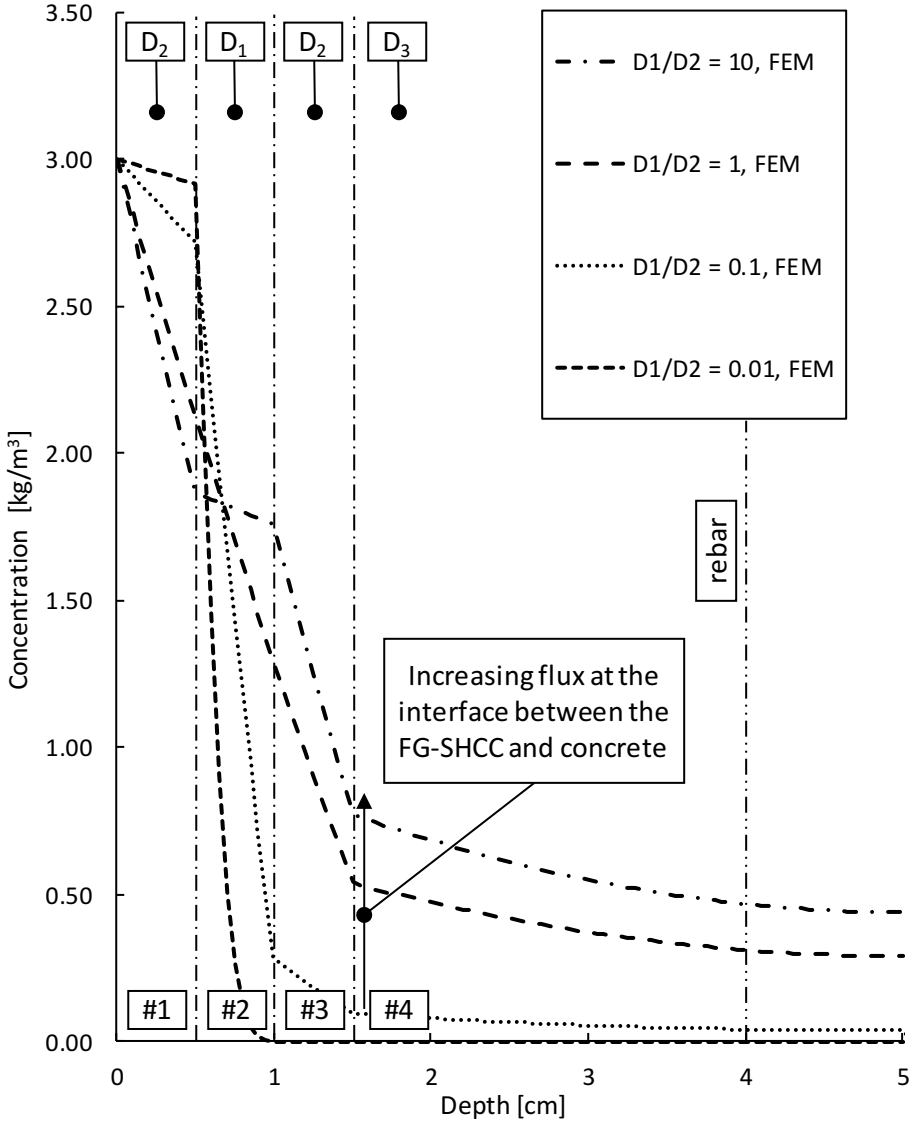

Fig. I.0.1 Mechanism of FGM

Appendix J

MATLAB code of chloride diffusion into FG-SHCC with mesh update by salt scaling

Matlab code used for calculation of chloride concentration with re-mashing in each time step as a representation of salt frost scaling effect.

```
%%%%
CL_bound=1.9;                    % [%] Chloride content seawater
CL_lim = 1.2;                    % [%] Limit concentration of chloride
%%%%

S = 0.000;                       % Scaled off material [mm]
%%%-- Mesh generation --%%%
mat_types = 3 ;                  % number of materials
Thickness=.01;                   % Thickness of a layer [m]
nL=6;                            % Number of SHCC material layers
Thtot = Thickness*nL;            % Total thickness of SHCC
nE=10;                           % Number of FE elements in one layer
nEtot = nE*nL;                   % Number of FE elements total
nNtot = nEtot+1;                 % Number of FE nodes total
nI = nL/mat_types;               % number of layers of one material
mat = zeros(nL,1);

for i = 1:mat_types
if i == 1
mat(i:nI,1) = i ;
```

```
elseif nI == 1
mat(i*nI,1) = i ;
else
mat(i*nI-(nI-1):i*nI,1) = i ;
end
end

%%%--- Creating space ---%%%
K=zeros(nNtot,nNtot);              % Empty stiffness matrix
C=zeros(nNtot,nNtot);              % Empty mass matrix
F=zeros(nNtot,1);                 % Empty forcing vector
Q=zeros(nNtot,1);                 % Initial forcing vector,

%%%--- Initial conditions ---%%%
T0=0;                                % Initial concentration [kg/m3]
CL_old=T0*ones(nNtot,1);           % Initial temperature in system [degC]
%%%--- Preparing matrices ---%%%
CL_new = CL_old;
Fold = F;
Fnew = Fold;
dt=0.05;                                    % Size of time step
t=1;                                  % Time [year]
CL_new = zeros (nNtot,1);

for n = 1:t/dt
for layers = 1:nL ;
if S == 0
dl=(Thickness)/nE;                 % Distance between nodes [m]
% Spatial discretisation of one layer
x_layer = [(layers-1)*Thickness:dl:(layers)*Thickness];
elseif S ~= 0 && layers > 1
dl=(Thickness)/nE;                 % Distance between nodes [m]
```

```
% Spatial discretisation of one layer
x_layer = [(layers-1)*Thickness:dl:(layers)*Thickness];
elseif S ~= 0 && layers == 1
% Distance between nodes in scaled layer [m]
dl=(Thickness-S)/nE;
% Spatial discretisation of one layer
x_layer = [S+(layers-1)*Thickness : dl : (layers)*(Thickness)];
end

if layers == 1
x = [x_layer] ;
end
if layers > 1
x = [x,x_layer(1,2:end)];
end
if layers == 1
a=2;
b=nE+1;
else
a=layers*nE-(nE-1)+1;
b=nE*layers+1;
end
for k = a:b                % Creates the element matrix
e(k-1,:) = [k-1 k mat(layers) dl];
end
end

if n>=1 && S ~= 0          %%% Update values in nodes after re-meshing
CL_old_update = zeros(size(CL_old));
for i=1:nEtot
CL_old_update(i) = (CL_old(i)-CL_old(i+1))/...
        ...(x_old(i+1)-x_old(i))*(x_old(i+1)-x(i))+CL_old(i+1) ;
```

```
end

CL_old_update(end) = CL_old(end) ;
CL_old_update(1,1) = CL_bound ;

figure(1)
plot(x_old(1:11),CL_old(1:11,1,1),...
        ...'bo-',x(1:11),CL_old_update(1:11,1,1),'rx-')
title('')
xlabel('Length')
ylabel('Concentration [%]')
CL_old = CL_old_update ;
CL_old(1,1) = CL_bound ;
end

%%% Diffusivity from surface layer to interface layer
eps = 0.05; % average strain used for equation in JSCE [%]
d_crack = 50*ones(nEtot,1);   % Crack width [micrometer]
H_dk=0.5;       % High quality uncracked diffusivity
N_dk=1.92;      % Normal quality uncracked diffusivity
L_dk=4.26;      % Low quality uncracked diffusivity
dk_database = [H_dk; N_dk; L_dk] ;
H_d0=1.47;      % High quality parameter D0
N_d0=1.91;      % Normal quality parameter D0
L_d0=2.23;      % Low quality parameter D0
d0_database = [H_d0; N_d0; L_d0] ;

D0homogen = 0.99 ;
Dkhomogen = 1.99;
pcx=2e4;                        % Chloride binding capacity [kg/m3]
A=1;                            % Element cross section [m2]
G=0;                            % Concentration source
```

```
%%%--- Assembling matrices ---%%%
l_sum = 0;
for k = 1:nEtot                    % Loop over all elements
nodes=e(k,1:2);                    % Identify nodes
% Diffusivity
if d_crack(k) == 0
dd = dk_database(e(k,3),1);
else
dd = dk_database(e(k,3),1) + d0_database(e(k,3),1)*...
        ...log10(eps*((d_crack(k,1))^2));
end

%%% Stiffness matrix %%%
dl=e(k,4);
Ke = ((A*dd)/dl)*[1 -1;-1 1] ;
Ce = ((pcx*A*dl)/6)*[2 1;1 2];       % Mass entry
% zero for no heat transfer on boundary with resistance
if nodes(1,1)==0
Fe = (G*A*dl)/2*[1;1] + h*A*CL_bound*[1;0] ;      % Forcing entry
else
Fe = (G*A*dl)/2*[1;1] ;
end
% Position stiffness entry at identified nodes
K(nodes,nodes)=K(nodes,nodes)+Ke;
% Position mass entry at identified nodes
C(nodes,nodes)=C(nodes,nodes)+Ce;
% Position forcing entry at identified nodes
F(nodes,1)=F(nodes,1)+Fe;
% Checking the possition of a node
l_sum = l_sum+dl;
end
```

```
%%%--- Time stepping ---%%%
CC=(C+0.5*dt*K);
DD=(C-0.5*dt*K);
% Crank-Nicolson ;
CL_new(2:end) = CC(2:end,2:end)\(DD(2:end,:)*...
        ...CL_old+dt*F(2:end)-CC(2:end,1)*(CL_bound)) ;
CL_new(1) = CL_bound;          % Boundary condition temperature
CL_old=CL_new;

figure(1)
plot(x,CL_new(:,1,1),'bo-')
title('Temperature distribution in rod')
xlabel('Length')
ylabel('Concentration [kg/m3]')

S=S+(0.005/(t/dt)); % Scaled off part in time period t/dt
x_old=x;
if n == 1
first_x = x_old;
first_Cl = CL_old;
end
end

figure(2)
plot(x,CL_new(:,1,1),'bo-',first_x,first_Cl(:,1,1),'bo-')
title('')
xlabel('Length')
ylabel('Concentration [%]')
```